Characterization of Wideband All-fiber Waveplates

Harsh M. Sanghvi

Thesis submitted to the faculty of the Virginia Polytechnic Institute and State University in partial fulfillment of the requirements for the degree of

Master of Science
In
Electrical Engineering

Rogers Stolen, Chair
Ira Jacobs
Ahmad Saafai-Jazi

April 27, 2004
Blacksburg, VA

Keywords: waveplates, optical fibers, polarization, birefringence, PM fibers

Characterization of Wideband All-fiber Waveplates

Harsh M. Sanghvi

Abstract

Many commercial and laboratory applications of fiber optics require an ability to manipulate, change and control the state of polarization of light. This is usually accomplished with bulk-optic wave plates which are inherently narrowband, bulky, and often require careful manual tuning and adjustments. H.C. Huang has recently proposed that a variably spun birefringent fiber with spin rate slowly varying from zero to very fast (or vice versa) will transform the state of polarization (SOP) from linear to circular (and vice versa). The most remarkable feature of a Huang fiber is that the transformation from linear to circular polarization is independent of wavelength over entire single mode range of the fiber.

In this thesis, using simulations and experiments we explore the properties of such a fiber element and investigate its similarities and differences as compared to a bulk-optic quarter-wave plate. In the simulations, we modeled the Huang fiber as a stack of birefringent waveplates and used this model verify the theoretically predicted polarization transformation behavior and the wideband nature of the Huang fiber. We analyzed the dependence of the polarization transformation by this device on various structural parameters and showed that while the fiber has loose tolerances with respect to the fiber length and the spin variation, it has a strong dependence on the maximum spin rate at the high-spun end. We investigated the PMD characteristics of the Huang fiber for short pulse applications. Using simulations we also verified that two such quarter wave-transforming fibers can be appropriately cascaded to obtain half-wave and full-wave transformation, analogous to bulk optics half wave and full wave plate respectively.

In the experiments we studied the polarization transformation behavior of a Huang fiber sample when it is excited by different input states of polarization both from the un-spun end and the high-spun end. We found that the results from the experiments strongly support the simulation results. The experiment was performed at 1310 nm and 1550 nm to verify the wideband nature of the Huang fiber sample. We found that the Huang fiber indeed performs the prescribed state of polarization transformation over a wide band.

Acknowledgements

I would like to thank my family for their continuous support and guidance that has made many of my achievements possible. I would like to thank my close friends Nitin Goel and Sudhanshu Mishra for their constant encouragement and critical remarks.

I would like to thank my advisor Dr. Rogers Stolen for many elucidating discussions that made this work possible. Finally, I would like to extend my sincere gratitude to Dr. H.C. Huang for providing the fiber sample used in experiments.

Table of Contents

Table of Figures

List of Tables

Introduction

Polarization is an important property of light, especially in the field of single mode fiber optics. The fundamental LP_{01} mode of optical fiber is two fold degenerate, in that a single mode fiber can be shown to support two orthogonally polarized LP_{01} modes [20]. In a hypothetical situation where an optical fiber with length invariant perfectly circular core/cladding geometry is laid perfectly straight without any external stresses or perturbations, two orthogonal polarization modes will have a same propagation constant and this fiber will behave as a truly single mode fiber. However such an idealized situation can hardly be achieved in practice due to manufacturing limitations and practical conditions. This causes the propagation constants of the two polarization modes to become non-degenerate. Practical single mode fibers support two polarization modes with propagation constants β_x and β_y. The difference between these propagation constants is called birefringence β. Two polarization modes beat along the fiber length and undergo all possible states of polarization while traveling distance $L_b = 2\pi/\beta$, called beatlength, along the fiber. In a standard single mode fiber the beat length varies along the fiber length, with time and with external surroundings of the fiber [6, 18]. Thus light coming out of a standard optical fiber has arbitrary state of polarization which varies with time.

Many fiber optics applications require specific state of polarization of light. For example: heterodyne detection scheme in coherent communications requires that light from the communication system and the light from the local oscillator have same state of polarization at the detector [19], Polarization based fiber optics sensors require accurate control over the SOP of light, Faraday effect based gyroscope needs circularly polarized input light [14]. Other applications require one to change the SOP of light for example in the case of coupling linearly polarized light from laser diode to a polarization maintaining fiber such that linearly polarized light is launched along one of the principal axes.

Bulk-optics waveplates can be used to change and control the state of polarization of light. However using bulk-optics waveplates require the light to be coupled out of and back in to the fiber using additional collimating optics. They also require continuous, manual adjustments and tuning. Another option that does not require collimating optics is LeFevre's in line fiber polarization controller which uses bend birefringence in an optical fiber to simulate retardation plates [9]. It has three fiber birefringent components; the first and the last are quarter-wave retarders while the second is a half-wave retarder. It can be shown that using this device any input SOP can be transformed to any output SOP. However it cannot maintain the output SOP over time and requires manual adjustments to the orientation of the fiber loops to restore the output SOP. Polarization controlling devices based on Faraday effect, Kerr effect and Pockels effect are commercially available but these devices tend to be very expensive [19]. In addition all the methods mentioned above have a disadvantage of being inherently narrowband. Consequently there is need for a polarization transforming device that performs prescribed SOP transformation over wide band, with minimum insertion loss and no manual tuning.

Recently H.C. Huang [1,2,3] has proposed that a variably spun birefringent fiber with spin rate slowly varying from zero-to-very fast will behave as a quarter wave transformer over a wide band. At first this proposition sounds strange and one suspects its veracity. It is known that spinning the preform during linear draw reduces the linear birefringence of the fiber [12]. The fiber drawn while spinning birefringent the preform will necessarily be less linearly birefringent. As mentioned earlier, the spin rate is slowly varied from zero to very fast. This implies that starting from purely linear birefringence at un-spun end, fiber becomes less and less linearly birefringent along its length and at the fast-spun end the linear birefringence will be minimum assuming sufficiently high spin rate at the fast-spun end. Thus at the fast-spun end, under the fast spun condition, the fiber can be approximated to be non-birefringent. The principal states of polarization for a linearly birefringent fiber are principal axes aligned linear polarizations [7, 11] and any state of polarization for a non-birefringent fiber say orthogonal circular polarization states.

From the above discussion one can try to explain the polarization transformation behavior of a Huang fiber by stating that there is a gradual evolution of the principal state of polarization from linear to circular polarization along the fiber. However this argument is not physically intuitive and skepticism remains. A detailed analysis of polarization transformation process in a Huang fiber by means of simulation and experiments is required to understand and establish its operation as a quarter waveplate. This is exactly the motivation for this work.

Thesis is organized in four chapters:

Chapter 1 discusses basic principles of polarization of light. We discuss different representations of SOP of light. We also briefly discuss the Jones matrix formalism and develop Jones matrix for a phase-shifter. This chapter provides an overview of concepts used in the later chapters.

Chapter 2 provides a detailed analytical framework for studying SOP transformation behavior of Huang plates. We discuss simulation model and present simulation results. We also study the dependence of the SOP transformation behavior on various structural parameters. We end by discussing the cascading of Huang plates to obtain half-wave and full-wave plate behavior.

In Chapter 3 we present the results of experiments that compliment the results from theory and simulations thereby establishing the operation of Huang plates as all-fiber wide band quarter waveplates.

Chapter 4 discusses conclusions and future work.

Chapter 1. Polarization of Light

In this chapter we will discuss some basic principles of polarization of light, different representations of states of polarization and Jones matrix formalism to study the propagation of states of polarization in optical devices. This chapter provides a quick overview of the concepts that will be extensively used in the next chapter while studying the polarization transformation behavior of Huang plates.

1.1 *Nature of light*

Light exhibits dual nature, particle nature and wave nature. Phenomena of absorption and emission of light can be best explained by treating light as packets of discrete amount (quanta) of energy and hence the particle nature. Properties of light such as interference, diffraction, reflection and polarization can be explained by treating light as electromagnetic fields propagating as waves through different media. Light can be thought of as a spatio-temporal field formed by coupling the electric field $\overline{\mathbf{E}}(r,t)$ and the magnetic field $\overline{\mathbf{H}}(r,t)$. Since $\overline{\mathbf{E}}(r,t)$ and $\overline{\mathbf{H}}(r,t)$ are both vectors (have magnitude and direction), the lightwave formed by coupling between them is necessarily also a vector [21]. Vector nature of light can be ignored and light can be treated as a scalar while solving the problems of diffraction, reflection, interference etc. However while treating the problem of polarization and the evolution of SOP during light transmission; it becomes necessary to treat light as a vector.

1.2 *Polarization of lightwaves*

Polarization of an optical wave is defined by how the direction of the vector associated with the electromagnetic field evolves temporally at a given point in space. If the evolution is same at every point in space the light is said to be polarized otherwise the light is said to be partially polarized or un-polarized.

Consider a monochromatic plane wave of angular frequency ω and of wave vector **k**, parallel to *z*-axis, propagating in an infinite, homogenous dielectric medium with no charges. At any point **Z(r)**, at any given time *t*, an electromagnetic field is also linked to this wave. Temporal evolution of this field at point **Z(r)** characterizes the polarization state of the wave. In optics electric field vector $\overline{\mathbf{E}}(r,t)$ is usually chosen to represent the electromagnetic field. In order to apply the theory to anisotropic media, electric induction vector $\overline{\mathbf{D}}(r,t)$, which is related to $\overline{\mathbf{E}}(r,t)$ as $\overline{\mathbf{D}}(r,t) = \bar{\varepsilon} \cdot \overline{\mathbf{E}}(r,t)$ is more commonly used [16]. In the case of homogenous plane waves in an infinite media, Maxwell's equation $\nabla \cdot \mathbf{D} = 0$ ensures that **D** and **k** vectors are perpendicular. If *z*-axis is along the propagation direction of the wave then we get $\mathbf{k} = k\hat{\mathbf{z}}$. Now the electric induction vector can be written as:

$$\mathbf{D}(z,t) = \mathbf{D}_0 \exp(-j(\omega t - kz)) \qquad 1.1$$

Where $k = nk_0 = n\omega/c$, *n*- is refractive index seen by the wave and $\mathbf{D_0}$ is a complex vector situated in the wave plane. $\mathbf{D_0}$ characterizes the state of polarization. In the Cartesian coordinate system with *z*-axis lying along the direction of the propagation and $\mathbf{D_0}$ lying in ***x-y*** plane we can decompose $\mathbf{D_0}$ as:

$$\mathbf{D}_0 = A_x e^{j\phi_x}\hat{\mathbf{x}} + A_y e^{j\phi_y}\hat{\mathbf{y}} \qquad 1.2$$

In the above equation A_x and A_y are real positive constants, ϕ_x and ϕ_y are modulo-2π phases. Considering the real part of Eq. (1.1) we get:

$$\begin{aligned} D_x(z,t) &= A_x \cos(\omega t - kz - \phi_x) \\ D_y(z,t) &= A_y \cos(\omega t - kz - \phi_y) \end{aligned} \qquad 1.3$$

Temporal evolution of $\mathbf{D}(z,t)$ vector describes the state of polarization of the optical wave and the complex vector, $\mathbf{D}_0$ fully describes this state. If a point **P** is associated with the tip of $\mathbf{D}(z,t)$ vector, it will usually describe an ellipse set in the wave plane. Such an

ellipse is called Lissajous ellipse (composition of two orthogonal vibrations of same frequency, different phase shifted amplitudes) see Figure 1-1. The most general state of polarization for a monochromatic plane wave in a homogenous medium is the state of elliptical polarization [17].

Putting $z = 0$ at origin, neglecting temporal terms in Eq. (1.3) and substituting $X = D_x$ and $Y = D_y$ we get:

$$\frac{X^2}{A_x^2} + \frac{Y^2}{A_y^2} - \frac{2XY\cos\phi}{A_x A_y} = \sin^2\phi \qquad 1.4$$

Where $\phi = \phi_x - \phi_y$ (modulo-2π) is the phase shift between orthogonal vibrations of $\mathbf{D}(z,t)$. In general the axes of the ellipse are not same as the reference axes ***x-y*** because of cross the term XY in Eq. (1.4). Also the ellipse is circumscribed by a rectangle of sides $2A_x$ and $2A_y$. Handedness of the ellipse is determined by the sign of phase shift ϕ. For *positive* ϕ point **P** rotates in an anticlockwise direction and the elliptically polarized light is said to be left-handed, for *negative* ϕ point **P** rotates in a clockwise direction and the elliptically polarized light is said to be right-handed. From Figure 1-1 axes of the ellipse can be readily determined by using a rotation matrix:

$$\mathbf{R}(\alpha) = \begin{bmatrix} \cos\alpha & \sin\alpha \\ -\sin\alpha & \cos\alpha \end{bmatrix} \quad \textit{thus}$$
$$\begin{bmatrix} X' \\ Y' \end{bmatrix} = \begin{bmatrix} \cos\alpha & \sin\alpha \\ -\sin\alpha & \cos\alpha \end{bmatrix} \begin{bmatrix} X \\ Y \end{bmatrix} \qquad 1.5$$

Also from Eq. (1.4) we can find the value of α as:

$$\tan 2\alpha = \frac{2A_x A_y}{A_x^2 - A_y^2}\cos\phi \qquad 1.6$$

In Figure 1-1 parameters α and ε characterize the orientation and the ellipticity of the polarization ellipse respectively.

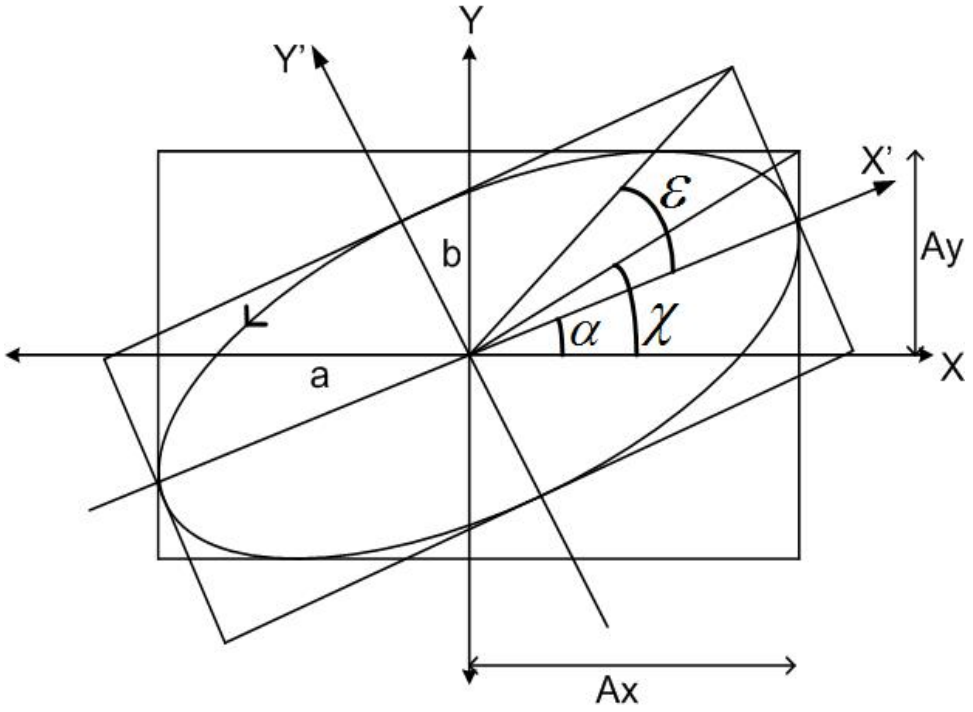

Figure 1-1 Lissajous polarization ellipse

From Eq. (1.4) it can be seen that relative values of the amplitudes A_x and A_y and the phase shift ϕ along with its sign determine the state of polarization of light. State of polarization will be linear if $\phi = 0$ *or* π. Eq. (1.4) becomes:

$$\left[\frac{X}{A_x} \pm \frac{Y}{A_y}\right]^2 = 0 \quad or$$
$$Y = \pm \frac{A_y}{A_x} X \qquad 1.7$$

The ellipse in Figure 1-1 becomes a line along one of the diagonals of the circumscribing rectangle.

If $\phi = \pm\pi/2$ the axes of the ellipse in Figure 1-1 get oriented along the reference coordinates axes. Now, if $A_x = A_y$ then the ellipse becomes a circle and we get a circularly polarized light. Eq. (1.4) becomes:

$$X^2 + Y^2 = A_x^2 \ (or A_y^2) \qquad 1.8$$

1.3 *Representations of States of polarization*

The representation for the SOP of light used in Eq. (1.3) is called trigonometric representation. Although it contains all the parameters to represent the SOP of light it is not mathematically convenient to handle. We therefore resort to different representations for the SOP of light that lend themselves to simpler mathematical manipulations. We will discuss the representations that we will use in next chapter.

Complex representation

If origin of phases is set at the phase of component of vibration in ***x***-direction, Eq. (1.2) can be rewritten as:

$$\mathbf{D}_0 = A_x \hat{\mathbf{x}} + A_y e^{j\phi} \hat{\mathbf{y}} \qquad 1.9$$

This is called complex representation for the SOP of light. Putting $\phi = 0$ in Eq. (1.9), we get a linearly polarized light oriented at an angle θ with respect to ***x***-axis as:

$$\mathbf{D}_0 = A\left[\cos\theta \ \hat{\mathbf{x}} + \sin\theta \ \hat{\mathbf{y}}\right] \qquad 1.10$$

Putting $\theta = 0 \ or \ \pi/2$ in Eq. (1.10), give the representations for ***x***-oriented and ***y***-oriented linearly polarized light respectively. The representation for circularly polarized light is obtained by putting $\phi = \pm\pi/2$ in Eq. (1.9) and we obtain:

$$\mathbf{D}_0 = A\left[\hat{\mathbf{x}} \pm j\hat{\mathbf{y}}\right] \qquad 1.11$$

Jones representation

R. C. Jones [5] introduced a matrix approach to solve the problems related to the polarization of light. In Jones representation the state of polarization is written as a two row vector called Jones vector:

$$\mathbf{A} = \begin{bmatrix} A_x e^{j\phi_x} \\ A_y e^{j\phi_y} \end{bmatrix} \qquad 1.12$$

It must be noted that multiplication of a Jones vector by any constant complex number does not alter the state of polarization of light and hence it is very convenient to work with normalized Jones vectors. In normalized Jones vectors sum of the squared amplitudes of two rows is equal to 1 i.e. $A_x^2 + A_y^2 = 1$

From Eq. (1.10) θ-oriented linearly polarized light can be represented by normalized Jones vector as:

$$A_{linear} = \begin{bmatrix} \cos\theta \\ \sin\theta \end{bmatrix} \qquad 1.13$$

From Eq. (1.11) circularly polarized light can be represented by normalized Jones vector as:

$$A_{circular} = \frac{1}{\sqrt{2}} \begin{bmatrix} 1 \\ \pm j \end{bmatrix} \qquad 1.14$$

From Figure 1-1 and the above discussion an elliptically polarized light can be represented by normalized Jones vector as:

$$A_{elliptical} = \begin{bmatrix} \cos\chi \\ \sin\chi \; e^{j\phi} \end{bmatrix} \qquad 1.15$$

Stokes parameters representation

Representations for the state of polarization of light discussed until now refer to the amplitudes of the lightwave components. In practice intensity is the quantity that can be directly measured. Therefore a representation of the SOP of light based on intensities would be practically more important [4]. Stokes parameter representation is such a representation. Let us consider Jones vector representation of a general SOP. Eq. (1.12) can be rewritten as:

$$\mathbf{A} = \begin{bmatrix} A_x \\ A_y e^{j\phi} \end{bmatrix} \qquad 1.16$$

Stokes parameters P_0, P_1, P_2 and P3 are defined as follows:

$$\begin{aligned} P_0 &= A_x^2 + A_y^2 \\ P_1 &= A_x^2 - A_y^2 \\ P_2 &= 2A_x A_y \cos\phi \\ P_3 &= 2A_x A_y \sin\phi \end{aligned} \qquad 1.17$$

It can be seen from Eq. (1.17) that:

$$P_1^2 + P_2^2 + P_3^2 = P_0^2 \qquad 1.18$$

Physically P_0 represents total intensity of an optical wave (I_0), P_1 represents the difference in the intensities of the linear components along ***x***-and ***y***-directions. Applying appropriate basis change to Eq. (1.16) we get:

$$A_{45^0} = \begin{bmatrix} A_x + A_y e^{j\phi} \\ A_x - A_y e^{j\phi} \end{bmatrix} \quad and \quad A_{circular} = \begin{bmatrix} A_x - jA_y e^{j\phi} \\ A_x + jA_y e^{j\phi} \end{bmatrix} \qquad 1.19$$

From Eq. (1.19) it can be shown that:

$$\begin{aligned} I_{+45} - I_{-45} &= 2A_x A_y \cos\phi = P_2 \\ I_{left\ \ circular} - I_{right\ \ circular} &= 2A_x A_y \sin\phi = P_3 \end{aligned} \qquad 1.20$$

Relationship of Stokes parameters to intensities can be summarized as:

$$\begin{aligned} P_0 &= I_x + I_y = I_0 \\ P_1 &= I_x - I_y \\ P_2 &= I_{+45^0} - I_{-45^0} \\ P_3 &= I_{left\ circular} - I_{righ\ circular} \end{aligned} \qquad 1.21$$

Thus by measuring the intensities I_0, I_x, I_y, I_{+45}, I_{-45}, $I_{left\ circular}$ and $I_{right\ circular}$ we can calculate Stokes parameters and thereby determine the SOP of light by direct intensity measurements. Standard Stokes parameters are given by:

$$\begin{aligned} S_0 &= P_0/P_0 = 1 \\ S_1 &= P_1/P_0 \\ S_2 &= P_2/P_0 \\ S_3 &= P_3/P_0 \end{aligned} \qquad 1.22$$

Standard Stokes parameters are collected in a vector **P** called stokes vector which describes the SOP of light. Table 1-1 lists standard Stokes vectors for some SOPs of light often encountered in practice.

SOP of light	**Standard Stokes Vector**
x-aligned linear	[1,1,0,0]
y-aligned linear	[1,-1,0,0]
$+45^0$- linear	[1,0,1,0]

-45^0- linear	[1,0,-1,0]
Right hand circular	[1,0,0,1]
Left hand circular	[1,0,0,-1]

Table 1-1 Standard Stokes vectors

Referring to Figure 1-1 we have:

$$\begin{aligned} \tan\chi &= \frac{A_y}{A_x} \\ \tan\varepsilon &= \frac{b}{a} \\ \tan 2\alpha &= \frac{2A_xA_y}{A_x^2 - A_y^2}\cos\phi \end{aligned} \qquad 1.23$$

Using relations of Eq. (1.23) in Eq. (1.17) and trigonometric manipulations it can be shown that:

$$\begin{aligned} S_1 &= \cos 2\varepsilon\cos 2\alpha = \cos 2\chi \\ S_2 &= \cos 2\varepsilon\sin 2\alpha = \sin 2\chi\cos\phi \\ S_3 &= \sin 2\varepsilon = \pm\sin 2\chi\sin 2\phi \end{aligned} \qquad 1.24$$

Poincairé sphere representation

If angles 2α and 2ε in Eq. (1.24) are considered as the polar angles of a spherical representation in a $S_1S_2S_3$ basis, the state of polarization with α-inclination and ε-ellipticity can be represented on surface of a unit sphere called Poincairé sphere [21]. See Figure 1-2.

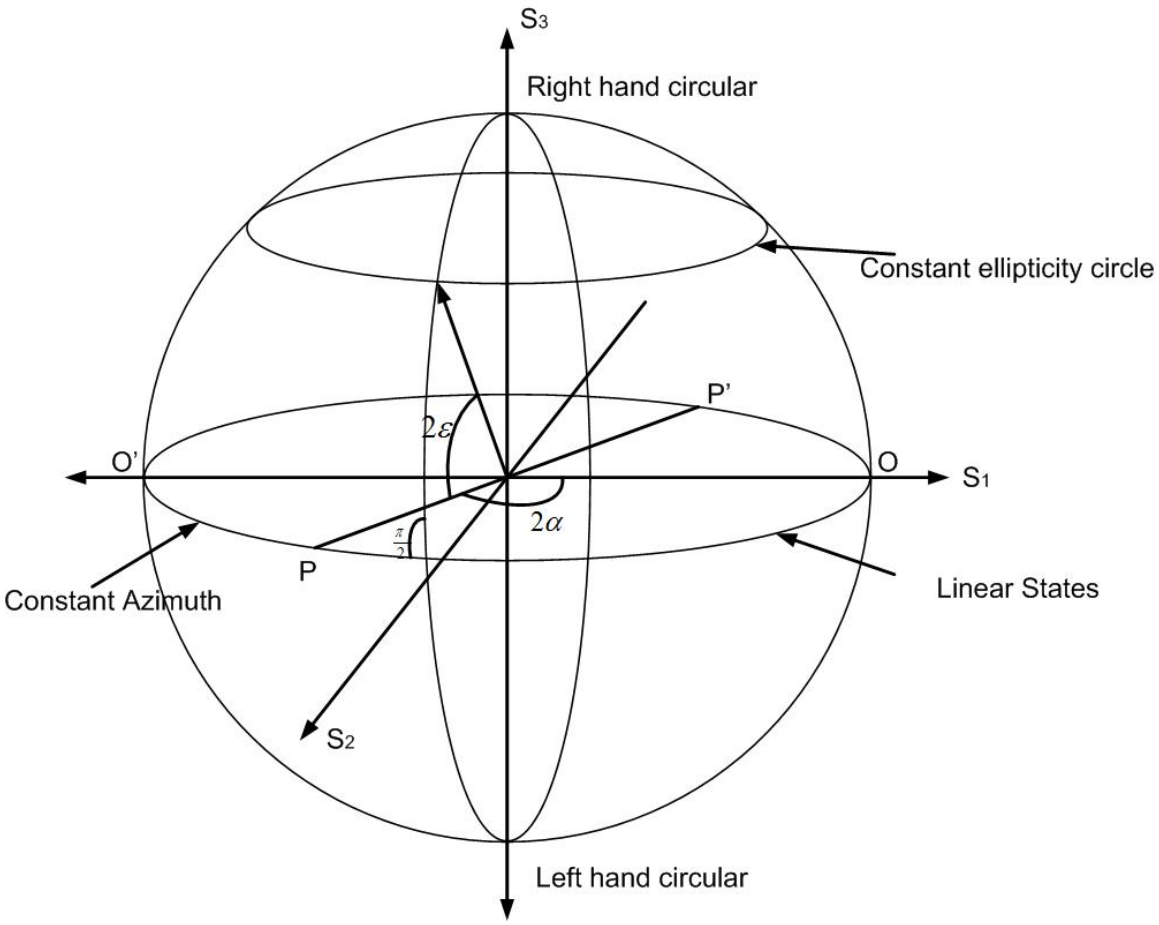

Figure 1-2 Poincairé sphere representation of SOP

On the Poincairé sphere equatorial circle is a locus of points ($\varepsilon = 0$) representing the linear states of polarization. The Points O and O' represent ***x***-and ***y***-aligned linear states of polarization respectively. Two orthogonal states are represented by the ends of a diameter of the sphere. In general each circle parallel to the equator represents the states of polarization having constant ellipticity. However the azimuth changes as we go around the circle. The poles represent a circularly polarized light with ellipticity ±1. The North Pole represents right circularly polarized light while the South Pole represents left circularly polarized light. Along a meridian on a Poincairé sphere the azimuth of an elliptical state of polarization remains constant while the ellipticity varies in the range [-1, 1]. Poincairé sphere is also a useful tool to treat the problems involving partially polarized light.

1.4 *Jones Matrices Formalism*

In this section we will present the Jones matrices formalism to study the propagation of a state of polarization in an optical device. Poole's [7] principal state model shows that for any elementary optical device there exist, two orthogonal polarization states ($\mathbf{A_1}$ and $\mathbf{A_2}$) that will propagate unaffected through the device such that their state of polarization will be preserved throughout the transmission. Such states of polarization are called principal states of polarization or eigen-states. Associated eigen-values λ_1 and λ_2 are descriptive of the phase retardation taken by the eigen-states during propagation through an optical device.

R.C. Jones [5] showed that any elementary optical device *viz* polarizer, retarder, rotator, etc., can be characterized by 2 x 2 linear matrix **M**. Using the properties of matrices it can be shown that the transmission of a state of polarization, through successive elementary optical devices, is reduced to a simple transformation of that state of polarization by a linear operator **M***. Where **M*** is a product of elementary linear operators **M** of successive optical devices taken in a reverse order.

Determination of Jones Matrices

If $\mathbf{A_1}$ and $\mathbf{A_2}$ are the eigen-states of an optical device in a chosen basis (say linear) and λ_1 and λ_2 are the associated eigen-values then it can be shown that:

$$\mathbf{A}_1 = \begin{bmatrix} u \\ v \end{bmatrix} \quad and \quad \mathbf{A}_2 = \begin{bmatrix} -v^* \\ u \end{bmatrix} \qquad 1.25$$

Here $\mathbf{A_1}$ and $\mathbf{A_2}$ are normalized Jones vectors. Jones matrix **M** of this optical element is a four-component 2 x 2 linear matrix:

$$\mathbf{M} = \begin{bmatrix} A & B \\ C & D \end{bmatrix} \qquad 1.26$$

From above discussions we know that **M** satisfies following equation:

$$\begin{aligned} \mathbf{M}\mathbf{A}_1 &= \lambda_1 \mathbf{A}_1 \\ \mathbf{M}\mathbf{A}_2 &= \lambda_2 \mathbf{A}_2 \end{aligned} \qquad 1.27$$

Eq. (1.27) can be solved to obtain elements of **M** as:

$$\mathbf{M} = \begin{bmatrix} \lambda_1 uu^* + \lambda_2 vv^* & (\lambda_1 - \lambda_2)uv^* \\ (\lambda_1 - \lambda_2)vu^* & \lambda_2 uu^* + \lambda_1 vv^* \end{bmatrix} \qquad 1.28$$

Thus the Jones matrix of an elementary optical component can be determined if its eigen-states and eigen-values are known in a given basis.

Jones matrix of a phase-shifter (waveplate)

Optical wave phase-shifters or wave plates are made of inherently birefringent materials such as crystal quartz, mica, etc. Consider a thin birefringent waveplate of thickness d having birefringence $\delta n = n_{ordinary} - n_{extra-ordinary}$. If this waveplate is illuminated by a monochromatic plane wave of wavelength λ then the phase difference ϕ picked up by the components of the plane wave traveling along the ordinary and the extra-ordinary axes is:

$$\phi = \frac{2\pi}{\lambda} \delta n \; d \qquad 1.29$$

Let the reference coordinate axes be oriented at an angle θ with respect to the internal birefringent axes of the waveplate as shown in Figure 1-3.

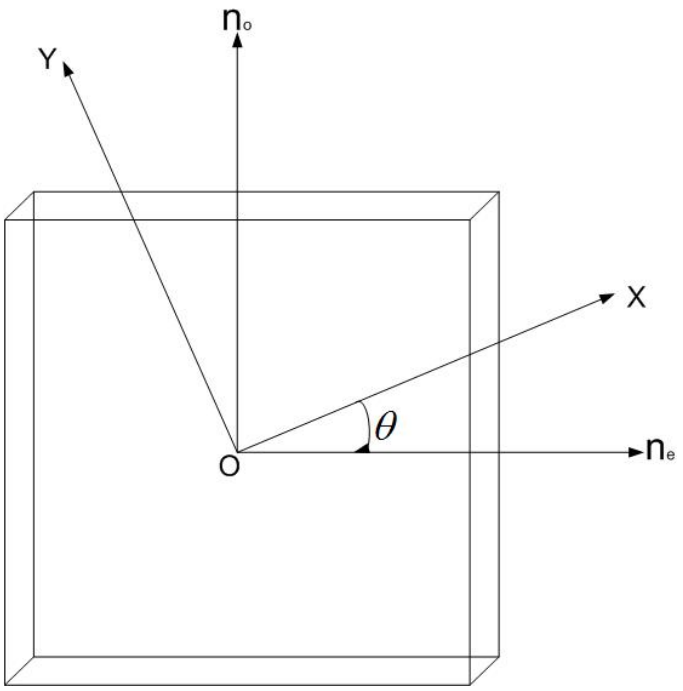

Figure 1-3 Linear Phase-shifter

The eigen-states of this waveplate are linear polarization states oriented along the internal birefringent axes. Hence in our basis (at angle θ with internal axes) they can be written in the normalized Jones vectors as follows:

$$\mathbf{A}_1 = \begin{bmatrix} \cos\theta \\ \sin\theta \end{bmatrix} \quad and \quad \mathbf{A}_2 = \begin{bmatrix} -\sin\theta \\ \cos\theta \end{bmatrix} \tag{1.30}$$

Associated eigen-values λ_1 and λ_2 are:

$$\begin{aligned} \lambda_1 &= e^{j\frac{\phi}{2}} \quad fast-\mathrm{mod}\,e \\ \lambda_1 &= e^{-j\frac{\phi}{2}} \quad slow-\mathrm{mod}\,e \end{aligned} \tag{1.31}$$

Putting Eq. (1.30) and Eq. (1.31) in Eq. (1.28) Jones matrix **M** for a phase-shifter can be obtained as:

$$\mathbf{M} = \begin{bmatrix} \cos^2\theta\, e^{j\frac{\phi}{2}} + \sin^2\theta\, e^{-j\frac{\phi}{2}} & \left(e^{j\frac{\phi}{2}} - e^{-j\frac{\phi}{2}}\right)\sin\theta\cos\theta \\ \left(e^{j\frac{\phi}{2}} - e^{-j\frac{\phi}{2}}\right)\sin\theta\cos\theta & \cos^2\theta\, e^{-j\frac{\phi}{2}} + \sin^2\theta\, e^{+j\frac{\phi}{2}} \end{bmatrix} \qquad 1.32$$

If the reference coordinate axes are oriented along the internal birefringent axes of the waveplate then putting $\theta = 0$ in Eq. (1.32), we have:

$$\mathbf{M} = \begin{bmatrix} e^{j\frac{\phi}{2}} & 0 \\ 0 & e^{-j\frac{\phi}{2}} \end{bmatrix} \qquad 1.33$$

For a quarter waveplate we have $\phi = \pi/2$, putting this value in Eq. (1.33), the Jones matrix for a quarter waveplate can be obtained as:

$$\mathbf{M} = \begin{bmatrix} e^{j\frac{\pi}{4}} & 0 \\ 0 & e^{-j\frac{\pi}{4}} \end{bmatrix} = e^{j\frac{\pi}{4}} \begin{bmatrix} 1 & 0 \\ 0 & -j \end{bmatrix} \qquad 1.34$$

If a θ-inclined linearly polarized light is incident on a quarter waveplate given by Eq. (1.34), the SOP of output light will be give by:

$$\begin{aligned} \mathbf{A}_{out} &= \mathbf{M}.\mathbf{A}_{in} \\ \mathbf{A}_{out} &= \begin{bmatrix} 1 & 0 \\ 0 & -j \end{bmatrix} \begin{bmatrix} \cos\theta \\ \sin\theta \end{bmatrix} \\ \mathbf{A}_{out} &= \begin{bmatrix} \cos\theta \\ -j\sin\theta \end{bmatrix} \end{aligned} \qquad 1.35$$

Figure 1-4 shows the SOP of the output light plotted on a Poincairé sphere when the orientation of input linear light, incident on the quarter waveplate, is varied from 0^0-to-350^0. As expected the SOP of the output light describes a meridian on the Poincairé

sphere indicating that output SOP has same azimuth but the ellipticity varies in the range [-1,1].

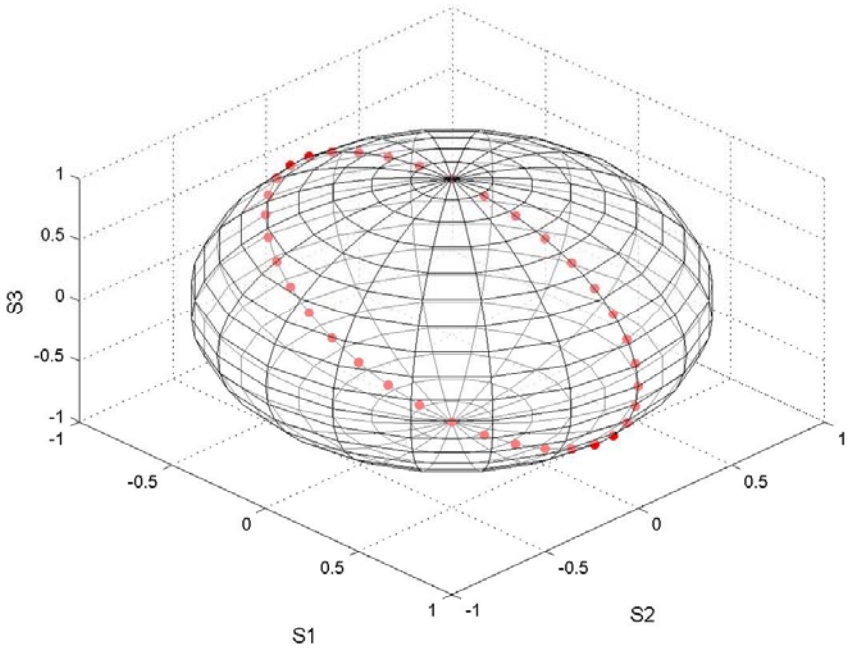

Figure 1-4 Output SOP when orientation of input linear light incident on quarter waveplate is varied from 0^0-to-350^0

Similarly behavior of half waveplates ($\phi = \pi$) and full waveplates ($\phi = 2\pi$) can be analyzed.

In this chapter we provided a quick overview of some basic concepts related to the polarization of optical lightwaves. Details can be obtained in any standard textbook on polarization. In the next chapter, we shall use these concepts to discuss the analysis of the polarization transformation behavior of all-fiber quarter waveplates.

Chapter 2. Wideband All-Fiber Waveplates

2.1 *Introduction*

In the previous chapter we described basic concepts of polarization of optical waves and various representations of state of polarization (SOP) of light. We also described analysis of propagation of states of polarization in optical devices using Jones matrix formulation. We developed Jones matrices for phase shifter (linear retarder) and observed evolution of output state of polarization on Poincairé sphere when linearly polarized light is incident on the input face of a quarter wave plate, at different angles with respect to internal birefringent axes.

In the present chapter we will use this background to analyze the polarization transformation behavior of wide-band all-fiber waveplates in general and all-fiber quarter waveplate in particular. This all-fiber wide-band quarter waveplate will be henceforth referred to as a Huang plate in recognition of principal inventor H.C. Huang [1, 2, 3]. We shall start by describing the structure of this novel device. Then we will present theoretical framework for analysis of polarization transformation behavior of the device based on solutions to coupled mode equations with variable coefficients, due to H.C. Huang. Analysis liberally uses concepts of Jones matrices and their algebraic manipulations described in the previous chapter. Solution gives us analytical expressions describing behavior of Huang plates. With simple straightforward logical approximation these expressions reduce to a very compact form that analytically predicts behavior of the device to different input states of polarization.

Expression derived from solution of coupled mode equations can be numerically simulated to understand the evolution of SOP along the length of the fiber. However, in the course of derivation and algebraic manipulations it is very easy to lose sight of the physical picture. Thus simulation of these equations does not provide any new insights in the behavior of the device and reduce to mere number crunching mechanism. Hence, we

develop simulations based on a simple and intuitive model consisting of a stack of birefringent waveplates. Such a model preserves the physical picture and provides more intuitive understanding of underlying principals. The fact that coupled mode equations, which are the starting point of theoretical analysis, are asymptotically derived from a model consisting of a stack of birefringent plates favors the choice of our simulation model. We will use analytical solution to predict behavior of Huang plate theoretically and then use our simulation model to verify this prediction numerically. Such an approach allows us to use elegantly compact analytical solutions while retaining a physical picture of the mechanism of operation of Huang plates. We will also show, by means of simulation, that Huang plates perform desired SOP transformation over wide range of wavelengths (over which fiber supports only LP_{01} mode).

In the following chapter we will present experimental results of SOP transformation by a Huang plate at 1310 nm and 1550 nm.

2.2 *Structure of Huang Plates*

In this section we will describe structure of the Huang plate which will be shown to work as an all-fiber wideband quarter wave plate. This polarization transforming device forms the basic element which can be cascaded in different fashion to obtain half waveplate or full waveplate behavior. Discussion of these concatenations will be postponed to the end of the chapter. Presently we will concentrate on Huang quarter waveplate.

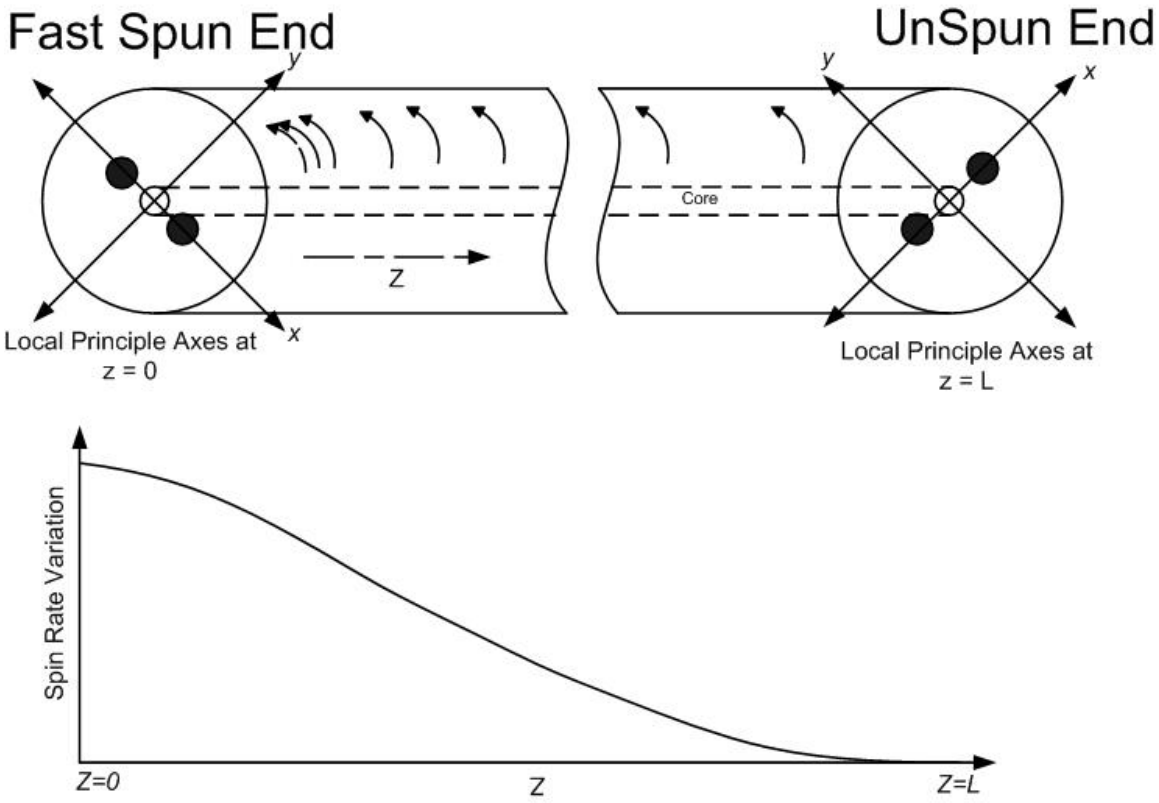

Structural Representation of Huang Quarter Wave Plate
(Adapted from Microwave Approach to Highly Irregular Fiber Optics, H. C. Huang, Wiley Series)

Figure 2-1 Structure of Huang Plate

Huang plate is a fiber element made by spinning a birefringent preform during a linear fiber draw with spin rate slowly varying from zero to very fast or conversely from very fast to zero. A schematic diagram is shown in Figure 2-1. In any kind of linearly birefringent fiber principal axes are defined by orientation of stress applying mechanism viz. stress applying rods. Fiber drawn by spinning a birefringent prefrom will have its principal axes rotating along the fiber length. Due to the varying spin rate say- from zero to very fast; axes along the fiber will equivalently rotate slowly initially and the rate of rotation slowly increases along the fiber length until there are several rotations per inherent un-spun fiber beat length towards the end of the fiber. The fiber structure has fairly loose tolerances with respect to length, spin rate variation and inherent birefringence of un-spun fiber. This is very favorable from manufacturing point of view. The fast spun requirement will be translated to a number during the course of analysis.

2.3 *Coupled mode analysis of Huang plates*

In this section we will present a theoretical analysis of Huang plates based on the coupled mode approach due to H. C. Huang [1,2,3]. We will start by specifying the choice of coordinates and base modes. After that, we will derive coupled mode equations for Huang plates in that, we will determine coupling coefficients for polarization modes. Next we will attempt to solve these coupled mode equations using appropriate substitutions and approximations. We will obtain general solutions and by applying appropriate initial conditions we will obtain particular solutions for given input SOP.

Coordinate system and base modes

Before attempting to derive the coupled mode equations it becomes necessary to specify the coordinate system (fixed or local) and base modes (linear or circular). Since the fiber under analysis is a spun fiber with spin rate varying along the fiber length, it is mathematically more convenient to use local coordinate system. In the local coordinate system the coordinate axes at any point **'z'** along the length of the fiber coincide with the principal axes at that point. In the case of a birefringent fiber the orientation of local principal axes is well defined [8]. Local principal axes of a Huang plate rotate along the fiber length with the rate of rotation slowly varying from zero to very fast. Hence, the coordinate axes also rotate at a variable rate as we go from un-spun end to high-spun end of the fiber. Assuming that at the un-spun end the local coordinate axes are same as the fixed coordinate axes, orientation of local axes at any point **'z'** along the fiber, with respect to fixed axes, will be given by:

$$\upsilon = \int_0^z \pm \tau(z) \cdot dz \qquad 2.1$$

Here $\tau(z)$ is spin-rate in radians/meter at point **'z'** along the fiber. Sign of $\pm\tau$ is to differentiate between clockwise or anti-clockwise spin. Local coordinates can be converted back to the fixed coordinate system by rotating the axes back by an amount $\mp\upsilon$; rotation matrix is given by:

$$\mathbf{R}(-\upsilon)=\begin{bmatrix}\cos(\upsilon) & -\sin(\upsilon)\\ \sin(\upsilon) & \cos(\upsilon)\end{bmatrix} \qquad 2.2$$

Choice of base modes (linear or circular) does not necessarily provide any advantage in selecting one or the other. We will use linear local base modes as they are typically easier to relate to in practice. Any SOP of optical light wave can thus be expressed in linear base modes as:

$$\mathbf{A}=\begin{bmatrix}\mathbf{A}_x e^{j\beta_x z}\\ \mathbf{A}_y e^{j\beta_y z}\end{bmatrix} \qquad 2.3$$

Where **'$\mathbf{A_x}$'** and **'$\mathbf{A_x}$'** are complex numbers and β_x and β_y are propagation constants of **'x'** and **'y'** components of the field in local coordinates.

Derivation of coupled mode equations

We follow the treatment proposed by McIntyre and Snyder [15] in which, a medium of infinite transverse dimensions can be expressed as a stack of plates. Wave fields in the next plate can be expressed in terms of the wave fields in the previous plate. Difference equations can be established by matching the wave fields at the interface between two adjacent plates. Desired coupled mode equations are obtained when thickness of the plates is allowed to go to zero.

The medium is modeled as a stack of birefringent plates with each plate having a thickness δz. Due to rotation, the birefringent axes of the next plate are oriented at an angle of $\delta\upsilon=\tau(z)\cdot\delta z$ with respect to those of the previous plate. Let z^- and z^+ be the coordinates of two adjacent plates 1 and 2 respectively. Linear modes in plates 1 and 2 can now be written as:

$$a_1(z^-) = \begin{bmatrix} a_x e^{-j\beta_x z^-} \\ a_y e^{-j\beta_y z^-} \end{bmatrix}$$
$$a_2(z^+) = \begin{bmatrix} (a_x + \delta a_x) e^{-j\beta_x z^+} \\ (a_y + \delta a_y) e^{-j\beta_y z^+} \end{bmatrix} \qquad 2.4$$

Here $a_x \equiv a_x(z^-), a_y \equiv a_y(z^-)$ and; $\delta a_x\ \delta a_y$ are incremental changes in the linear mode from z^- to z^+ in local coordinates. Since, axes of plate 2 are rotated by an amount $\delta\upsilon = \tau(z)\cdot\delta z$ with respect to axes of plate 1 and the fields should match at the interface in same coordinate system; we have:

$$a_2(z^+) = \mathbf{R}(\delta\upsilon) a_1(z^-) \qquad 2.5$$

Putting Eq. (2.4) and Eq. (2.2) in Eq. (2.5) and using relation $\tau(z)\cdot\delta z \approx 0$; since $\delta z \approx 0$; thus $\cos(\tau(z)\cdot\delta z) \approx 1$ and $\sin(\tau(z)\cdot\delta z) \approx \tau(z)\cdot\delta z$; also at the interface $z^- = z^+ = z$; we get:

$$\begin{aligned} \delta a_x e^{-j\beta_x z} &= a_y e^{-j\beta_y z}(\tau(z)\cdot\delta z) \\ \delta a_y e^{-j\beta_y z} &= -a_x e^{-j\beta_x z}(\tau(z)\cdot\delta z) \end{aligned} \qquad 2.6$$

Using substitutions:

$$\begin{aligned} \bar{a}_x &= a_x e^{-j\beta_x z} \\ \bar{a}_y &= a_y e^{-j\beta_y z} \end{aligned} \qquad 2.7$$

in Eq. (2.6) we get:

$$\begin{aligned} \frac{d\bar{a}_x}{dz} &= -j\beta_x \bar{a}_x + \tau(z)\bar{a}_y \\ \frac{d\bar{a}_y}{dz} &= -\tau(z)\bar{a}_x - j\beta_y \bar{a}_y \end{aligned} \qquad 2.8$$

Let $\delta\beta = \beta_y - \beta_x$ be the difference in propagation constants of **'x'** and **'y'** modes and $\beta = (\beta_x + \beta_y)/2$ be the average propagation constant of two modes. Extracting common phase factor $e^{-j\beta z}$ from $\bar{a}_x$ and $\bar{a}_y$, we get:

$$\begin{aligned} \bar{a}_x(z) &= A_x(z)\, e^{j\frac{\delta\beta}{2}z} \\ \bar{a}_y(z) &= A_y(z)\, e^{-j\frac{\delta\beta}{2}z} \qquad where: \\ A_x(z) &= a_x\, e^{-j\beta z} \qquad and \\ A_y(z) &= a_y\, e^{-j\beta z} \end{aligned} \tag{2.9}$$

Putting Eq. (2.9) in Eq. (2.8), we get:

$$\begin{aligned} \frac{dA_x}{dz} &= j\frac{\delta\beta}{2}A_x + \tau(z)\,A_y \\ \frac{dA_y}{dz} &= -\tau(z)\,A_x - j\frac{\delta\beta}{2}A_y \end{aligned} \tag{2.10}$$

Eq. (2.10), defined in local coordinates, is now in terms of two readily measurable quantities; $\delta\beta$ can be directly related to the beatlength of the un-spun fiber while $\tau(z)$ is rate at which the preform was spun while linear draw.

In Eq. (2.10) modes that are coupled by geometrical spinning of the axes are local modes defined in the local coordinate system. Coupling coefficient is exactly equal to the local spin rate; also we note that the coupling mechanism due to spinning does not modify the propagation constants of the local modes. Above derivation tacitly assumed plane wave propagation in an infinite transverse medium and the wave guiding effects, that would be present in an actual fiber, were ignored. However it has been shown in literature [15] that coupling coefficient, in spun fiber derived after taking wave guiding effect in to account, deviates little from $\tau(z)$ derived above.

In summary, the Huang plate, which is a spun fiber with the spin rate slowly varying from zero to very fast, is described by a set of coupled mode equations with variable

cross coupling coefficients $\tau(z)$; in local coordinates. Next we will attempt to solve Eq. (2.10).

Solution using method of diagonalization

In this section we will employ the method of diagonalization to solve Eq. (2.10). However, in order to facilitate a better understanding and ease of mathematics we will assume that spin rate is constant i.e. $\tau(z) = \tau$. In other words the fiber is spun at a uniform rate and not at a rate varying from zero to very fast. Using constant spin rate will illustrate the principal of method of diagonalization more clearly. Once we reach a point where we cannot go any further without considering the varying spin rate we will modify the equations to accommodate the variation in spin rate. Putting $\tau(z) = \tau$ in eq. (2.10) we have:

$$\begin{aligned} \frac{dA_x}{dz} &= j\frac{\delta\beta}{2}A_x + \tau A_y \\ \frac{dA_y}{dz} &= -\tau A_x - j\frac{\delta\beta}{2}A_y \end{aligned} \qquad 2.11$$

Eq. (2.11) is a set of coupled mode equations with constant coefficients in local coordinates, descriptive of a uniformly spun fiber element. Eq. (2.11) can be written in a matrix form as:

$$\begin{aligned} &\frac{d\mathbf{A}}{dz} = \mathbf{K}\mathbf{A} \qquad where: \\ &\mathbf{A} = \begin{bmatrix} A_x \\ A_y \end{bmatrix} \\ &\mathbf{K} = \begin{bmatrix} \frac{j\delta\beta}{2} & \tau \\ -\tau & -\frac{j\delta\beta}{2} \end{bmatrix} \end{aligned} \qquad 2.12$$

Here ***A*** is a column matrix whose elements are the linear modes that are coupled by geometrical spinning of axes and **K** is a square matrix whose elements are descriptive of the fiber structure regardless of the excitation conditions. Diagonal elements of **K** represent residual linear birefringence of the fiber and its off-diagonal elements represent the coupling coefficients between linear modes in local coordinates. The method of diagonalization is a mathematical technique by which, matrix **K** (representing the coupled difference equations) is transformed in to a diagonal matrix. In other words, new diagonal matrix will represent two independent difference equations which can be solved separately and in a straight forward manner. We introduce the following transformation:

$$\begin{aligned} &\mathbf{A} = \mathbf{O}\mathbf{W} \qquad or; \\ &\mathbf{W} = \mathbf{O}^{-1}\mathbf{A} \end{aligned} \tag{2.13}$$

Where, **O** is a diagonalizing matrix whose elements have to be determined and **W** is a column matrix whose elements are related to elements of **A** by inverse $\mathbf{O}^{-1}$ transformation as shown above. Elements of **W** are called normal modes. Normal modes will be explained more clearly later.

Putting Eq. (2.13) in Eq. (2.12), we get:

$$\begin{aligned} &\frac{d\mathbf{W}}{dz} = \Lambda\mathbf{W} \\ &\Lambda = \mathbf{O}^{-1}\mathbf{K}\mathbf{O} \end{aligned} \tag{2.14}$$

Now, if Λ as defined above becomes a diagonal matrix with its off-diagonal elements zero, equation $d\mathbf{W}/dz = \Lambda\mathbf{W}$ will represent two independent ordinary difference equations. This requirement implies that **O** cannot arbitrary and can be determined as follows.

$$\mathbf{K}\mathbf{O} = \mathbf{O}\Lambda \tag{2.15}$$

$$\begin{bmatrix} \frac{j\delta\beta}{2} & \tau \\ -\tau & -\frac{j\delta\beta}{2} \end{bmatrix} \begin{bmatrix} O_{11} & O_{12} \\ O_{21} & O_{22} \end{bmatrix} = \begin{bmatrix} O_{11} & O_{12} \\ O_{21} & O_{22} \end{bmatrix} \begin{bmatrix} \lambda_1 & 0 \\ 0 & \lambda_2 \end{bmatrix} \tag{2.16}$$

Using simple matrix multiplication and assuming non-zero values for elements of **O**, eigen values λ_1 and λ_2 can determined to be:

$$\lambda_1 = +j\left[\tau^2 + \left(\frac{\delta\beta}{2}\right)^2\right]^{1/2}$$
$$\lambda_2 = -j\left[\tau^2 + \left(\frac{\delta\beta}{2}\right)^2\right]^{1/2} \qquad 2.17$$

The diagonal matrix Λ is then given by:

$$\Lambda = \begin{bmatrix} jg & 0 \\ 0 & -jg \end{bmatrix}$$
$$g = \left[\tau^2 + \left(\frac{\delta\beta}{2}\right)^2\right]^{1/2} \qquad 2.18$$

Using the condition of normalization $\sqrt{|O_{11}|^2 + |O_{21}|^2} = 1$ and $\sqrt{|O_{12}|^2 + |O_{22}|^2} = 1$ (conservation of power); we can evaluate elements of **O** as:

$$O_{11} = O_{22} = \frac{\tau}{\sqrt{\tau^2 + \left(g - \frac{\delta\beta}{2}\right)^2}}$$
$$O_{12} = O_{21} = \frac{j\left(g - \frac{\delta\beta}{2}\right)}{\sqrt{\tau^2 + \left(g - \frac{\delta\beta}{2}\right)^2}} \qquad 2.19$$

Observing Eq. (2.19); if numerator of O_{11} and O_{21} are taken as the base and the leg of a right angle triangle then denominator will be the hypotenuse of this triangle and we have: $O_{11} = O_{22} = \cos\varphi$ and $O_{12} = O_{21} = j\sin\varphi$; so that, $\tan\varphi = \left[g - (\delta\beta/2)\right]/\tau$ or, $\tan(2\varphi) = \tau/(\delta\beta/2)$. Thus **O** can be written as:

$$\mathbf{O} = \begin{bmatrix} \cos\phi & j\sin\phi \\ j\sin\phi & \cos\phi \end{bmatrix}$$

$$\mathbf{O}^{-1} = \begin{bmatrix} \cos\phi & -j\sin\phi \\ -j\sin\phi & \cos\phi \end{bmatrix}$$

$$\varphi = \frac{1}{2}\tan^{-1}\left[\frac{\tau}{\delta\beta/2}\right] = \frac{1}{2}\tan^{-1}(2Q) \qquad 2.20$$

where

$$Q = \frac{\tau}{\delta\beta} = \frac{L_b}{L_s}$$

Here $L_b = 2\pi/\delta\beta$ is the beatlength of the un-spun fiber and $L_S = 2\pi/\tau$ is the spin pitch of the spun fiber. Putting Eq. (2.18) in Eq. (2.14), we get:

$$\frac{dW_1}{dz} = \lambda_1 W_1$$
$$\frac{dW_2}{dz} = \lambda_2 W_2 \qquad 2.21$$

Where λ_1 and λ_2 are defined in Eq. (2.17). Thus the solutions are:

$$W_1(z) = e^{jgz}\ W_1(0)$$
$$W_2(z) = e^{-jgz}\ W_2(0) \qquad 2.22$$

Modes W_1 and W_2 which were earlier called normal modes are exactly the eigen-functions of uniformly spun fiber element. Associated eigen-values are as given by Eq. (2.17). Eq. (2.22) can be written in matrix form as:

$$\mathbf{W}(z) = \widetilde{\Lambda}\,\mathbf{W}(0) \qquad \textit{where,}$$
$$\widetilde{\Lambda} = \begin{bmatrix} e^{jgz} & 0 \\ 0 & e^{-jgz} \end{bmatrix} \qquad 2.23$$

Here, $\widetilde{\Lambda}$ is a diagonal matrix whose diagonal elements are the eigen-functions. Solution can now be obtained for local modes **A** using transformation in Eq. (2.13). If we write the initial condition as:

$$\begin{aligned}
\mathbf{A}(0) &= \begin{bmatrix} A_x(0) \\ A_y(0) \end{bmatrix} \\
\mathbf{W}(0) &= \mathbf{O}^{-1}\mathbf{A}(0) \\
\mathbf{W}(z) &= \widetilde{\Lambda}\mathbf{W}(0) \\
\mathbf{A}(z) &= \mathbf{O}\mathbf{W}(z) \qquad \textit{thus}
\end{aligned} \qquad 2.24$$

$$\begin{aligned}
\mathbf{A}(z) &= \mathbf{O}\widetilde{\Lambda}\mathbf{O}^{-1}\mathbf{A}(0) \\
&= \mathbf{T}_l\mathbf{A}(0) \qquad \textit{where} \\
\mathbf{T}_l &= \mathbf{O}\widetilde{\Lambda}\mathbf{O}^{-1}
\end{aligned}$$

where $\mathbf{T_l}$ is the transfer matrix of uniformly spun fiber in local co-ordinates. This matrix connects SOP of the output light **A** (z) to that of the input light **A** (0) such that when the input SOP is given, SOP of the output light can be readily determined using single matrix operation.

In summary, the method of diagonalization was illustrated for simplified case of a uniformly spun fiber element which is described by a set of coupled mode equations with constant coupling coefficients. In that, with the help of transformation Eq. (2.13), the original simultaneous (coupled) differential equations for **A** were transformed into independent (un-coupled) differential equations for **W**. The ordinary differential equations for **W** are readily solvable and the solution is in exponential form given by Eq. (2.23). These solutions can be readily converted back to the solutions for local modes **A** by using the inverse transformation in Eq. (2.13). In the above process matrix **O** is a diagonalizing matrix which transforms matrix **K** (non-zero off-diagonal elements) to a diagonal matrix Λ.

The elements of matrix **W** are called the '*normal modes*' and it was shown that they are exact eigen-functions. However, these modes obtained by transformation of **A** are

defined in the '*normal coordinates*'. Normal coordinates are different from the local coordinates, in which modes of **A** are defined, due to transformation of Eq. (2.13). These normal coordinates do not have a physical significance, in that it is not possible to determine the orientation of normal coordinates in laboratory. The concept of normal modes is a mathematical abstraction that is employed to simplify the analysis. Thus they must be treated only as matrix elements that are related to local modes by transformation Eq. (2.13).

We have now introduced basic concepts of the method of diagonalization and terminology involved therein. At this point we will go back to Eq. (2.11) and re-substitute $\tau = \tau(z)$. In other words we will consider variation in the spin rate along the fiber length. In the following section we shall see how and where the analysis presented above must be altered to accommodate the variation of spin rate in Huang plates. We shall find the concepts for the uniformly spun fiber given in this section very helpful in visualizing and solving this seemingly difficult problem.

Extension of Method of Diagonalization for Huang plates

A Huang fiber is a variably spun birefringent fiber element with the spin rate slowly varying from zero to very fast. Such a variably spun fiber element was shown to be described by a set of coupled mode equations with variable cross-coupling coefficients (proportional to the local spin rate $\tau(z)$), in local coordinates. We repeat Eq. (2.10):

$$\begin{aligned} \frac{dA_x}{dz} &= j\frac{\delta\beta}{2}A_x + \tau(z)A_y \\ \frac{dA_y}{dz} &= -\tau(z)\,A_x - j\frac{\delta\beta}{2}A_y \end{aligned} \qquad 2.25$$

This can be rewritten in matrix form as:

$$\frac{d\mathbf{A}}{dz} = \mathbf{K}(z)\ \mathbf{A}$$
$$\mathbf{K}(z) = \begin{bmatrix} j\frac{\delta\beta}{2} & \tau(z) \\ -\tau(z) & -j\frac{\delta\beta}{2} \end{bmatrix} \qquad 2.26$$

Here $\tau(z)$ and hence $\mathbf{K}(z)$ are functions of 'z'.

In the previous section, we solved for local modes **A** from normal modes **W** and we used transformation **A=OW**. For the case of a uniformly spun fiber element the diagonalizing matrix **O** has constant elements given by Eq. (2.20) because spin rate τ was a constant. Since in Huang plates spin rate is a function of distance $\tau(z)$ if we want to use the same transformation above the diagonalizing matrix no longer remains a constant but becomes a function of distance 'z'. Mathematically:

$$\mathbf{A} = \mathbf{O}(z)\ \mathbf{W}$$
$$\mathbf{O}(z) = \begin{bmatrix} \cos\varphi & j\sin\varphi \\ j\sin\varphi & \cos\varphi \end{bmatrix}$$
$$\varphi \equiv \varphi(z) = \frac{1}{2}\tan^{-1}\left[2Q(z)\right] \qquad 2.27$$
$$Q(z) = \frac{\tau(z)}{\delta\beta} = \frac{L_b}{L_s(z)}$$

Putting the transformation of Eq. (2.27) in Eq. (2.26) we have:

$$\frac{d[\mathbf{O}(z)\mathbf{W}]}{dz} = \mathbf{K}(z)\mathbf{O}(z)\mathbf{W}$$

$$\mathbf{O}(z)\frac{d\mathbf{W}}{dz} + \frac{d\mathbf{O}(z)}{dz}\mathbf{W} = \mathbf{K}(z)\mathbf{O}(z)\mathbf{W}$$

$$\mathbf{O}(z)\frac{d\mathbf{W}}{dz} = \mathbf{K}(z)\mathbf{O}(z)\mathbf{W} - \frac{d\mathbf{O}(z)}{dz}\mathbf{W}$$

Hence

$$\frac{d\mathbf{W}}{dz} = \mathbf{O}^{-1}(z)\mathbf{K}(z)\mathbf{O}(z)\mathbf{W} - \mathbf{O}^{-1}(z)\frac{d\mathbf{O}(z)}{dz}\mathbf{W}$$

$$\frac{d\mathbf{W}}{dz} = \left[\mathbf{O}^{-1}(z)\mathbf{K}(z)\mathbf{O}(z) - \mathbf{O}^{-1}(z)\frac{d\mathbf{O}(z)}{dz}\right]\mathbf{W}$$

$$\frac{d\mathbf{W}}{dz} = \mathbf{N}(z)\mathbf{W} \qquad 2.28$$

$$\mathbf{N}(z) = \mathbf{O}^{-1}(z)\mathbf{K}(z)\mathbf{O}(z) - \mathbf{O}^{-1}(z)\frac{d\mathbf{O}(z)}{dz}$$

Comparing Eq. (2.28) to Eq. (2.14) we note a distinctive difference between Λ of Eq. (2.14) and $\mathbf{N}(z)$ of Eq. (2.28). While $\Lambda = \mathbf{O}^{-1}\mathbf{K}\mathbf{O}$ for the case of a uniformly spun fiber is exactly diagonalized, matrix $\mathbf{N}(z)$ for the case of a Huang plate is not diagonal. This is because $\mathbf{N}(z)$ has an extra derivative term. Thus, for the case of a Huang plate W_1 and W_2 do not satisfy independent differential equations separately. They still remain coupled by the term $\mathbf{O}^{-1}(z)[d\mathbf{O}(z)/dz]$. However this term is very small, if the variation in the spin rate is very small, compared to the first term $\mathbf{O}^{-1}(z)\mathbf{K}(z)\mathbf{O}(z)$.

W_1 and W_2 for the case of Huang plate remain weakly coupled through the derivative term in $\mathbf{N}(z)$ and are not the eigen-modes. However for the case of slowly varying spin rate the coupling is very weak and they behave almost like eigen-modes, hence they are called quasi-eigen-modes or super-modes. In event that $d\tau/dz \to 0$, the coupling term

between W_1 and W_2 vanishes and they become eigen-modes (this is the case of uniformly spun fiber).

Referring to expression for $\mathbf{N}(z)$ in Eq. (2.28) it has been shown [22] that:

$$\mathbf{N}(z) = \begin{bmatrix} jg & -j\dfrac{d\varphi}{dz} \\ -j\dfrac{d\varphi}{dz} & -jg \end{bmatrix}$$
$$g \equiv g(z) = \pi(1+4Q^2)^{1/2},\ Q \equiv Q(z) \qquad 2.29$$
$$\frac{d\varphi}{dz} = (1+4Q^2)^{-1}\left(\frac{dQ}{dz}\right)$$
$$= \frac{1}{2\pi}(1+4Q^2)^{-1}\left(\frac{d\tau}{dz}\right)$$

Assuming slowly varying spin rate over the entire length of the fiber approximate solution for Eq. (2.26) can be derived by iterative process. The zeroth-order approximation is given by:

$$W_1(z) \approx W_1(0)\ e^{\,j\int_0^z g\ dz}$$
$$W_2(z) \approx W_2(0)\ e^{\,-j\int_0^z g\ dz} \qquad 2.30$$

where $W_{1,2}(0) = W_{1,2}(z)\big|_{z=0}$. The first order iterative solution is given by:

$$W_1(z) \approx e^{j\rho}\left\{W_1(0) - W_1(0)\int_0^z \frac{d\varphi}{dz}e^{-2j\rho}\left(\int_0^z \frac{d\varphi}{dz}e^{2j\rho}dz\right)dz - jW_2(0)\int_0^z \frac{d\varphi}{dz}e^{-2j\rho}dz\right\}$$
$$W_2(z) \approx e^{-j\rho}\left\{W_2(0) - W_2(0)\int_0^z \frac{d\varphi}{dz}e^{2j\rho}\left(\int_0^z \frac{d\varphi}{dz}e^{-2j\rho}dz\right)dz - jW_1(0)\int_0^z \frac{d\varphi}{dz}e^{2j\rho}dz\right\} \qquad 2.31.$$

In the above equation:

$$\varphi \equiv \varphi(z) = \frac{1}{2}\tan^{-1}(2Q)$$
$$Q \equiv Q(z) = \frac{\tau(z)}{\delta\beta} \qquad 2.32$$
$$\rho \equiv \rho(z) = \int_0^z g\ dz = \int_0^z \pi(1+4Q^2)^{1/2}\ dz$$

From $W_1(z)$ and $W_2(z)$ obtained above the local modes $A_1(z)$ and $A_2(z)$ can be readily obtained using the transformation $\mathbf{A}(z) = \mathbf{O}(z)\mathbf{W}(z)$. Also the excitation condition (SOP at the input) which is given in terms of local modes $\mathbf{A}(0)$, can be readily converted to initial values for $\mathbf{W}(0)$ using the same transformation.

Solutions for end-to-end SOP evolution

In the previous section the solutions to variably coupled mode equations (descriptive of Huang plate structure) were derived. Given the fiber structure parameters beatlength L_b, spin rate $\tau(z)$, fiber length L and initial SOP, we can compute the SOP of the light at any point along the fiber. However in most practical applications, we only require to know the end-to-end SOP transformation of the device. The analytical equations can be simplified to a great extent if we desire to find only the SOP of the light at the output of the fiber for given input SOP.

The spin rate at the un-spun end is zero ($\tau(0) = 0$). From Eq. (2.27), $\varphi = 0$ and $\mathbf{O}(0) \equiv \mathbf{O}_0$ becomes:

$$\mathbf{O}_0 = \mathbf{O}_0^{-1} = \begin{bmatrix} 1 & 0 \\ 0 & 1 \end{bmatrix} \qquad 2.33$$

The spin rate at the fast spun end is very high ($\tau(L) >> \delta\beta$). From Eq. (2.27), $\varphi = \pi/4$ and $\mathbf{O}(L) \equiv \mathbf{O}_F$ becomes:

$$\mathbf{O}_F \rightarrow \frac{1}{\sqrt{2}}\begin{bmatrix} 1 & j \\ j & 1 \end{bmatrix}$$
$$\mathbf{O}_F^{-1} \rightarrow \frac{1}{\sqrt{2}}\begin{bmatrix} 1 & -j \\ -j & 1 \end{bmatrix} \qquad 2.34$$

With slowly varying spin rate along the entire length of the fiber the zeroth-order solution for **W** given in Eq. (2.30) is suitable. This essentially means that the off-diagonal terms of $\mathbf{N}(z)$ are negligibly small for slowly varying spin rate. Eq. (2.30) can now be rewritten in matrix form as:

$$\mathbf{W}(L) \rightarrow \tilde{\Lambda}\mathbf{W}(0)$$
$$\tilde{\Lambda} = \begin{bmatrix} e^{j\rho} & 0 \\ 0 & e^{-j\rho} \end{bmatrix} \qquad 2.35$$

$$\rho \equiv \rho(L) = \int_0^L g \; dz$$
$$= \int_0^L \pi \left[1 + 4\left(L_b / L_S\right)^2\right]^{1/2} \; dz \qquad 2.36$$

Parameter ρ is an important parameter descriptive of the fiber structure and is called '*global structural parameter*'. Putting Eq. (2.27) in Eq. (2.35) and using Eq. (2.33), Eq. (2.34); the solution for end to end SOP transformation in Huang plate can be found. For input at un-spun end the solution is:

$$\mathbf{A}(L) = \mathbf{T}_l \mathbf{A}(0)$$
$$\mathbf{T}_l = \mathbf{O}_F \tilde{\Lambda} \mathbf{O}_0^{-1} \qquad 2.37$$

For input at high spun end the solution is:

$$\mathbf{A}(L) = \mathbf{T}_l \mathbf{A}(0)$$
$$\mathbf{T}_l = \mathbf{O}_0 \tilde{\Lambda} \mathbf{O}_F^{-1} \qquad 2.38$$

These equations will be extensively used in later sections to analyze polarization transformation behavior of Huang plates.

In summary we have presented analytical solution for SOP transformation characteristics of Huang plates. In the following section we will discuss our simulation model. Next, we shall employ the analytical solutions, developed in this section, to predict the output SOP for different input SOP and use simulation as a tool to verify (and validate) these predictions.

2.4 *Simulation model*

In this section we will discuss the simulation model used to simulate the behavior of Huang plates when it is excited by different SOP from both the high-spun and the un-spun end. It is possible to simulate Eq. (2.30) or Eq. (2.31) and use appropriate formulae to determine the SOP evolution along the fiber. However, these equations are for super-modes (section 2.3). The super-modes **W** are defined in the normal coordinates. The normal coordinates were discussed to have no geometrical meaning. In other words, modes **W** were required to simplify the analysis and can be considered to be a set of numbers that are related to the local modes **A** defined in the local coordinates by transformation Eq. (2.27). In the course of the derivation and involved mathematical manipulations it is very easy to lose the view of the physical picture of the SOP transformation process. With this viewpoint in mind we go back to the starting point of the analysis where (section 2.3) the spun fiber was modeled by a stack of birefringent plates.

We modeled Huang plate as a stack of birefringent plates (Figure 2-2 Simulation Model) where, each plate is rotated with respect to the previous plate in the stack and the amount of rotation slowly increases along the length of the fiber. We used the linear base modes. The calculations were performed in the local coordinates however the SOP at each point along the fiber will be shown in both the local coordinates and the fixed

laboratory coordinates. We also computed the Stokes parameters for the SOP of the light at each point along the fiber and plotted the SOP evolution on a Poincairé sphere.

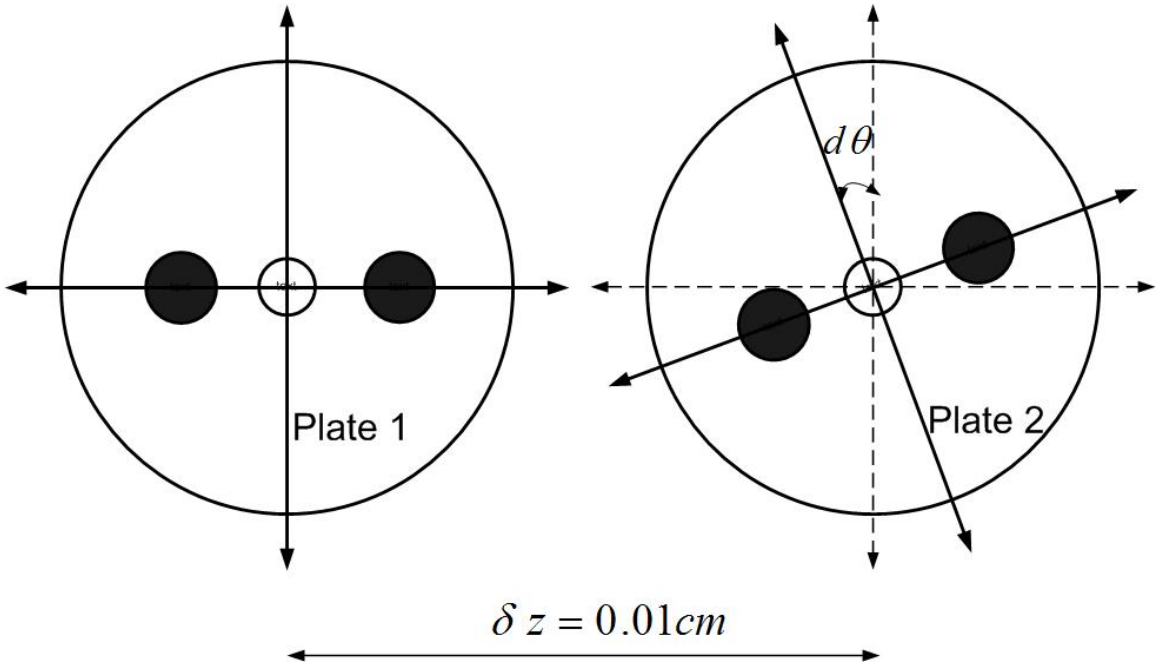

Figure 2-2 Simulation Model

Simulation parameters

Wavelength of operation

The SOP transformation of Huang plates was simulated over a wide wavelength range 1μm –to- 2μm to verify its wide-band nature. For verification of other SOP transformation properties the simulation was performed at 1μm.

Beat-length and propagation constant difference ($\delta\beta$)

The un-spun fiber beatlength was chosen to be 2 *cm* at $1\mu m$. Using $\delta n = \lambda / L_b$ we get a δn=0.00005 at $1\mu m$. The difference in propagation constant of two modes can be calculated using $\delta\beta = (2\pi/\lambda)\cdot\delta n$. Here $\delta\beta = 100\pi\ rad/m$ at $1\mu m$.

Fiber Length (L), step size (δz) and number of iterations

The fiber length was chosen to be $1m$. The step size of 0.01 cm was used. Hence, the number of iterations is $(L/\delta z) = 10000$. Simulation was performed for different fiber lengths keeping the step size constant. Step size of 0.01 cm means there are (2/0.01=) 200 birefringent plates within one un-spun beatlength of the fiber. High number of birefringent plates per beat length ensures that the model remains adiabatic.

Spin rate ($\tau(z)$)

From section 2.2, we know that Huang plate is a variably spun fiber element with the spin rate slowly varying from zero to very fast. These three conditions: 1. zero spun at one end, 2. very high spin rate at the other end and 3. Slow variation of spin rate from one end to other; are the most important structural parameters of Huang plates and exclusively determine its behavior.

We modeled the spin rate using the following equation:

$$
\begin{aligned}
Q(z) &= Q_{\max}\left[\frac{1}{2} \pm \frac{1}{2}\cos(\pi \frac{z}{L})\right]^{\gamma} \\
Q(z) &= \frac{\tau(z)}{\delta\beta} \\
\tau(z) &= Q(z)\cdot\delta\beta
\end{aligned}
\qquad 2.39
$$

Here γ determines the location of the maximum slope along the fiber. A value of $\gamma = 1$ was used in general. It was found that the γ value does not have a much impact on final results. The '+' sign in Eq. (2.39) implies input from high spun end and '-' implies input from the un-spun end. The parameter $Q_{\max}$ determines the maximum spin rate. The larger the value of $Q_{\max}$ the better but from point of view of manufacturing limitations we have

to limit its value to a reasonable number. The value used in our simulations was $Q_{\max} = 50$. The practical limitation of $Q_{\max}$ will be addressed later.

The angle between the principal axes of two adjacent plates can be determined as:

$$d\theta = \tau(z) \cdot \delta z \qquad 2.40$$

Figure 2-3 shows $d\theta$ in radians when the input is un-spun end ('-' sign in Eq. (2.39)). Figure 2-4 shows $d\theta$ in radians when the input is high-spun end ('+' sign in Eq. (2.39)). Figure 2-5 shows that the slowly varying spin rate condition is satisfied by Eq. (2.39), the maximum variation being ~2.5 x 10^{-4} radians/m.

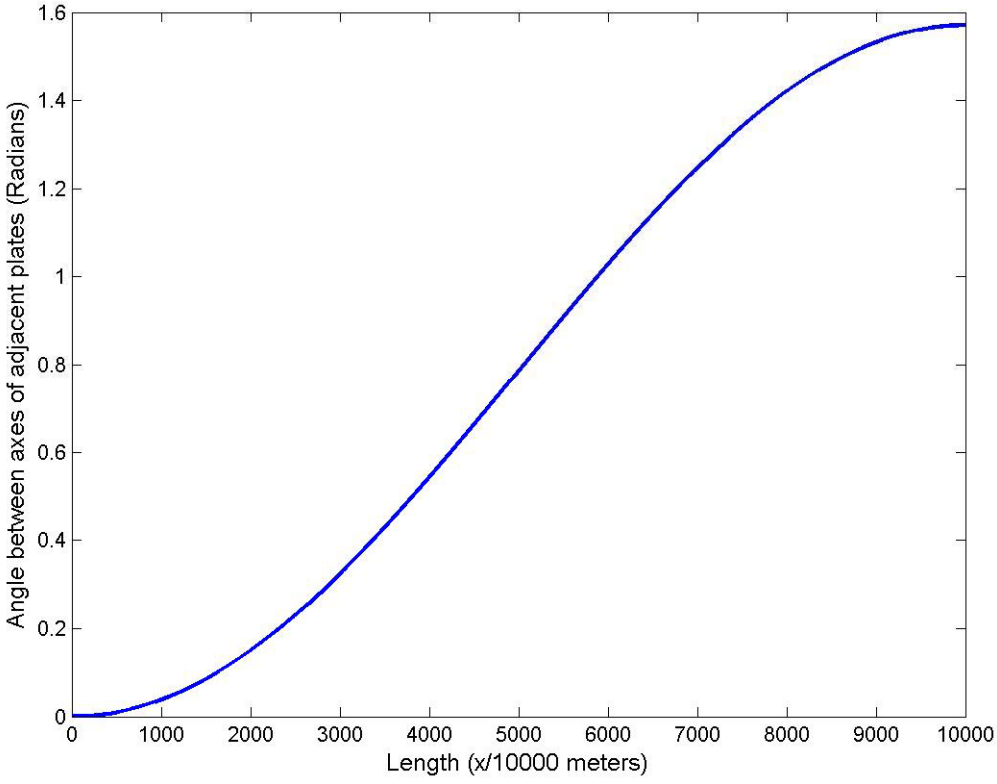

Figure 2-3 Angular rotation between axes of adjacent birefringent plates (Input Un-spun end)

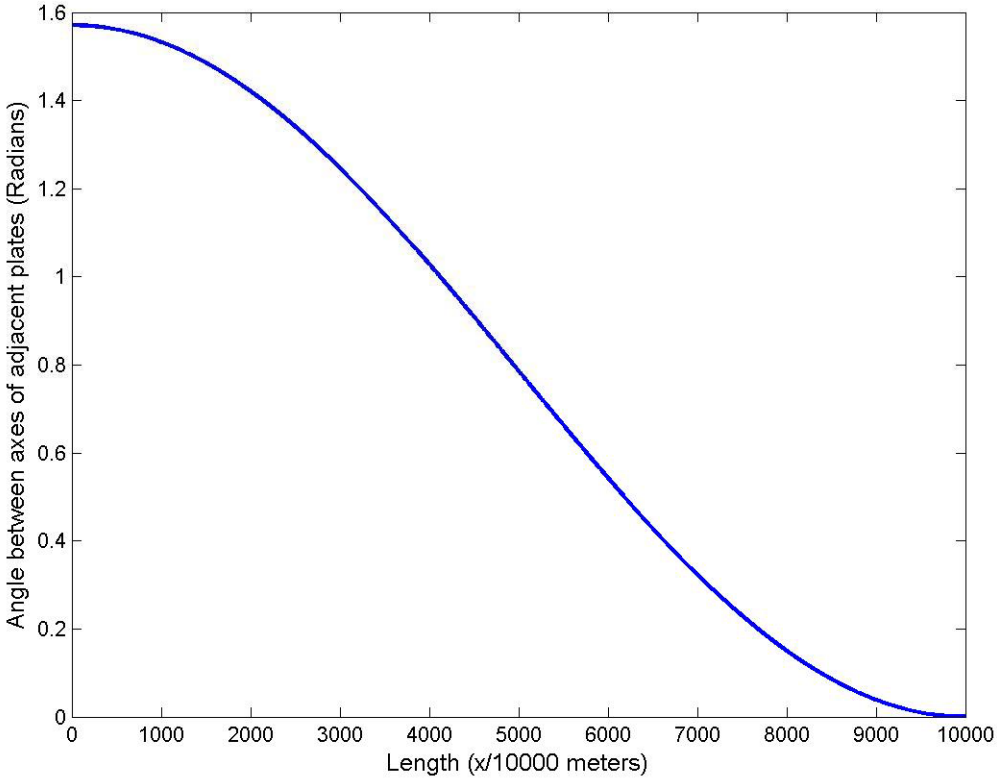

Figure 2-4 Angular rotation between axes of adjacent birefringent plates (Input high-spun end)

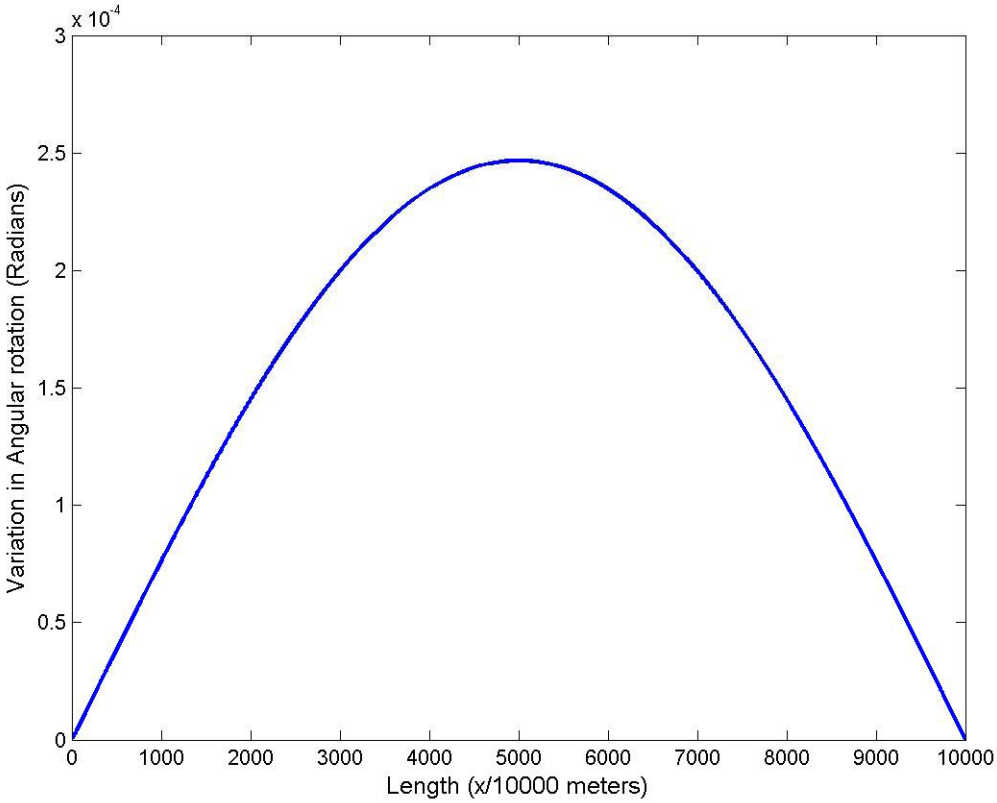

Figure 2-5 Slow spin rate variation

If we increase the value of $Q_{\max}$ we must correspondingly decrease the value of the step-size (δz) used in order to keep the model adiabatic or physically correct. It can be shown that for a given step size δz the maximum value for $Q_{\max}$ should be such that the corresponding maximum value of $d\theta \leq \pi/2$. This is an important point that should be kept in mind to avoid misinterpretation of simulations results.

Simulation algorithm

The simplicity of our simulation model will be evident in this section. The simulation algorithm has two simple matrix multiplications that are repeatedly performed for each birefringent plate. The SOP of light is expressed as a Jones vector as in Eq. (2.3). Consider plate 'n' in the stack of birefringent waveplates. Light at the output of this waveplate can be written as:

$$\mathbf{A}_n^+ = \begin{bmatrix} A_{x_n} \\ A_{y_n} \end{bmatrix} \qquad 2.41$$

Where, '+' superscript indicates output of plate 'n', A_{x_n} and A_{y_n} are complex numbers and are defined in the local coordinates $[x_n,y_n]$ at output of plate 'n'. The local axes of the next plate 'n+1' are expressed in the local coordinates $[x_{n+1},y_{n+1}]$ and they make an angle $d\theta(n+1)$ with the axes of plate 'n'. Rotating A_n^+ by an angle $d\theta(n+1)$, we get:

$$A_{n+1}^- = \begin{bmatrix} \cos[d\theta(n+1)] & \sin[d\theta(n+1)] \\ -\sin[d\theta(n+1)] & \cos[d\theta(n+1)] \end{bmatrix} \begin{bmatrix} A_{x_n} \\ A_{y_n} \end{bmatrix} \qquad 2.42$$

Now, due to the inherent birefringence ($\delta\beta \quad rad/m$) of the waveplate; the elements of A_{n+1}^- will experience a phase retardation given by:

$$A_{n+1}^+ = \begin{bmatrix} e^{j\frac{\delta\beta}{2}} & 0 \\ 0 & e^{-j\frac{\delta\beta}{2}} \end{bmatrix} A_{n+1}^- \qquad 2.43$$

The process is repeated for the next birefringent waveplate in the stack. The SOP at the output of each waveplate can be converted back to the fixed coordinates by accumulating the total rotation of the local axes and rotating the coordinate axes back by that amount using Eq. (2.2). Stokes parameters were also calculated. Detailed MATLAB program can be found in the Appendix.

In summary we discussed our simulation model, simulation parameters and simulation algorithm in detail. This simple model gives a lot of physical insight into a seemingly complex SOP transformation process of Huang plates. In the next section we will use the analytical model developed in the previous section to predict the output SOP for a given input SOP. We shall then use our simulation model to verify (and validate) this prediction. In that we will see the SOP evolution along the fiber length in the local coordinates, the fixed coordinates and on the Poincairé sphere. Thus our simulation

model serves to validate the analytical theory and to provide the physical picture of the SOP transformation without resorting to complicated calculations.

2.5 *SOP transformation behavior of Huang plates*

In this section we will analyze the SOP transformation behavior of Huang plates and establish its operation as an all-fiber quarter-wave plate over wide bandwidth. In the case of uniform waveguide transmission, the problems relating to the SOP evolution and transformation are often classified based on the involvement of either single eigen-mode or both the eigen-modes. The eigen-modes are also called the principal polarization states (PSP) [7] and for a given waveguide they form a pair of orthogonal states of polarization for which the field pattern (and SOP) remains unchanged during transmission, except for a phase shift descriptive of wave motion. However, when the SOP of light launched in the waveguide is not one of the eigen-modes (or PSP) then, both the eigen-modes propagate. Thus for non-eigen input SOP, dual eigen-mode transmission causes a beating pattern whose amplitude varies periodically along the waveguide. This period is called the beat length. A similar approach can be adopted for Huang plates because SOP transformation in Huang plates can be described in terms of a set of supermodes **W** (Section 2.3). These supermodes were said to be quasi-eigen-modes in that, very weak coupling term in Eq. (2.29) can be ignored to obtain Eq. (2.35). In other words if the SOP of input light is such that it excites only one of the supermodes either W_1 or W_2 then, from Eq. (2.35) it can be seen that the transmission will involve only that mode. This eigen-mode-like behavior of supermodes **W** can be used to classify the SOP transformation problems in to a broad category depending on whether it involves only one or both supermodes. Further classification can be based on whether the light is input at the un-spun end or the high-spun end. As will be seen in this section unlike bulk optics waveplates, Huang plates are not symmetrical. In that, Huang plates behave differently depending on which end is used as the input end of the fiber.

In section 2.3 supermodes were **W** (defined in normal co-ordinates) were said to be a set of numbers that are related to the local modes (defined in local co-ordinates) by Eq.

(2.27). Thus we can translate the requirement for single supermode transmission to the requirement for the SOP of input light; at un-spun end and high-spun fiber end using Eq. (2.27). Let the desired supermode for single supermode transmission be W_1. Mathematically:

$$\mathbf{W} = \begin{bmatrix} 1 \\ 0 \end{bmatrix} \qquad 2.44$$

Using Eq. (2.27) and Eq. (2.33) the SOP of input light at the un-spun end for single supermode (W_1) transmission is:

$$\begin{aligned} \mathbf{A}(0) &= \mathbf{O}_0.\mathbf{W} \\ \mathbf{A}(0) &= \begin{bmatrix} 1 & 0 \\ 0 & 1 \end{bmatrix}\begin{bmatrix} 1 \\ 0 \end{bmatrix} \\ &= \begin{bmatrix} 1 \\ 0 \end{bmatrix} \qquad \equiv \text{'}\mathbf{x}\text{'}\,\textit{aligned linear} \end{aligned} \qquad 2.45$$

Similarly, the SOP of input light at the un-spun end for single supermode (W_2) transmission is:

$$\mathbf{A}(0) = \begin{bmatrix} 0 \\ 1 \end{bmatrix} \qquad \equiv \text{'}\mathbf{y}\text{'}\,\textit{aligned linear} \qquad 2.46$$

Thus in terms of local modes, the principal states of polarization of a Huang plate at un-spun end are principal axes aligned linearly polarized light. If the input light is not principal axis aligned linearly polarized light then transmission takes place by dual supermode process.

Using Eq. (2.27) and Eq. (2.34) the SOP of input light at the high-spun end for single supermode (W_1) transmission is:

$$\mathbf{A}(0) = \mathbf{O}_F . \mathbf{W}$$

$$\mathbf{A}(0) = \frac{1}{\sqrt{2}} \begin{bmatrix} 1 & j \\ j & 1 \end{bmatrix} \begin{bmatrix} 1 \\ 0 \end{bmatrix} \qquad 2.47$$

$$= \frac{1}{\sqrt{2}} \begin{bmatrix} 1 \\ j \end{bmatrix} \qquad \equiv \textit{Right hand circular}$$

Similarly, the SOP of input light at the high-spun end for single supermode (W_2) transmission is:

$$\mathbf{A}(0) = \frac{1}{\sqrt{2}} \begin{bmatrix} 1 \\ -j \end{bmatrix} \qquad \equiv \textit{Left hand circular} \qquad 2.48$$

Thus in terms of local modes, the principal states of polarization of a Huang plate at high-spun end are right and left handed circularly polarized light. If the input light is not right or left handed circularly polarized light then transmission takes place by dual supermode process.

We have determined the principal states of polarization for Huang plates at the un-spun end and the high-spun. In the following section we shall discuss the SOP transformation behavior of a Huang plate by single supermode process followed by SOP transformation by dual-supermode process.

SOP transformation by single supermode process

Input un-spun end

As discussed in the previous section, the principal states of polarization at the un-spun end are principal axes aligned linearly polarized light. Let **'x'**-aligned linearly polarized light be input at the un-spun end of a Huang plate.

$$\mathbf{A}(0) = \begin{bmatrix} 1 \\ 0 \end{bmatrix} \qquad 2.49$$

Using Eq. (2.37), Eq. (2.33) and Eq. (2.34), we get:

$$\begin{aligned}
&\mathbf{A}(L) = \mathbf{O}_F \widetilde{\Lambda} \mathbf{O}_0^{-1} \mathbf{A}(0) \\
&\mathbf{A}(L) = \frac{1}{\sqrt{2}} \begin{bmatrix} 1 & j \\ j & 1 \end{bmatrix} \begin{bmatrix} e^{j\rho} & 0 \\ 0 & e^{-j\rho} \end{bmatrix} \begin{bmatrix} 1 & 0 \\ 0 & 1 \end{bmatrix} \begin{bmatrix} 1 \\ 0 \end{bmatrix} \\
&\mathbf{A}(L) = \frac{1}{\sqrt{2}} \begin{bmatrix} 1 \\ j \end{bmatrix} e^{j\rho}
\end{aligned} \qquad 2.50$$

The resulting light at the output given by Eq. (2.50) is a circularly polarized light. The handedness (right or left) depends on the direction in which the observer looks at the light. For convenience let Eq. (2.50) represent right circularly polarized light. Thus input **'x'** aligned linearly polarized light at the un-spun end is transformed to a right circularly polarized light at the output high-spun end. The factor $e^{j\rho}$ is the phase term descriptive of the wave motion.

Simulations were performed using **'x'** aligned linear light as the input from the un-spun end. Figure 2-6 and Figure 2-7 show the evolution of the amplitude and the phase along the fiber length respectively. All the power is launched in the **'x'** mode, as we go down the fiber more and more power is coupled from the **'x'** mode to the **'y'** mode and they carry equal power at the high-spun end. The phase difference evolves from zero at the un-spun end to a value of $d\varphi = \pi/2 = 1.57\, radians$ at the high spun end. Thus the **'x'** aligned linearly polarized light exits as a right circularly polarized light at the high-spun end. Figure 2-8 and Figure 2-9 show the evolution of the SOP from the un-spun end to the high-spun end and the initial and the final SOP on a Poincairé sphere respectively. Stokes vector for input light is **S = (1, 1, 0, 0)** descriptive of the **'x'** aligned linearly polarized light and that of the output light is **S = (1, 0, 0, 1)** descriptive of the right circularly polarized light. Figure 2-10–to- Figure 2-13 the evolution of the SOP in the fixed laboratory coordinates (coinciding with the local coordinates at the un-spun end).

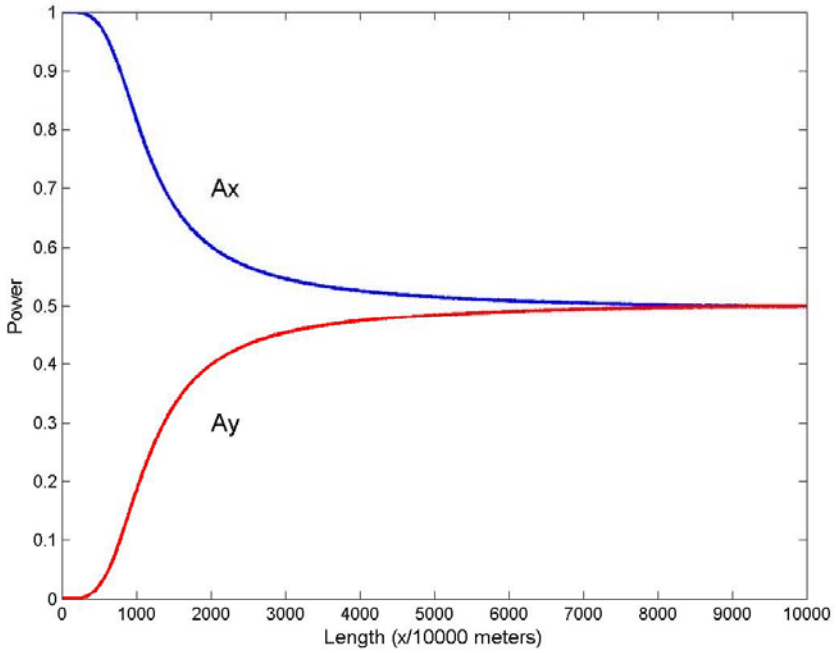

Figure 2-6 Evolution of amplitude in local coordinates

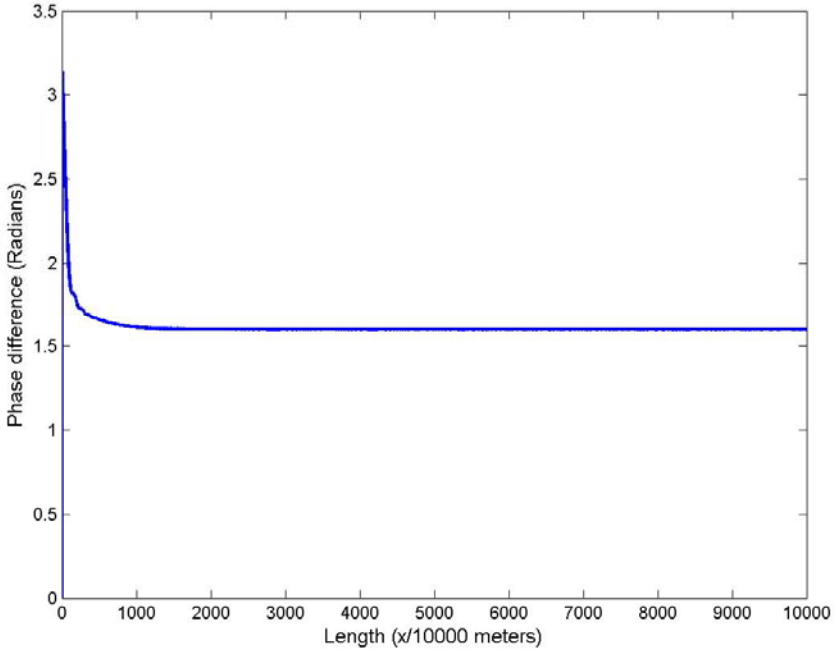

Figure 2-7 Evolution of phase difference in local coordinates

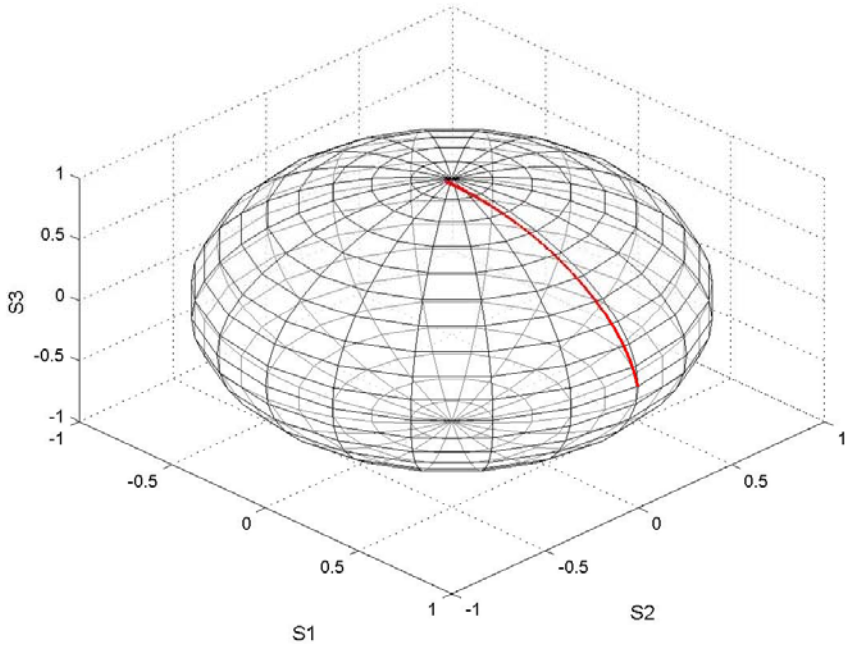

Figure 2-8 SOP Evolution on Poincairé sphere (local coordinates)

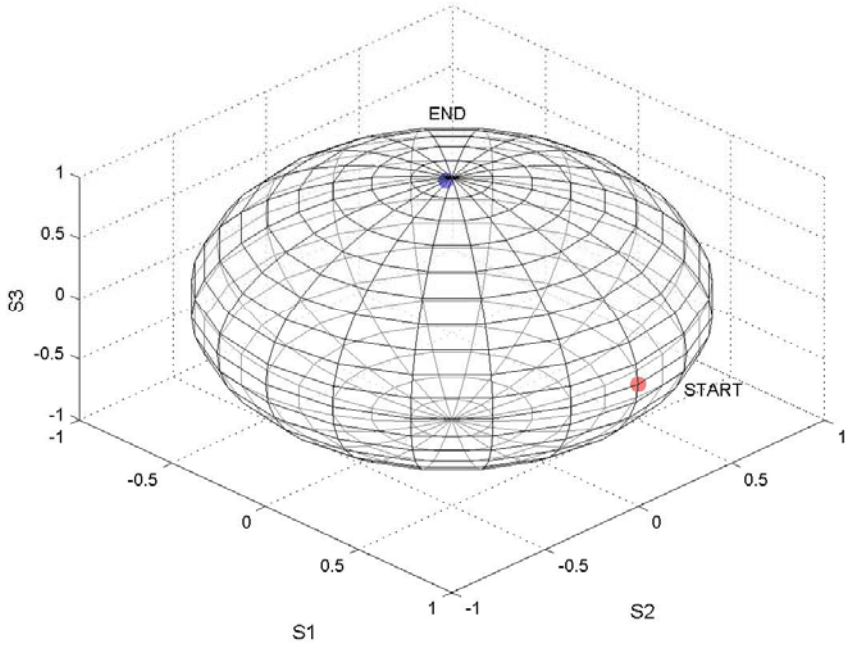

Figure 2-9 Initial and final SOP on Poincairé sphere (local coordinates)

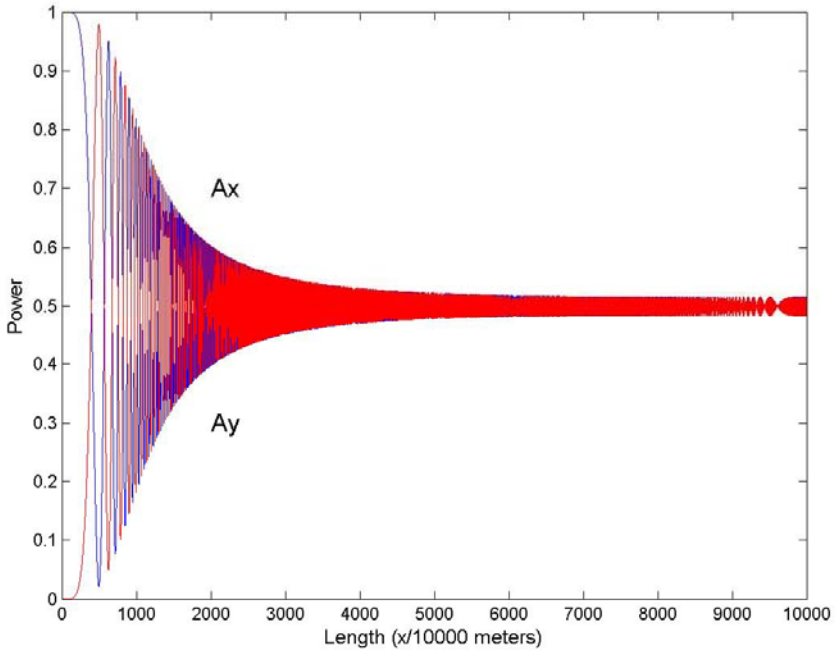

Figure 2-10 Evolution of amplitude in fixed coordinates

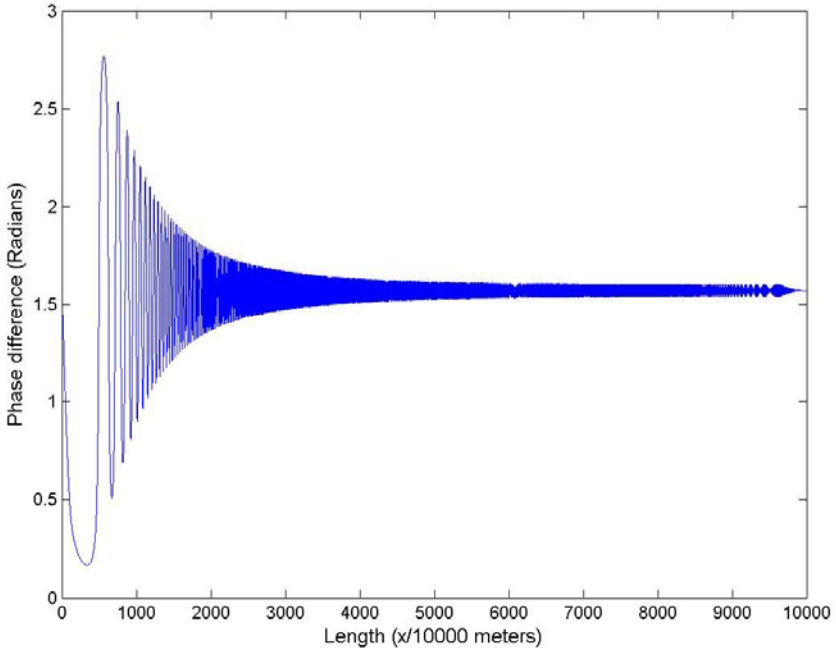

Figure 2-11 Evolution of phase difference in fixed coordinates

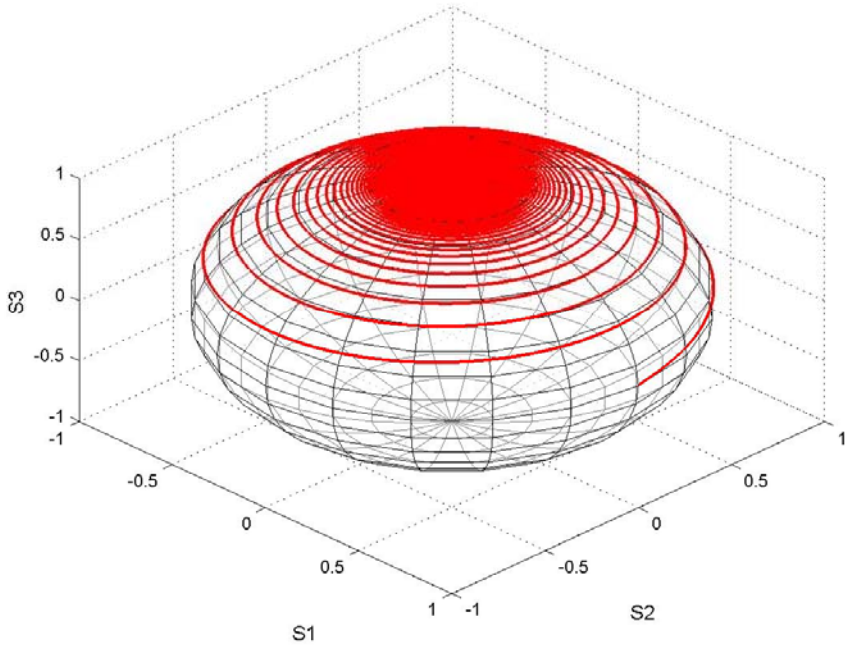

Figure 2-12 SOP Evolution on Poincairé sphere (fixed coordinates)

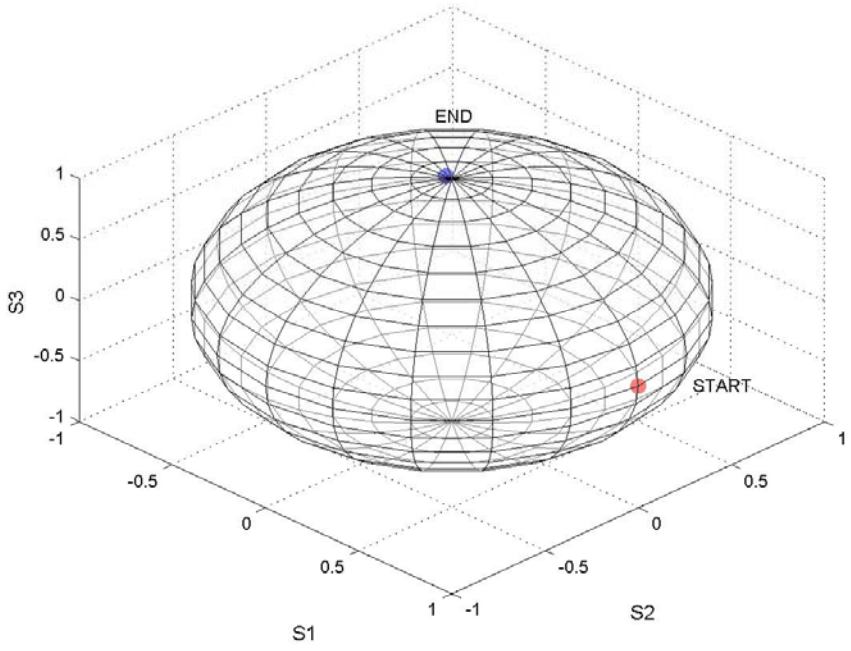

Figure 2-13 Initial and final SOP on Poincairé sphere (fixed coordinates)

Let **'y'**-aligned linearly polarized light be input at the un-spun end of a Huang plate.

$$\mathbf{A}(0) = \begin{bmatrix} 0 \\ 1 \end{bmatrix} \qquad 2.51$$

Using Eq. (2.37), Eq. (2.33) and Eq. (2.34), we get:

$$\begin{aligned} \mathbf{A}(L) &= \mathbf{O}_F \widetilde{\Lambda} \mathbf{O}_0^{-1} \mathbf{A}(0) \\ \mathbf{A}(L) &= \frac{1}{\sqrt{2}} \begin{bmatrix} 1 & j \\ j & 1 \end{bmatrix} \begin{bmatrix} e^{j\rho} & 0 \\ 0 & e^{-j\rho} \end{bmatrix} \begin{bmatrix} 1 & 0 \\ 0 & 1 \end{bmatrix} \begin{bmatrix} 0 \\ 1 \end{bmatrix} \\ \mathbf{A}(L) &= \frac{1}{\sqrt{2}} \begin{bmatrix} 1 \\ -j \end{bmatrix} e^{-(j\rho - \frac{\pi}{2})} \end{aligned} \qquad 2.52$$

The resulting light at the output given by Eq. (2.52) is a left circularly polarized light. Thus input **'y'** aligned linearly polarized light at the un-spun end is transformed to a left circularly polarized light at the output high-spun end. The factor $e^{-(j\rho - \frac{\pi}{2})}$ is the phase term descriptive of the wave motion.

Simulations were performed using the **'y'** aligned linear light as theinput from the un-spun end. Figure 2-14 and Figure 2-15 show the evolution of the amplitude and the phase along the fiber length respectively. All the power is launched in the **'y'** mode, as we go down the fiber more and more power is coupled from the **'y'** mode to the **'x'** mode and they carry equal power at the high-spun end. The phase difference evolves from zero at the un-spun end to a value of $d\varphi = -\pi/2 = -1.57\, radians$ at the high spun end. Thus the **'y'** aligned linearly polarized light exits as a left circularly polarized light at the high-spun end. Figure 2-16 and Figure 2-17 show the evolution of the SOP from the un-spun end to the high-spun end and the initial and the final SOP on a Poincairé sphere respectively. Stokes vector for the input light is **S = (1, -1, 0, 0)** descriptive of the **'y'** aligned linearly polarized light and that of the output light is **S = (1, 0, 0, -1)** descriptive of the left circularly polarized light. Figure 2-18–to-Figure 2-21 show the evolution of the SOP in the fixed laboratory coordinates (coinciding with the local coordinates at the un-spun end).

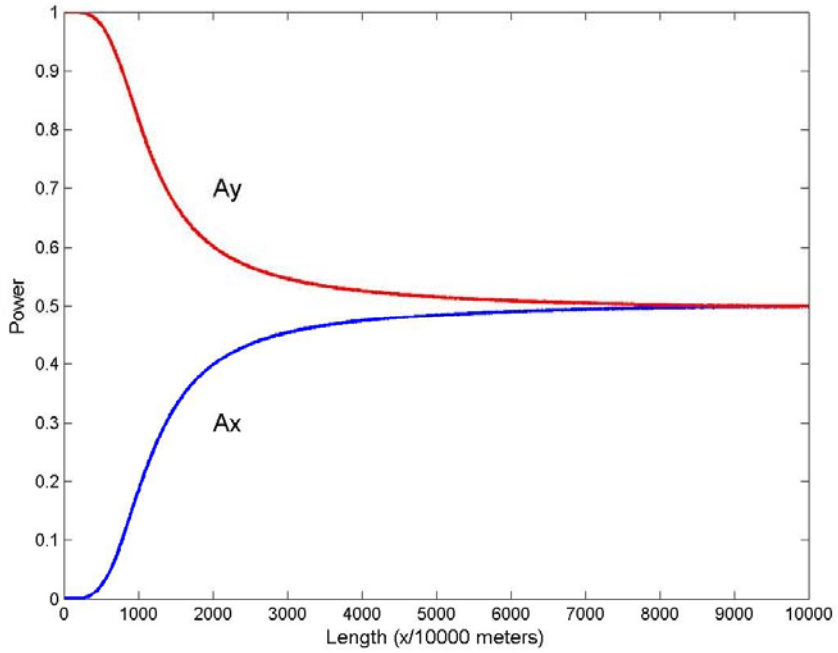

Figure 2-14 Evolution of amplitude in local coordinates

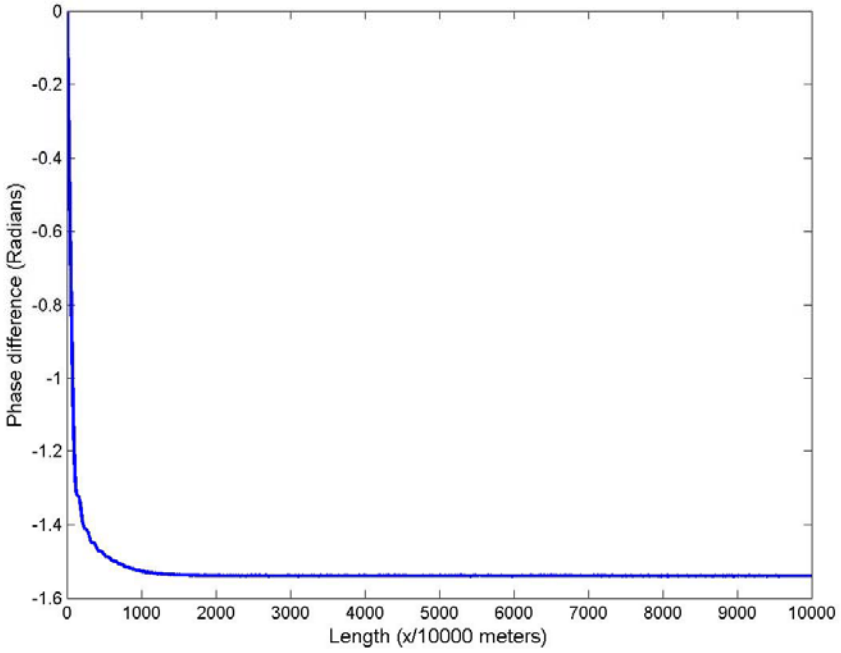

Figure 2-15 Evolution of phase difference in fixed coordinates

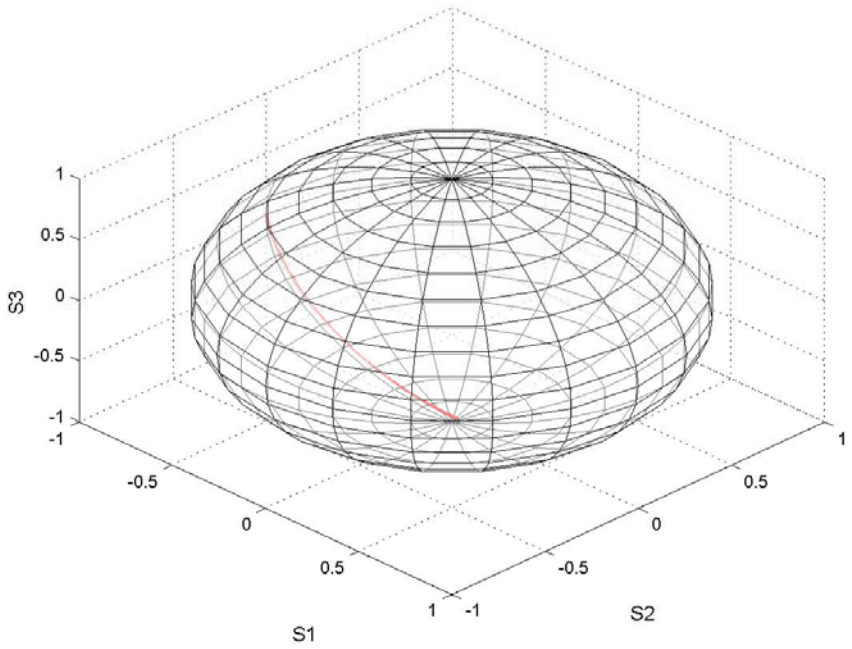

Figure 2-16 SOP evolution on Poincairé sphere (local coordinates)

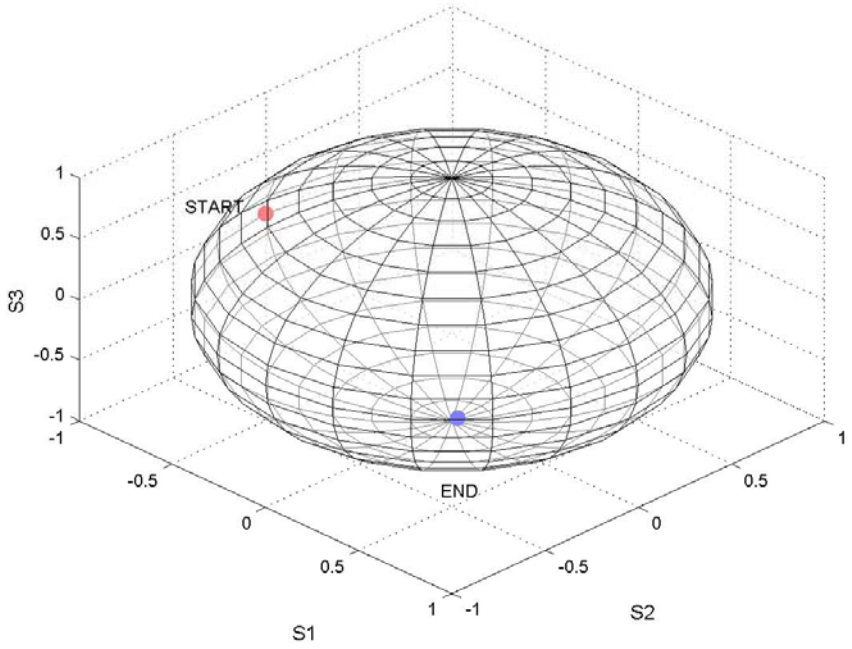

Figure 2-17 Initial and final SOP on Poincairé sphere (local coordinates)

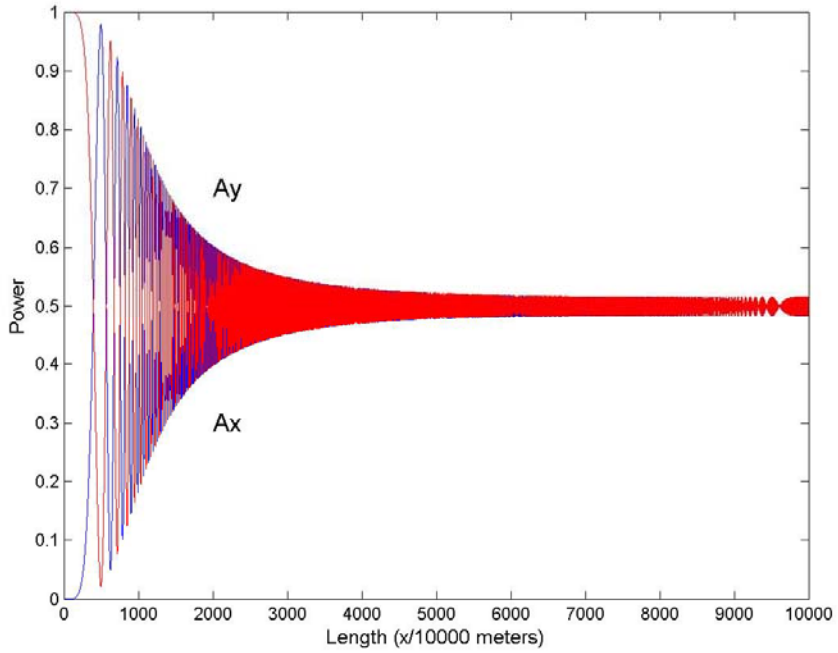

Figure 2-18 Evolution of amplitude in fixed coordinates

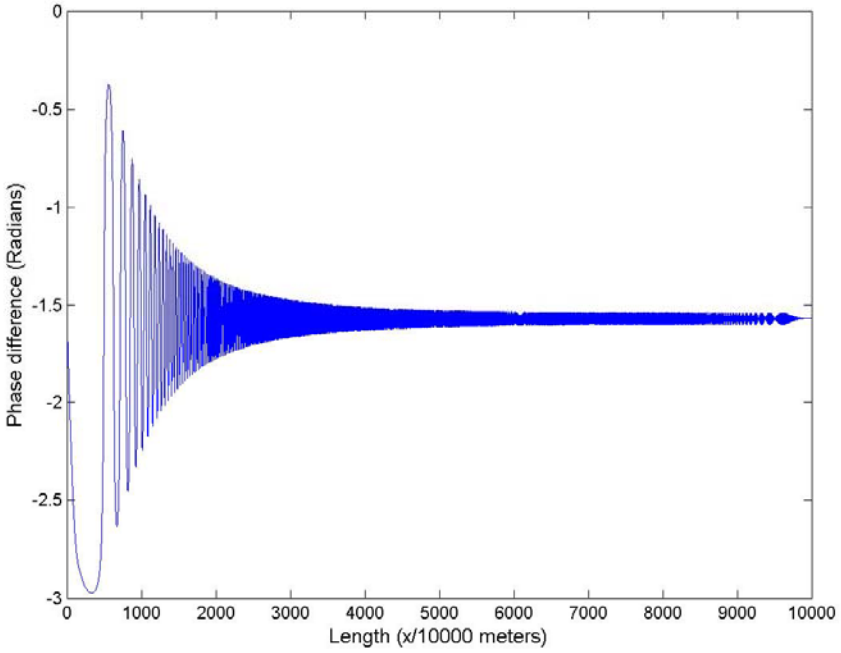

Figure 2-19 Evolution of phase in fixed coordinates

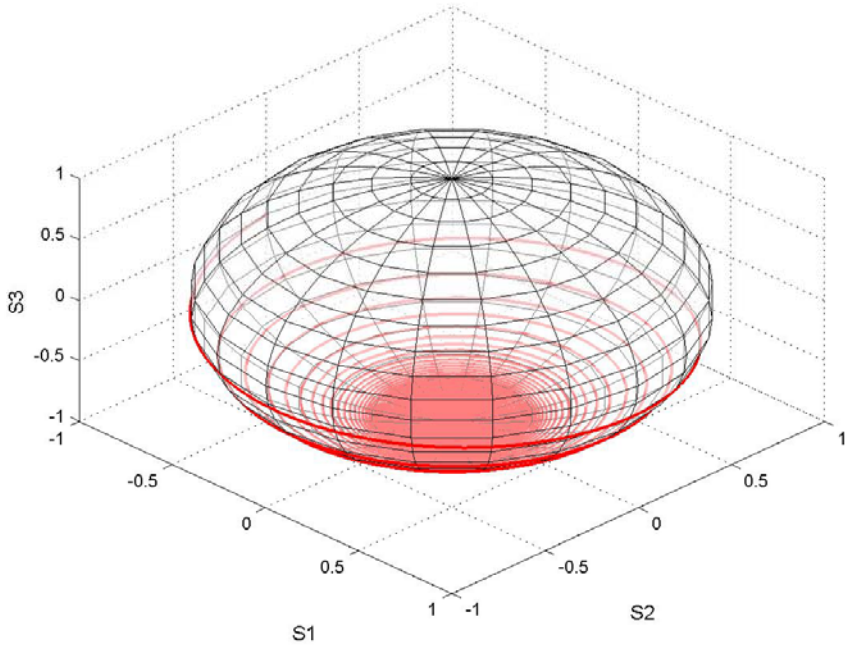

Figure 2-20 SOP evolution on Poincairé sphere (fixed coordinates)

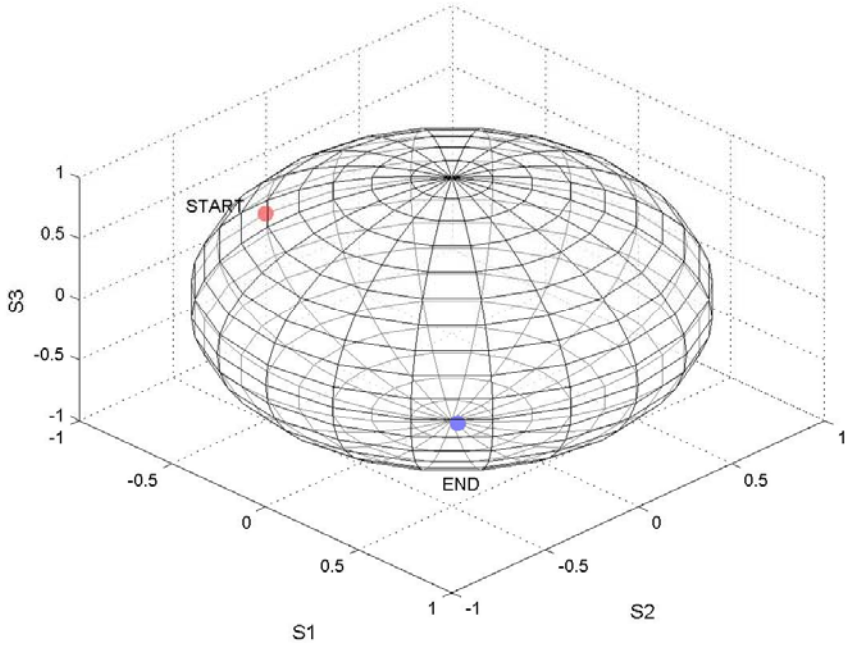

Figure 2-21 Initial and final SOP on Poincairé sphere (fixed coordinates)

Input high-spun end

Principal states of polarization at the high-spun end are right and left handed circularly polarized light. Let **'right'**-handed circularly polarized light be input to the high-spun end of a Huang plate.

$$\mathbf{A}(0) = \frac{1}{\sqrt{2}}\begin{bmatrix}1\\ j\end{bmatrix} \qquad 2.53$$

Using Eq. (2.37), Eq. (2.33) and Eq. (2.34), we get:

$$\begin{aligned}\mathbf{A}(L) &= \mathbf{O}_0\tilde{\Lambda}\mathbf{O}_F^{-1}\mathbf{A}(0)\\ \mathbf{A}(L) &= \frac{1}{2}\begin{bmatrix}1 & 0\\ 0 & 1\end{bmatrix}\begin{bmatrix}e^{j\rho} & 0\\ 0 & e^{-j\rho}\end{bmatrix}\begin{bmatrix}1 & -j\\ -j & 1\end{bmatrix}\begin{bmatrix}1\\ j\end{bmatrix} \qquad 2.54\\ \mathbf{A}(L) &= \begin{bmatrix}1\\ 0\end{bmatrix}e^{j\rho}\end{aligned}$$

The resulting light at the output given by Eq. (2.54) is **'x'** aligned linearly polarized light. Thus input **'right'**-handed circularly polarized light at the high-spun end is transformed to a **'x'** aligned linearly polarized light at the output un-spun end. The factor $e^{j\rho}$ is the phase term descriptive of the wave motion.

Simulations were performed using **'right'**-handed circularly polarized light as input from the high-spun end. Figure 2-22 and Figure 2-23 show the evolution of the amplitude and phase along the fiber length respectively. Equal power is launched in the **'x'** mode and the **'y'** mode. As we go down the fiber more and more power is coupled from the **'y'** mode to the **'x'** mode and all the power is transferred to the **'x'** mode at the un-spun end. The phase difference evolves from $d\varphi = \pi/2 = 1.57\,radians$ at the high-spun end to $0\ radians$ at the un-spun end. Thus **'right'** handed circularly polarized light exits as **'x'** aligned linearly polarized light at the un-spun end. Figure 2-24 and Figure 2-25 show the evolution of the SOP from the high-spun end to the un-spun end and the initial and the final SOP on a Poincairé sphere respectively. Stokes vector for the input light is **S = (1, 0, 0, 1)** descriptive of a **'right'**-handed circularly polarized light and that of the output light is **S = (1, 1, 0, 0)** descriptive of a **x'** aligned linearly polarized light. Figure 2-26–to-

Figure 2-29 show the evolution of the SOP in the fixed laboratory coordinates (coinciding with the local coordinates at the un-spun end).

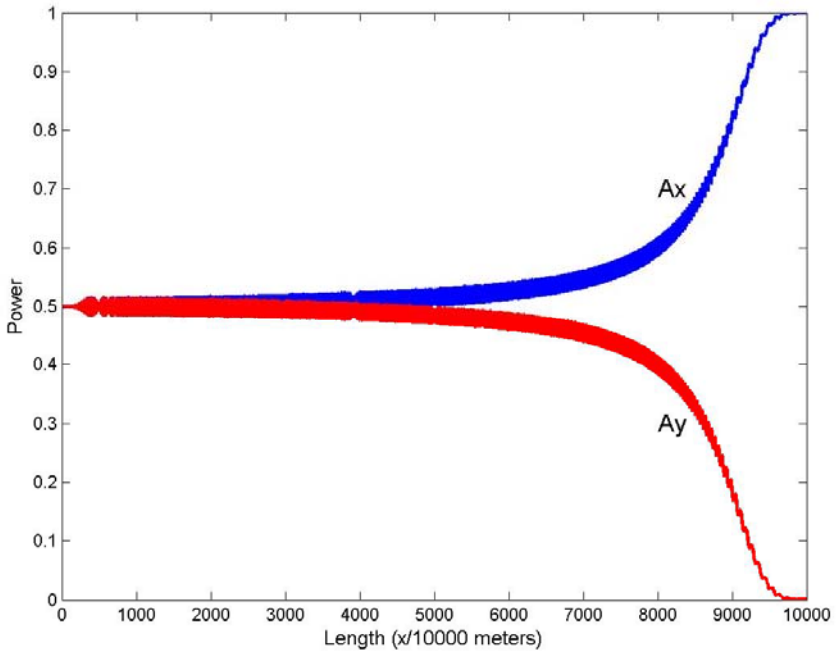

Figure 2-22 Evolution of amplitude in local coordinates

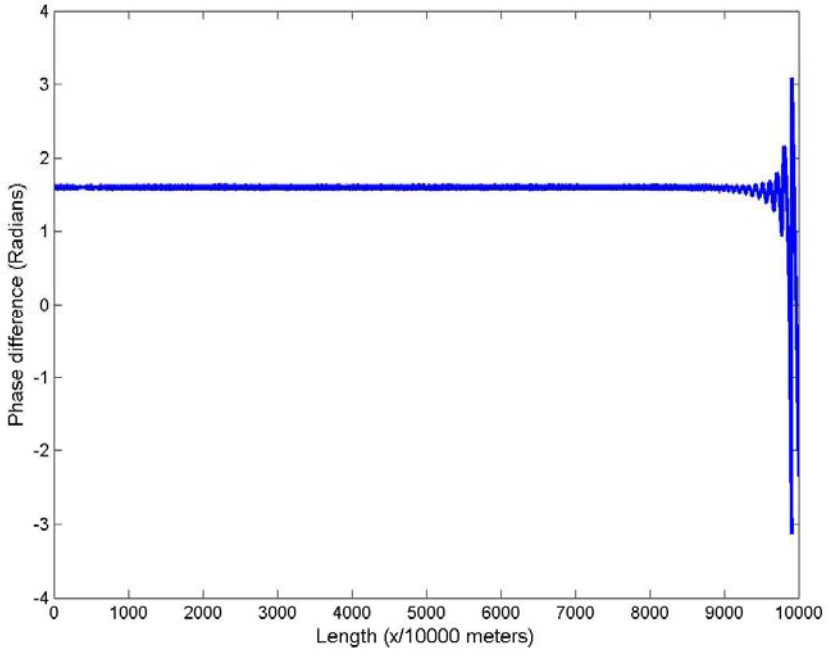

Figure 2-23 Evolution of phase difference in local coordinates

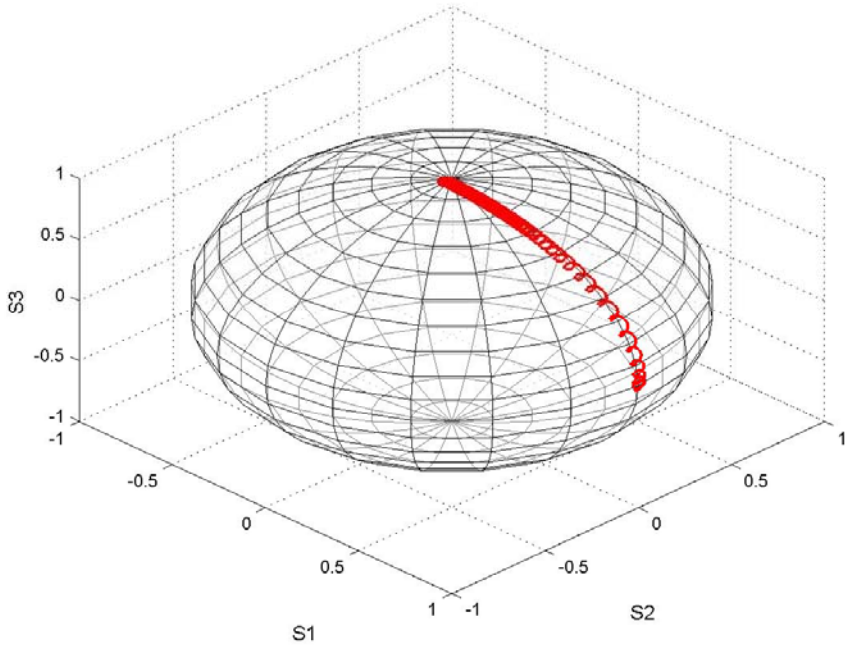

Figure 2-24 SOP evolution on Poincairé sphere (fixed coordinates)

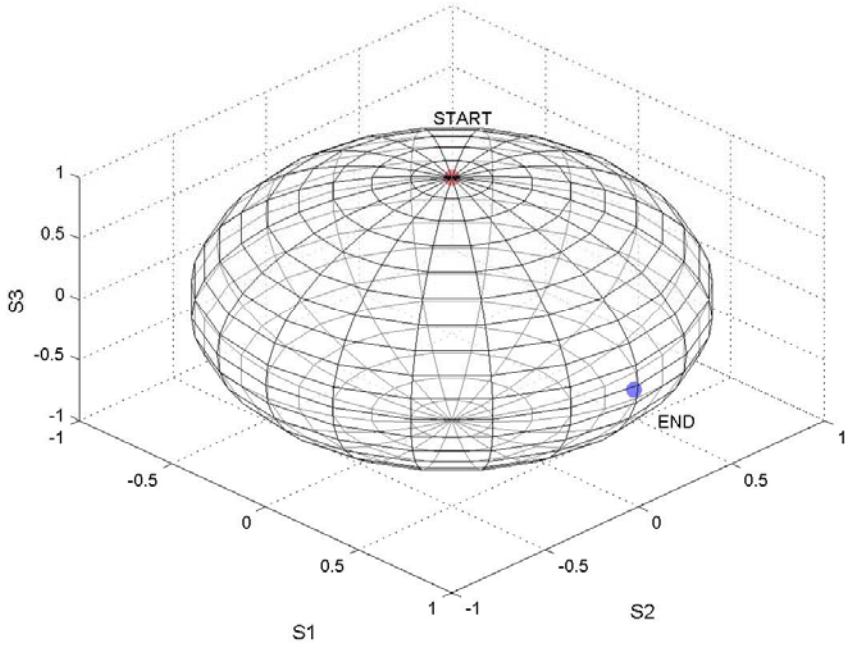

Figure 2-25 Initial and final SOP on Poincairé sphere (fixed coordinates)

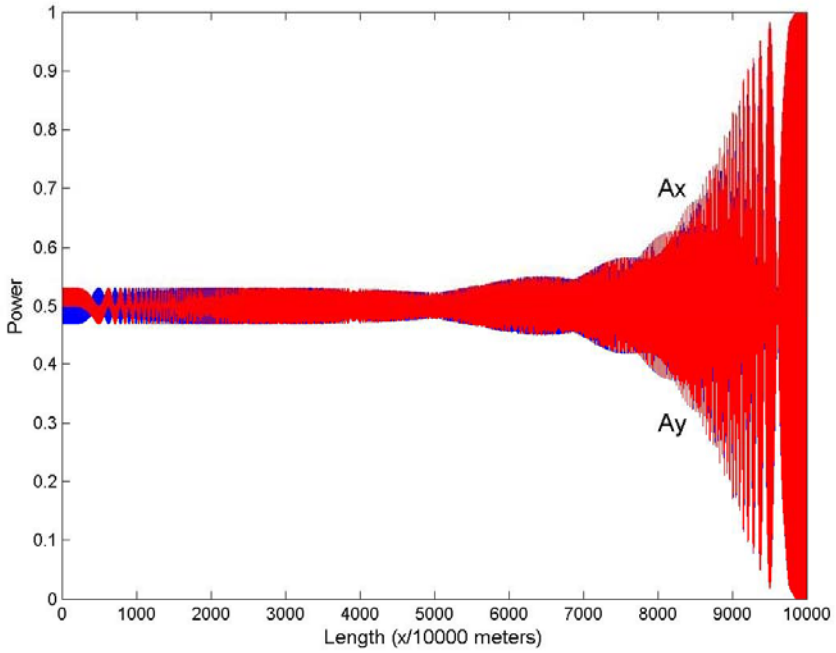

Figure 2-26 Evolution of amplitude in fixed coordinates

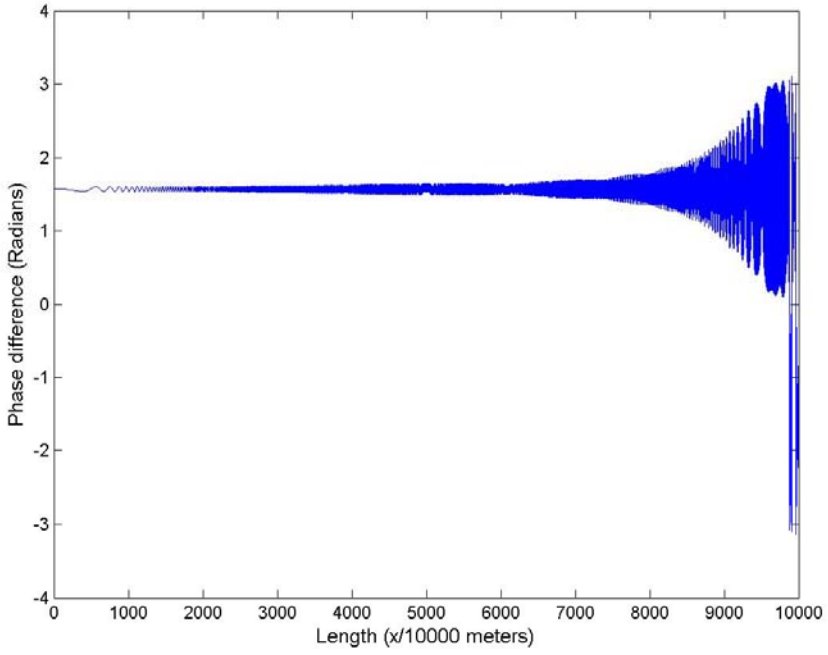

Figure 2-27 Evolution of phase difference in fixed coordinates

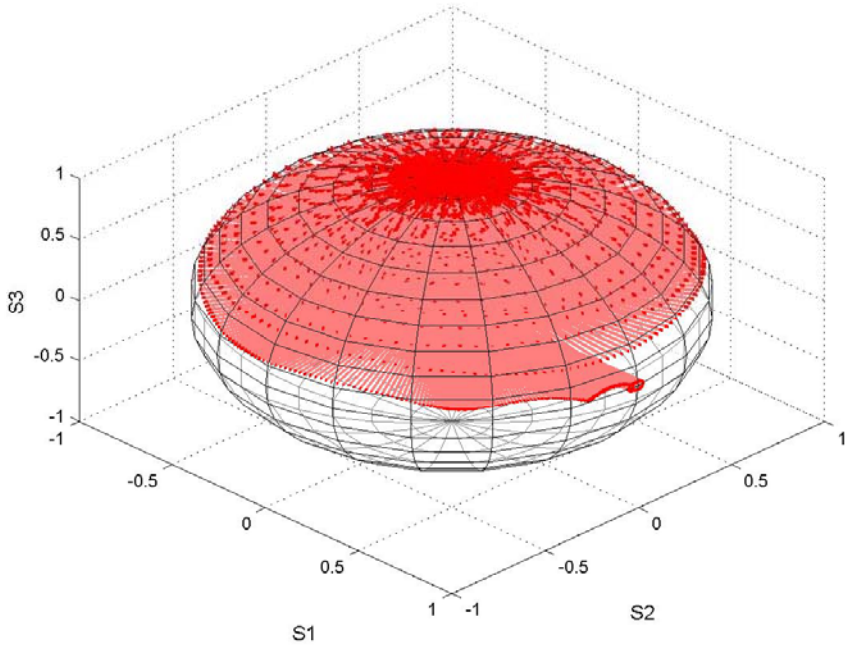

Figure 2-28 SOP evolution on Poincairé sphere (fixed coordinates)

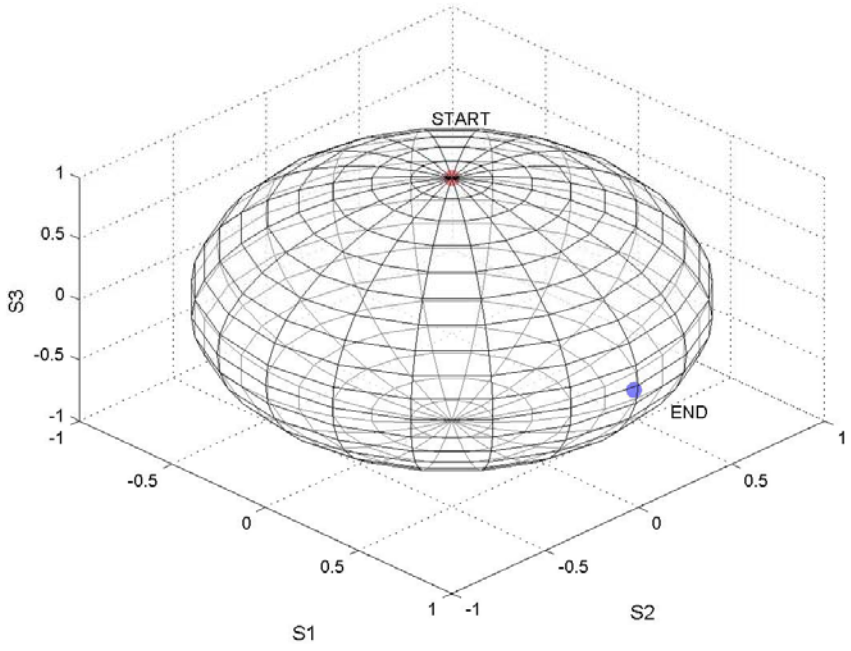

Figure 2-29 Initial and final SOP on Poincairé sphere (fixed coordinates)

Let **'left'**-handed circularly polarized light be input at the high-spun end of a Huang plate.

$$\mathbf{A}(0) = \frac{1}{\sqrt{2}}\begin{bmatrix} 1 \\ -j \end{bmatrix} \qquad 2.55$$

Using Eq. (2.37), Eq. (2.33) and Eq. (2.34), we get:

$$\begin{aligned} \mathbf{A}(L) &= \mathbf{O}_0 \widetilde{\Lambda} \mathbf{O}_F^{-1} \mathbf{A}(0) \\ \mathbf{A}(L) &= \frac{1}{2}\begin{bmatrix} 1 & 0 \\ 0 & 1 \end{bmatrix}\begin{bmatrix} e^{j\rho} & 0 \\ 0 & e^{-j\rho} \end{bmatrix}\begin{bmatrix} 1 & -j \\ -j & 1 \end{bmatrix}\begin{bmatrix} 1 \\ -j \end{bmatrix} \\ \mathbf{A}(L) &= \begin{bmatrix} 0 \\ 1 \end{bmatrix} e^{-j(\rho+\frac{\pi}{2})} \end{aligned} \qquad 2.56$$

The resulting light at the output given by Eq. (2.56) is **'y'** aligned linearly polarized light. Thus input **'left** -handed circularly polarized light at the high-spun end is transformed to a **'y'** aligned polarized light at the output un-spun end. The factor $e^{-j(\rho+\frac{\pi}{2})}$ is the phase term descriptive of wave motion.

Simulations were performed using **'left'**-handed circularly polarized light as input from the high-spun end. Figure 2-30 and Figure 2-31 show the evolution of the amplitude and the phase along the fiber length respectively. Equal power is launched in the **'x'** mode and the **'y'** mode. As we go down the fiber more and more power is coupled from the **'x'** mode to the **'y'** mode and all the power is transferred to the **'y'** mode at the un-spun end. The phase difference evolves from $d\varphi = -\pi/2 = -1.57\, radians$ at the high-spun end to $0\ radians$ at the un-spun end. Thus **'left'** handed circularly polarized light exits as a **'y'** aligned linearly polarized light at the un-spun end. Figure 2-32 and Figure 2-33 show the evolution of the SOP from the high-spun end to the un-spun end and the initial and the final SOP on a Poincairé sphere respectively. Stokes vector for the input light is **S = (1, 0, 0, -1)** descriptive of a **'left'**-handed circularly polarized light and that of the output light is **S = (1, -1, 0, 0)** descriptive of a **'y'** aligned linearly polarized light. Figure 2-34–to-Figure 2-37 show the evolution of the SOP in the fixed laboratory coordinates (coinciding with the local coordinates at the un-spun end).

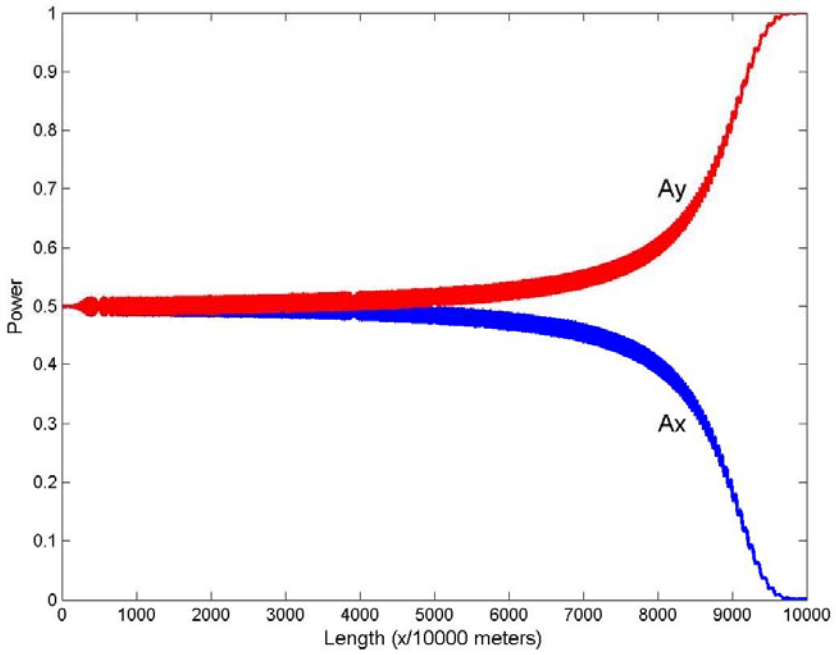

Figure 2-30 Evolution of amplitude in local coordinates

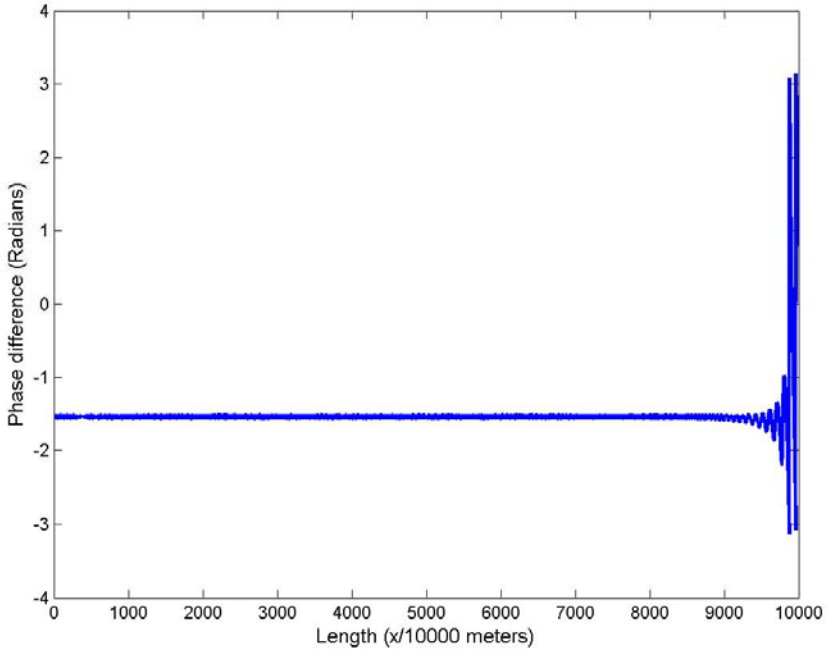

Figure 2-31 Evolution of phase difference in local coordinates

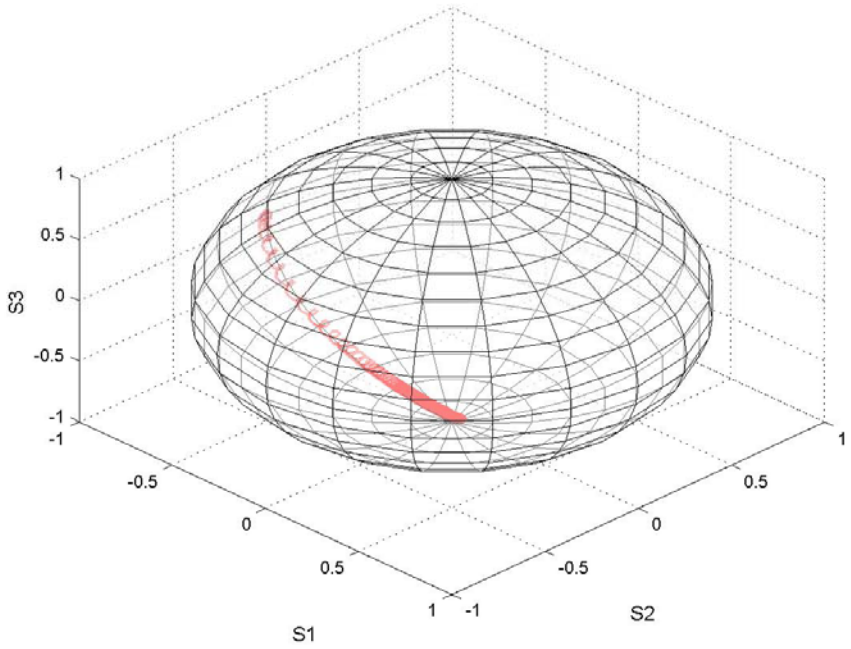

Figure 2-32 SOP evolution on Poincairé sphere (local coordinates)

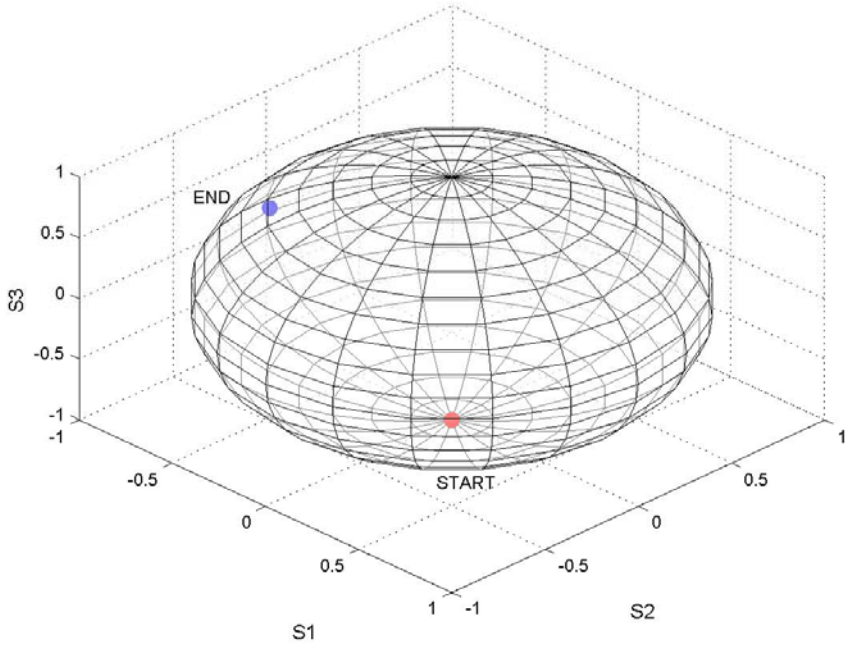

Figure 2-33 Initial and final SOP on Poincairé sphere (local coordinates)

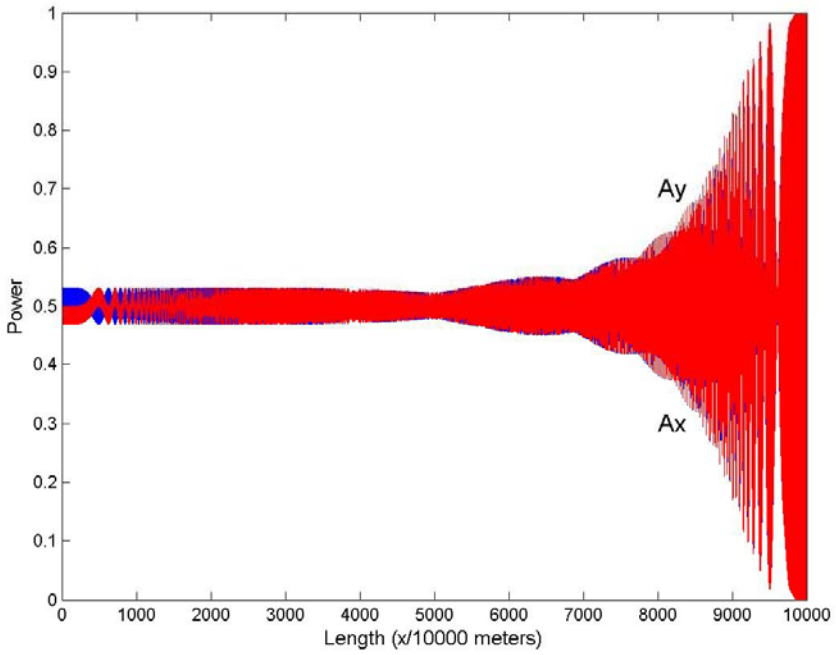

Figure 2-34 Evolution of amplitude in fixed coordinates

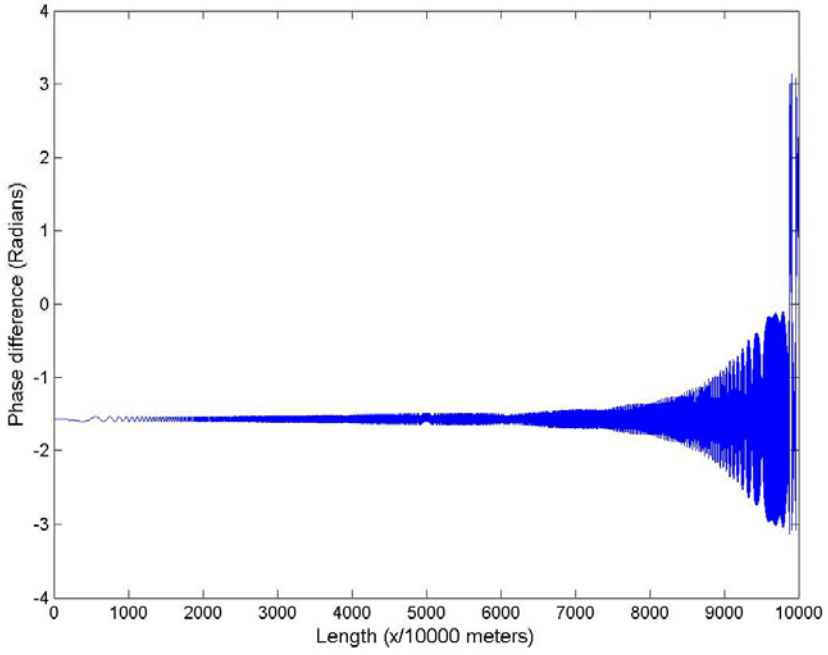

Figure 2-35 Evolution of phase difference in fixed coordinates

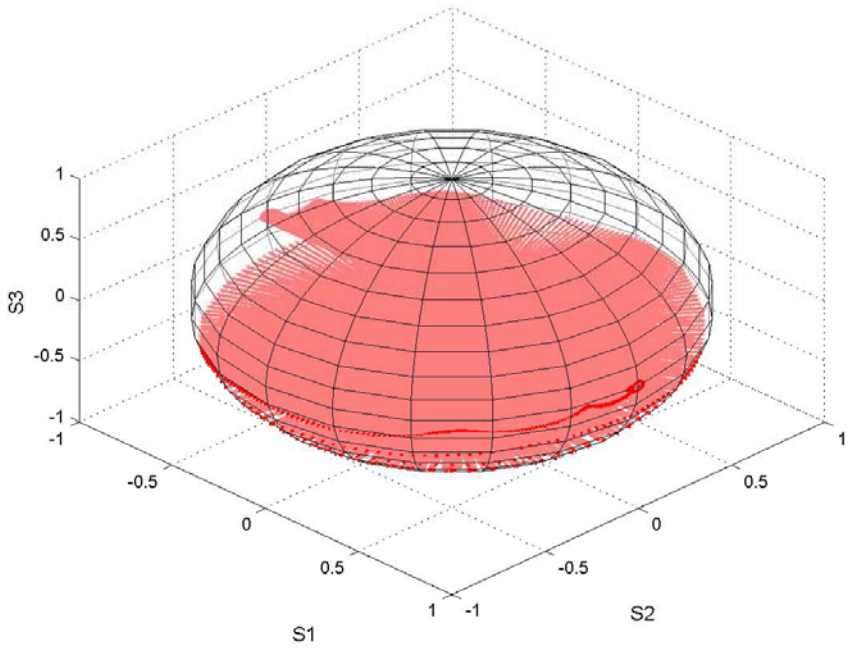

Figure 2-36 SOP evolution on Poincairé sphere (fixed coordinates)

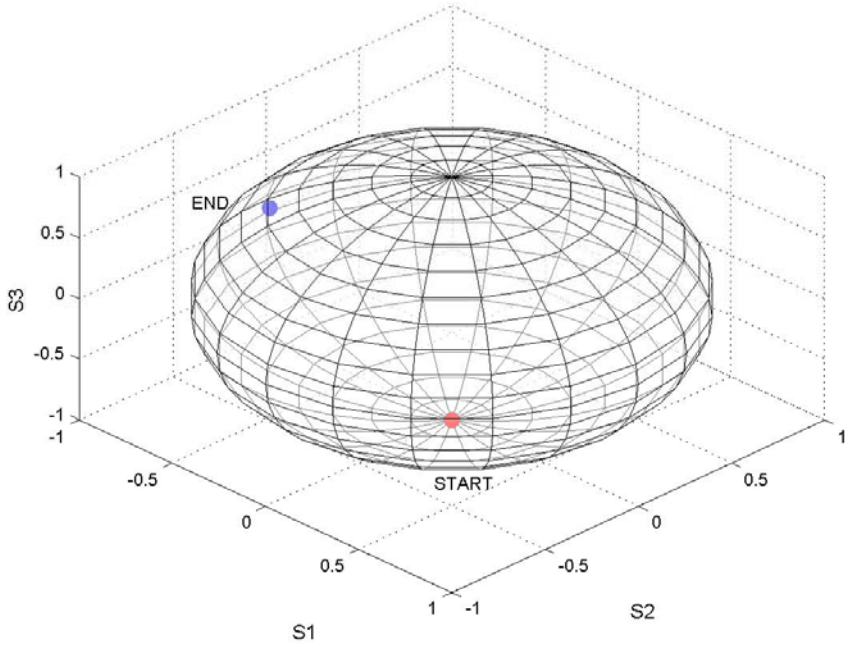

Figure 2-37 Initial and final SOP on Poincairé sphere (fixed coordinates)

Quarter waveplate –like behavior and wideband nature of Huang plates

The results from the analytical model and the simulation presented in previous two sections indicate that Huang plates behave like bulk-optic quarter waveplates. When a linearly polarized light is incident on a face of a bulk-optic waveplate making an angle of 45^0 with its internal birefringent axes, it exits as a circularly polarized light from the other face; and vice versa. Principal axes aligned linearly polarized light input at the un-spun end of a Huang plate exits as circularly polarized light at the high-spun end and vice versa. Thus, the behavior of a Huang plate is analogous to 45^0 excitation of a bulk-optic quarter waveplate. However there are some important differences.

The first most important difference is that while bulk-optic waveplates behave identically irrespective of the face on which the light is input, Huang plates behave differently depending on whether the light is input on the un-spun end or the high spun end. In other words the structure is asymmetrical and one needs to specify the appropriate input end at all times. The second difference lies in the basic principal of operation of the two devices. Bulk-optics quarter waveplate works on the principal that the ordinary and the extraordinary waves pick up a phase difference while propagating through an inherently birefringent material. This phase difference can be adjusted as desired, (e.g. $\pi/2$ for quarter waveplates) by adjusting the thickness of the waveplate, at a particular wavelength. However the phase difference will be different at any other wavelength and hence the bulk-optic waveplates are inherently narrowband in nature. In the case of Huang plates the Principal states of polarization at the un-spun end are principal axes aligned linearly polarized light and circularly polarized light at the high-spun end. Huang plates work on the principle that there is a slow and steady evolution of the principal state of polarization from linear to circular (and vice versa), while propagating through a slowly varying fiber structure which is several orders of magnitude longer than the un-spun beatlength. This evolution is independent of the wavelength so long as the fiber remains single mode at that wavelength.

Mathematically the only wavelength dependent term in the analysis (Section 2.3) is the un-spun beatlength L_b that appears in the global structural parameter (ρ) in Eq. (2.36). However for the SOP transformation by the single supermode process the term ρ is absorbed in the phase term and does not affect the SOP of the output light [see Eq. (2.50), (2.52), (2.54), (2.56)]. We verified the wideband nature of Huang plates by the means of simulation. We used **'x'**-aligned linear light as input at the un-spun end and observed the SOP of the output light at the high-spun end over a wavelength range $1\ \mu m - 2\ \mu m$ in steps of $0.1\ \mu m$. The SOP of the output light was plotted on a Poincairé sphere as shown in Figure 2-38. The SOPs of output light over wavelength range $1\ \mu m - 2\ \mu m$ are so close that they appear as a single point. Figure 2-39 shows zoomed diagram of the Poincairé sphere.

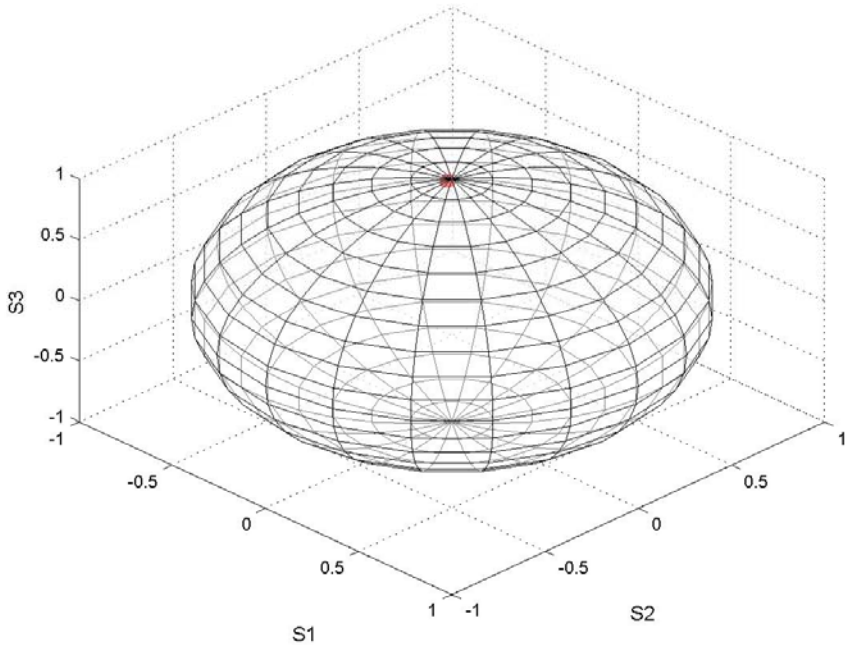

Figure 2-38 SOP of output light for principal axis aligned linear input at unspun end from 1um to 2 um (wideband nature)

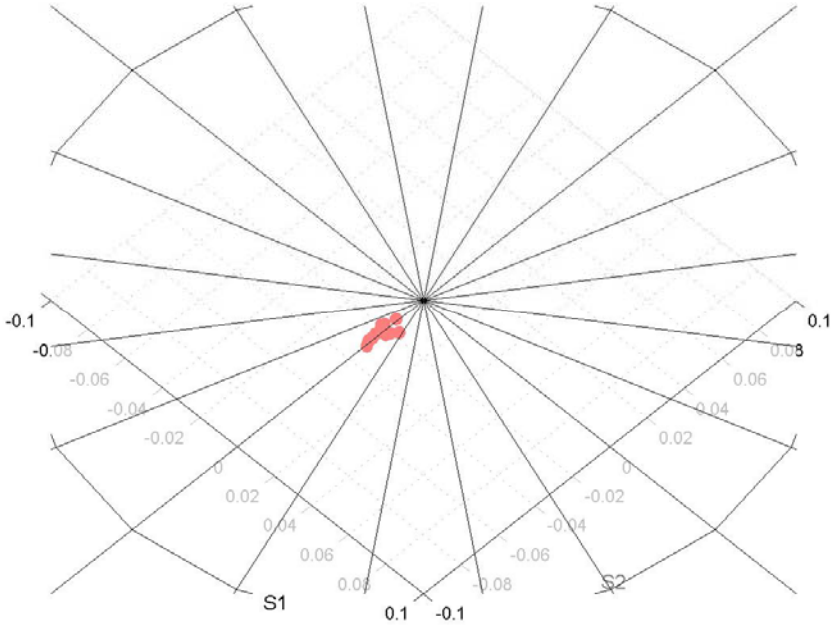

Figure 2-39 SOP of output light for principal axis aligned linear input at unspun end from 1um to 2 um (wideband nature) - Zoomed

SOP transformation by dual supermode process

In the previous section we established the quarter waveplate- like behavior of the Huang plates when the SOP transformation takes place by the single supermode process. In other words when the input SOP matches the principal state of polarization at the input end, the SOP transformation takes place by single supermode process and the device performs linear to circular (and vice versa) SOP transformation like a bulk-optic quarter waveplate. If the input SOP does not match the principal state of polarization at the input end then both the supermodes (W_1 *and* W_2) are excited and the SOP transformation takes place by the dual supermode process i.e. by beating of W_1 *and* W_2. In this section we shall analyze and simulate the SOP transformation by dual supermode process in Huang plates

Input un-spun end

With input at the un-spun end if the SOP of the input light is not principal axes aligned linearly polarized light then the SOP transformation takes place by the dual supermode process. Let right handed circularly polarized light be input at the un-spun end of the fiber:

$$\mathbf{A}(0) = \frac{1}{\sqrt{2}}\begin{bmatrix}1\\ j\end{bmatrix} \qquad 2.57$$

Using Eq. (2.37), Eq. (2.33) and Eq. (2.34), we get:

$$\begin{aligned}&\mathbf{A}(L) = \mathbf{O}_F \widetilde{\Lambda}\, \mathbf{O}_0^{-1}\mathbf{A}(0)\\ &\mathbf{A}(L) = \frac{1}{2}\begin{bmatrix}1 & j\\ j & 1\end{bmatrix}\begin{bmatrix}e^{j\rho} & 0\\ 0 & e^{-j\rho}\end{bmatrix}\begin{bmatrix}1 & 0\\ 0 & 1\end{bmatrix}\begin{bmatrix}1\\ j\end{bmatrix}\\ &\mathbf{A}(L) = \begin{bmatrix}\cos(90-\rho)\\ \sin(90-\rho)\end{bmatrix} e^{j(\frac{\pi}{2})}\end{aligned} \qquad 2.58$$

Thus output light at the high-spun end is linearly polarized light and is oriented at an angle of $(90-\rho)$ in the local coordinates at the high-spun end and is multiplied by a phase factor $e^{i\frac{\pi}{2}}$ descriptive of the wave motion. We simulated the behavior of a Huang plate excited by right circularly polarized light input at the un-spun end. Figure 2-40 shows the evolution of the amplitude in fixed coordinates. Figure 2-41shows the initial and the final SOP on a Poincairé sphere. At the input un-spun end **'x'** and **'y'** carry equal power, and both the supermodes are excited, the super modes beat along the fiber length such that a linearly polarized light exits at the output high-spun end. This light was found to make an angle of $0.3575\ radians = 20.48^0$ in the local coordinates. Since analytically the output linear light makes an angle of $(90-\rho)$ in the local coordinates we have:

$$\begin{aligned}&90-\rho = 20.48\\ &\rho = 69.51^0\end{aligned} \qquad 2.59$$

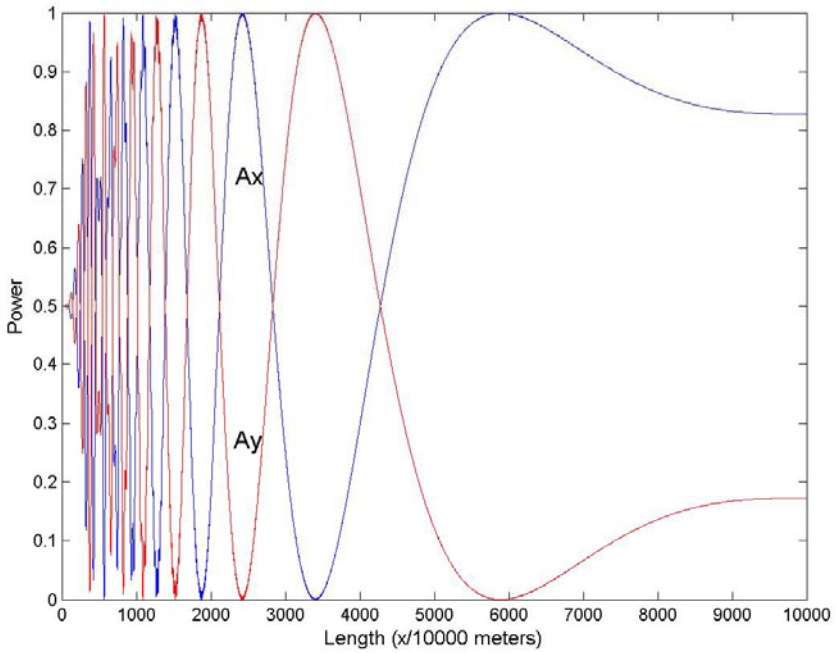

Figure 2-40 Evolution of amplitude on fixed coordinates

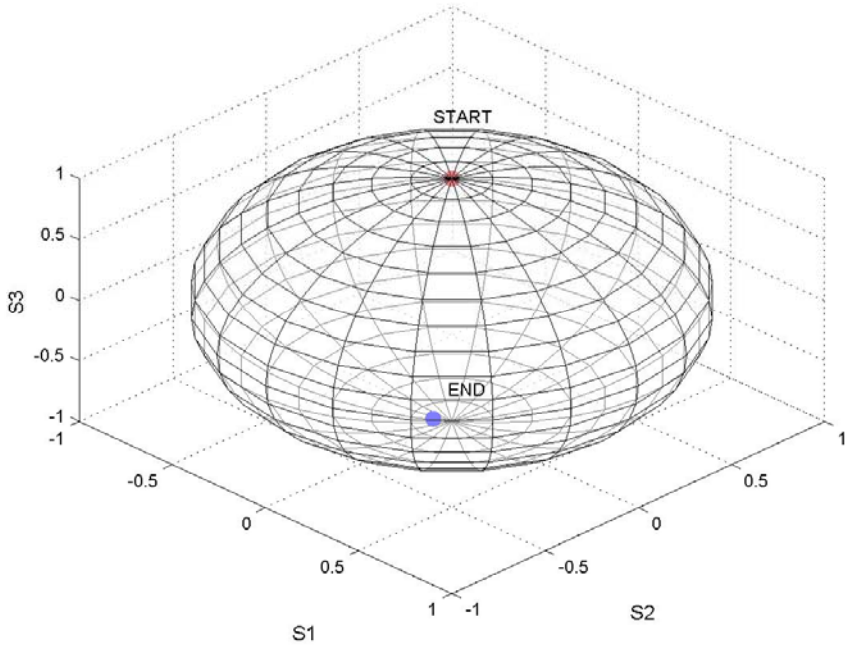

Figure 2-41 Initial and final SOP on Poincairé sphere (fixed coordinates)

Let left handed circularly polarized light be input at the un-spun end of the fiber:

$$\mathbf{A}(0) = \frac{1}{\sqrt{2}}\begin{bmatrix} 1 \\ -j \end{bmatrix} \tag{2.60}$$

Using Eq. (2.37), Eq. (2.33) and Eq. (2.34), we get:

$$\begin{aligned} &\mathbf{A}(L) = \mathbf{O}_F \widetilde{\Lambda} \mathbf{O}_0^{-1} \mathbf{A}(0) \\ &\mathbf{A}(L) = \frac{1}{2}\begin{bmatrix} 1 & j \\ j & 1 \end{bmatrix}\begin{bmatrix} e^{j\rho} & 0 \\ 0 & e^{-j\rho} \end{bmatrix}\begin{bmatrix} 1 & 0 \\ 0 & 1 \end{bmatrix}\begin{bmatrix} 1 \\ -j \end{bmatrix} \\ &\mathbf{A}(L) = \begin{bmatrix} \cos(\rho) \\ \sin(\rho) \end{bmatrix} \end{aligned} \tag{2.61}$$

Thus output light at the high-spun end is linearly polarized light and is oriented at an angle of ρ in the local coordinates at the high-spun end. We simulated the behavior of a

Huang plate excited by left circularly polarized light input at the un-spun end. Figure 2-42 shows the evolution of the amplitude in the fixed coordinates and Figure 2-43 shows the initial and the final SOP on a Poincairé sphere. At the input un-spun end **'x'** and **'y'** carry equal power, and both the supermodes are excited, the super modes beat along the fiber length such that a linearly polarized light exits at the output high-spun end. This light was found to make an angle of 1.2133 *radians* $= 69.51^0$ in the local coordinates. Since analytically the output linear light makes an angle of ρ in the local coordinates we have $\rho = 69.51^0$ as in Eq. (2.59).

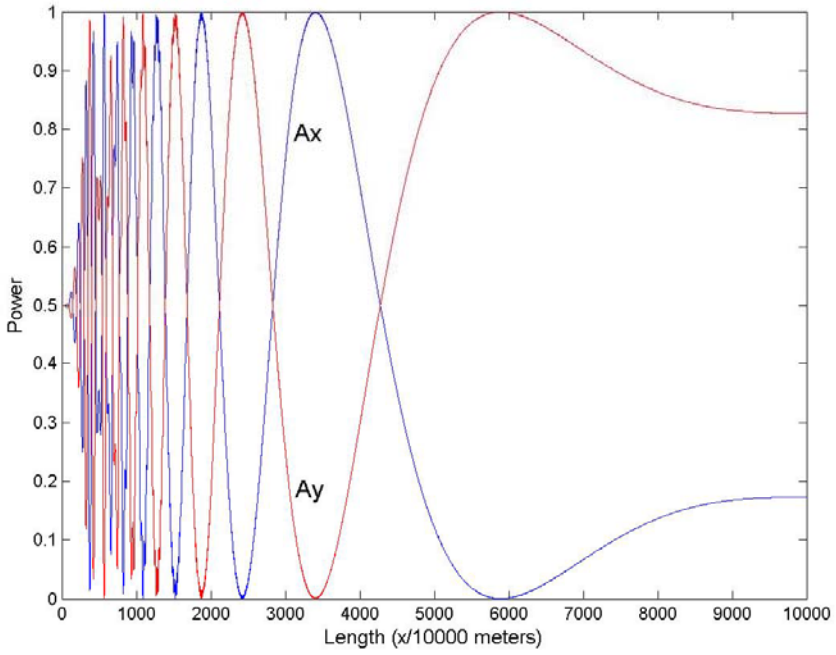

Figure 2-42 Evolution of amplitude in fixed coordinates

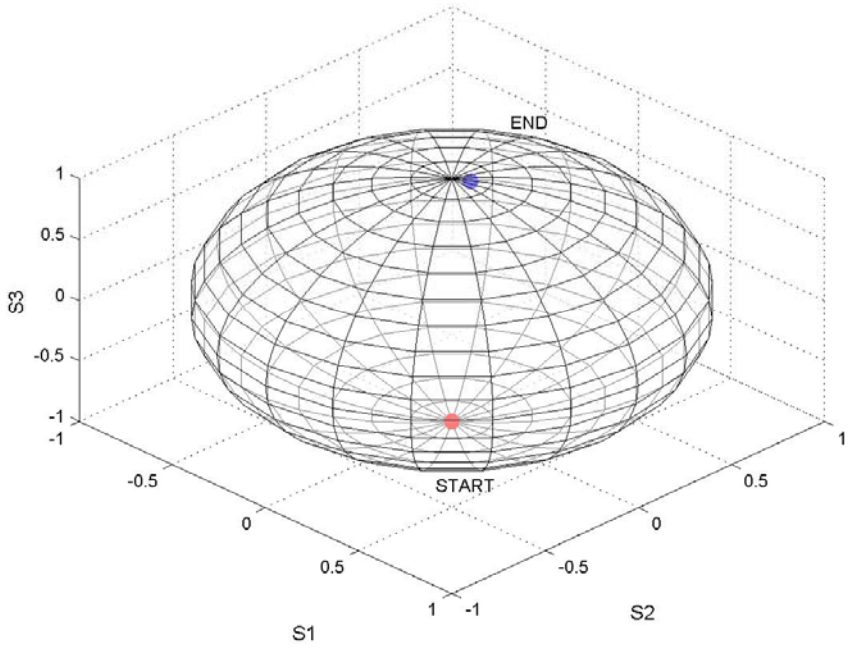

Figure 2-43 Initial and final SOP on Poincairé sphere (fixed coordinates)

The parameter ρ defined in Eq. (2.32) is a wavelength dependent term and will vary with the wavelength. Value of parameter ρ determines the location of the corresponding principal axes at the high-spun end and these axes rotate with the wavelength. The direct implication of this property is that the SOP transformation behavior of a Huang plate by the dual supermode process is wavelength dependent. While the SOP transformation from circular to linear polarization will take place (by the dual supermode process) independent of the wavelength the orientation of output linear light will be wavelength dependent. On the other hand the SOP transformation by single supermode process is completely wavelength independent.

We simulated this effect by varying the wavelength from 1 *um* to 2 *um* in steps of 0.01 *um*. The input was left-circularly polarized light at the un-spun end. Figure 2-44 shows computed value of parameter ρ (from output SOP) plotted against the wavelength. Figure 2-45 shows the orientation of the output linear light at the high-spun end as a function of

the wavelength. The points circle around the Poincairé sphere along its diameter indicating linear light of different orientations.

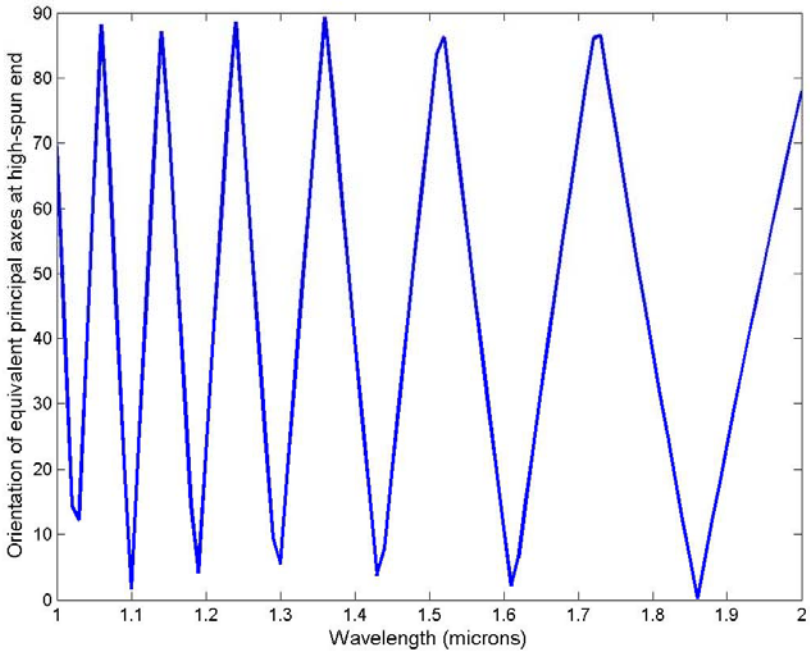

Figure 2-44 Orientation of the equivalent principal axes at high-spun end is wavelength dependent

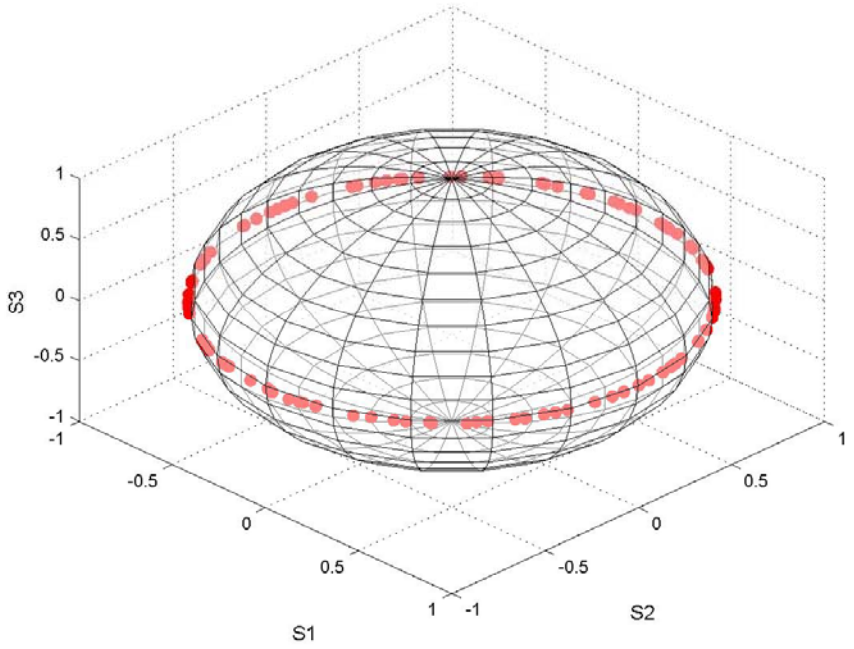

Figure 2-45 Wavelength dependence of orientation of principal axes at high-spun end plotted on Poincairé sphere.

Let linearly polarized light making an angle θ be input at the un-spun end of the fiber:

$$\mathbf{A}(0) = \begin{bmatrix} \cos\theta \\ \sin\theta \end{bmatrix} \tag{2.62}$$

Using Eq. (2.37), Eq. (2.33) and Eq. (2.34), we get:

$$\begin{aligned} \mathbf{A}(L) &= \mathbf{O}_F \widetilde{\Lambda} \mathbf{O}_0^{-1} \mathbf{A}(0) \\ \mathbf{A}(L) &= \frac{1}{\sqrt{2}} \begin{bmatrix} 1 & j \\ j & 1 \end{bmatrix} \begin{bmatrix} e^{j\rho} & 0 \\ 0 & e^{-j\rho} \end{bmatrix} \begin{bmatrix} 1 & 0 \\ 0 & 1 \end{bmatrix} \begin{bmatrix} \cos\theta \\ \sin\theta \end{bmatrix} \\ \mathbf{A}(L) &= \frac{1}{\sqrt{2}} \begin{bmatrix} \cos(\theta) e^{j\rho} + j\sin(\theta) e^{-j\rho} \\ j\cos(\theta) e^{j\rho} + \sin(\theta) e^{-j\rho} \end{bmatrix} \end{aligned} \tag{2.63}$$

Eq. (2.63) gives a general expression for the SOP of output light when input is θ-inclined linearly polarized light at the un-spun end. For $\theta = 0^0$ the input light is principal axis aligned and Eq. (2.63) gives a right circular light at high-spun end. Similarly, $\theta = 90^0$ is also a principal axis aligned linear light and Eq. (2.63) gives left circular light at the high-spun end. For $\theta = 45^0$, Eq. (2.63) gives a linearly polarized light at the output high-spun end. Thus as angle θ varies from $0^0 - 90^0$ the SOP at the output high-spun end goes from circular- elliptical-linear- opposite elliptical- opposite circular. This can be seen from Figure 2-46 which shows that the SOP of the output light at the high-spun end traces a longitude on a Poincairé sphere when the orientation of input linear light is varied from $0^0 - 350^0$.

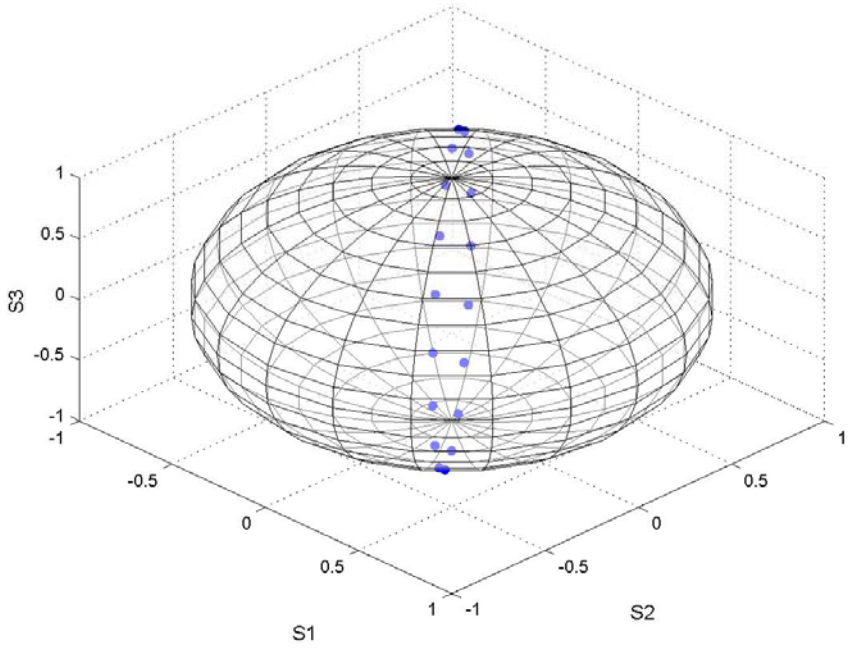

Figure 2-46 Output SOP when linearly polarized light at different orientation input at un-spun end

Input High-spun end

Principal states of polarization at the high-spun end are right and left circularly polarized light. If the SOP of the input light is not circular then both the supermodes are excited

and transmission takes place by the dual supermode process. In this section we will analyze and simulate the behavior of a Huang plate when non-circularly polarized light excites the high-spun end.

Let θ-inclined linearly polarized light be input at the high-spun end:

$$\mathbf{A}(0) = \begin{bmatrix} \cos\theta \\ \sin\theta \end{bmatrix} \tag{2.64}$$

Using Eq. (2.37), Eq. (2.33) and Eq. (2.34), we get:

$$\begin{aligned} &\mathbf{A}(L) = \mathbf{O}_0 \widetilde{\Lambda} \mathbf{O}_F^{-1} \mathbf{A}(0) \\ &\mathbf{A}(L) = \frac{1}{\sqrt{2}} \begin{bmatrix} 1 & 0 \\ 0 & 1 \end{bmatrix} \begin{bmatrix} e^{j\rho} & 0 \\ 0 & e^{-j\rho} \end{bmatrix} \begin{bmatrix} 1 & -j \\ -j & 1 \end{bmatrix} \begin{bmatrix} \cos\theta \\ \sin\theta \end{bmatrix} \\ &\mathbf{A}(L) = \frac{1}{\sqrt{2}} \begin{bmatrix} e^{j(\rho-\theta)} \\ -je^{-j(\rho-\theta)} \end{bmatrix} = \frac{1}{\sqrt{2}} \begin{bmatrix} e^{j(\rho-\theta)} \\ e^{-j(\frac{\pi}{2}+\rho-\theta)} \end{bmatrix} \end{aligned} \tag{2.65}$$

Eq. (2.65) gives an expression for the SOP of the output light at the un-spun end when θ-inclined linearly polarized light is input at the high-spun end. Let ζ be the phase difference between the components of $\mathbf{A}(L)$ in Eq. (2.65). We have:

$$\begin{aligned} \zeta &= -(\frac{\pi}{2} + \rho - \theta) - (\rho - \theta) \\ \zeta &= -\frac{\pi}{2} - 2\rho + 2\theta \end{aligned} \tag{2.66}$$

From Eq. (2.66) if the input linear light at the high spun is inclined by $\theta = \rho$ in the local coordinates then the phase difference of the output light will be $-\pi/2$ i.e. the output light at the un-spun end will be left circularly polarized. We simulated the behavior of a Huang plate excited by ρ-inclined linearly polarized light at the high-spun end. The numerical value of $\rho = 69.51^0$ was determined in the previous section by means of the simulation in Eq. (2.59). Figure 2-47 shows the evolution of the amplitude along the fiber length in the fixed coordinates. The SOP transformation takes place by the dual supermode process

where two super modes beat along the fiber length with varying beatlength in such a manner that they carry equal amount power at the output un-spun end. Figure 2-48 shows the initial and the final SOP plotted on a Poincairé sphere. The initial SOP can be seen as a dot on the equator on the back surface of the Poincairé sphere. The final SOP is at the south-pole indicating a left circularly polarized light at the output un-spun end.

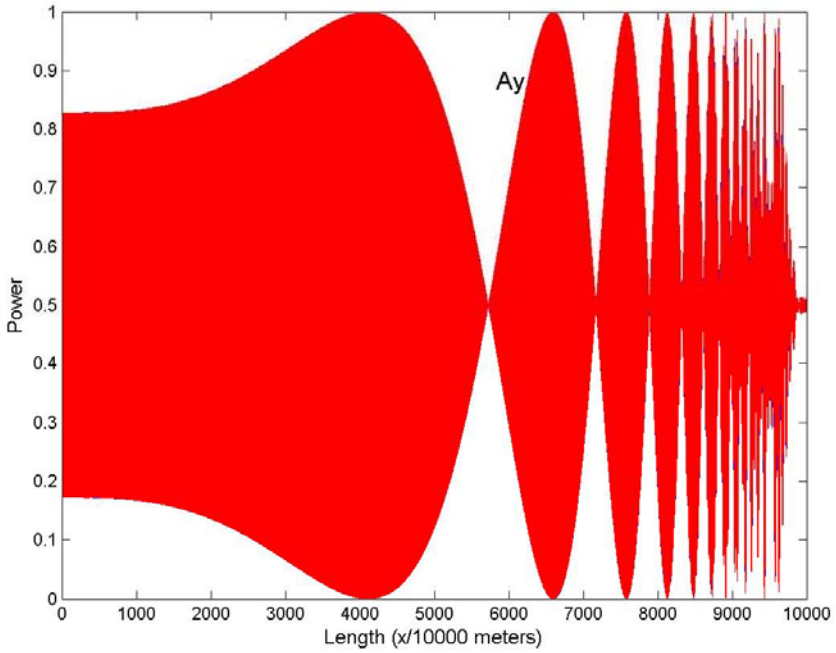

Figure 2-47 Evolution of amplitude when ρ-inclined linearly polarized light excites high spun end (fixed coordinates)

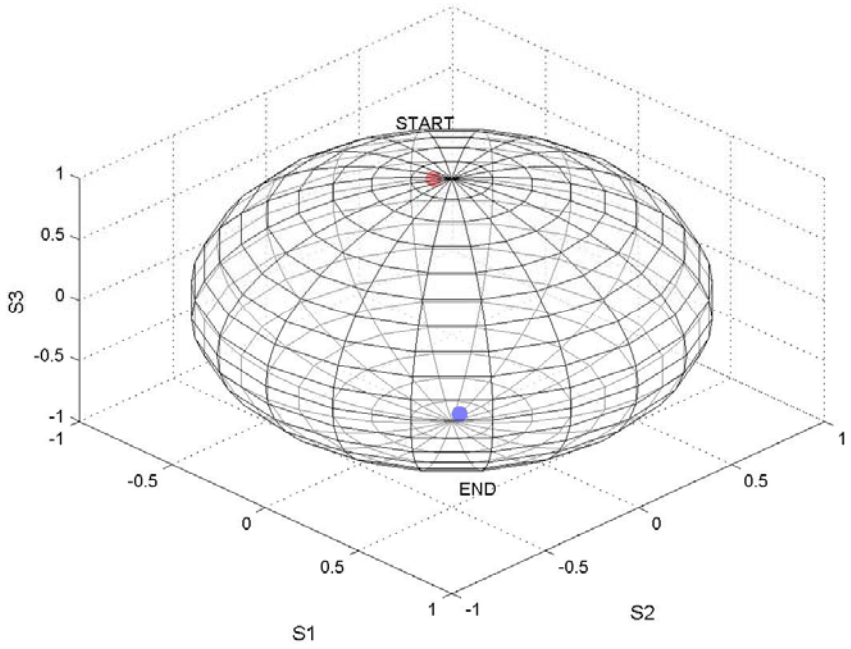

Figure 2-48 Initial and Final SOP on Poincairé sphere (fixed coordinates)

From Eq. (2.66) if the input linear light at the high spun is inclined by $\theta = \rho + \pi/4$ in local coordinates then the phase difference of the output light will be 0^0 i.e. the output light at the un-spun end will be linearly polarized. We simulated the behavior of a Huang plate excited by $\rho + \pi/4 = 114.51^0$-inclined linearly polarized light at the high-spun end. Figure 2-49 shows the evolution of amplitude along the fiber length in the fixed coordinates. Figure 2-50 shows the initial and the final SOP plotted on a Poincairé sphere. The initial SOP can be seen as a dot on the equator on the right side of the Poincairé sphere. The final SOP is shown by the dot on the equator towards left side of the Poincairé sphere indicating a linear SOP at the output un-spun end.

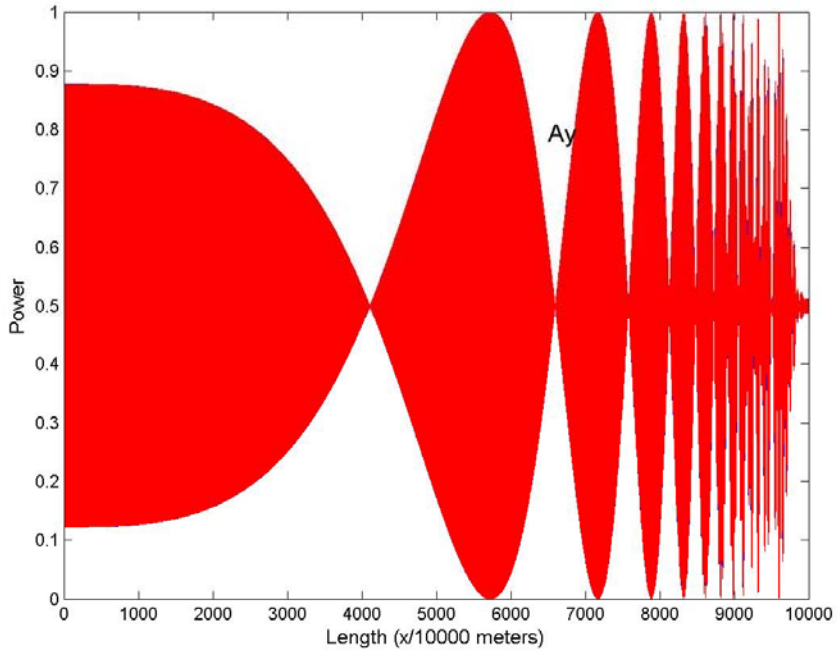

Figure 2-49 Evolution of amplitude for (ρ+45^0)-inclined linear excitation at high-spun end (fixed coordinates)

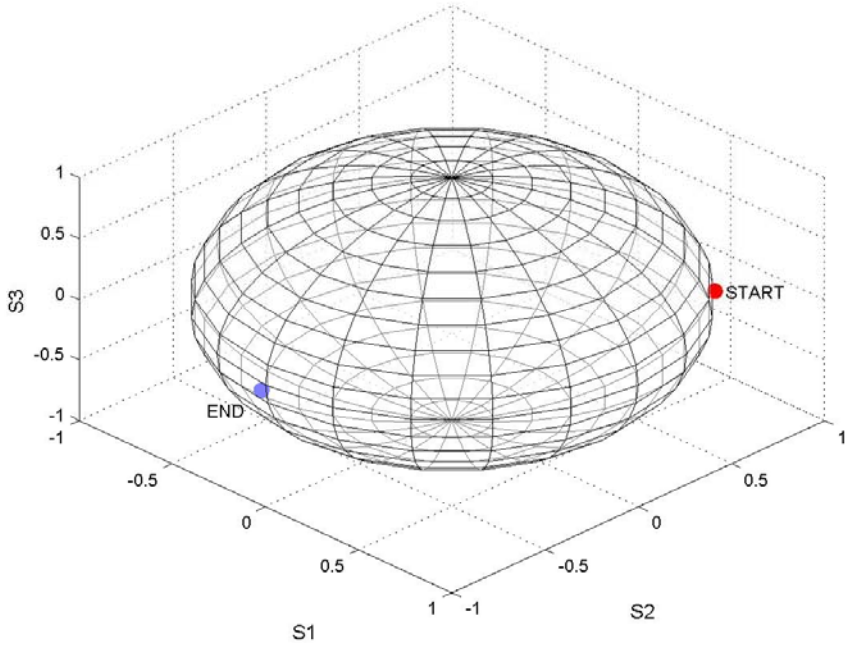

Figure 2-50 Initial and final SOP on Poincairé sphere (fixed coordinates)

Similarly for $\theta = \rho + \pi/2$-inclined input linear light at the high-spun end, Eq. (2.66) suggests that the output light at the un-spun end will be right circularly polarized. Figure 2-51 shows the initial and the final SOP plotted on a Poincairé sphere. The SOP of the output light from the un-spun end can be seen as the dot at the north-pole of the Poincairé sphere indicating right circularly polarized light.

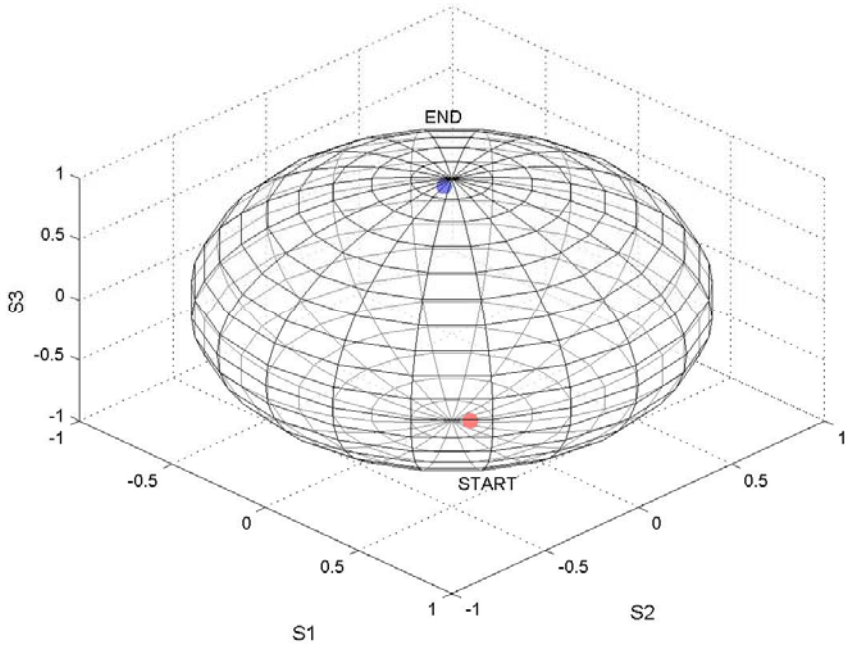

Figure 2-51 Initial and final SOP on Poincairé sphere (fixed coordinates)

Linearly polarized light can be considered as a linear combination of right and left circularly polarized light. We have shown that the circularly polarized light input on the high-spun end exits as a principal axis aligned linearly polarized light at the un-spun end. Thus when linearly polarized light is input at the high spun end power exiting in the **'x'** and the **'y'** directions at the un-spun end must be equal. This property is referred to as the '*equal power division property*'. From Eq. (2.65) it can be seen that:

$$|A_1|^2 = |A_2|^2 = 0.5 \qquad 2.67$$

We simulated the behavior of a Huang plate with θ-inclined linearly polarized light exciting the high-spun end with θ varying from 0^0-350^0. Figure 2-52 shows the power division factor defined as $|A_1|^2 / |A_2|^2$.

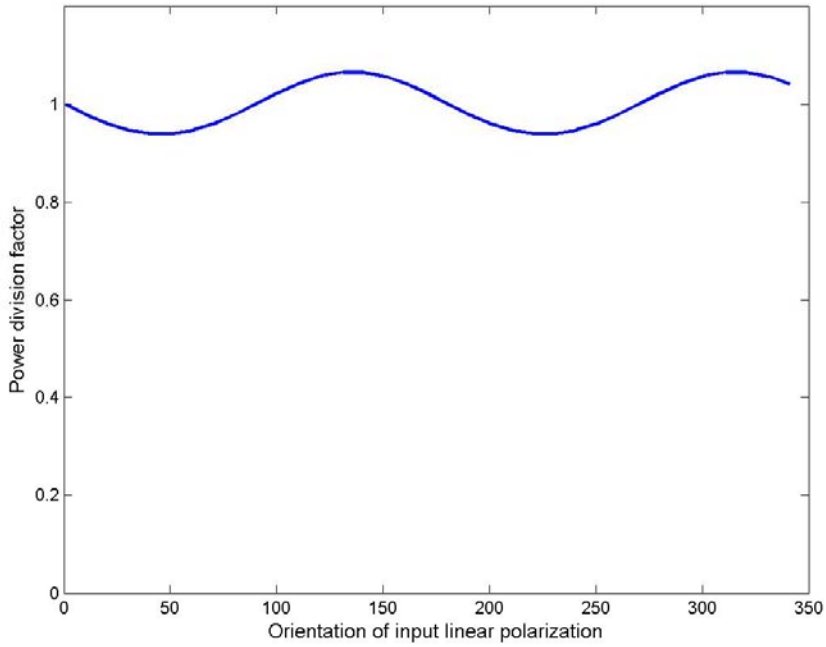

Figure 2-52 Power division factor ($|A_1|^2 / |A_2|^2$)

Single supermode process v/s dual supermode process

In case of the single supermode process light is launched at the input end (un-spun or high-spun) so that the SOP of the input light matches one of the principal states of polarization (linear or circular) at that end. There is a gradual evolution the principal state of polarization and hence, that of the SOP of the input light as it propagates to the output end. Only one supermode is involved throughout the transmission. The wavelength dependent term ρ appears in the phase term of the transformed light e.g. Eq. (2.50). This results in a wavelength independent SOP transformation by the single supermode process. On the other end the SOP transformation by the dual supermode process involves both the supermodes. Two supermodes beat and exchange power as they

propagate down the fiber in a fashion that a desired SOP transformation can be achieved for an appropriate input SOP. However since beating of the modes is involved this process is prone to the variation in the external environment of the fiber and the Huang plate behavior may change with the changes in the surrounding conditions. Also the wavelength dependent term ρ now appears inside the Jones vector of the transformed light (Eq. (2.58)) and determines the SOP of the output light. In other words the SOP transformation by the dual-supermode process is a wavelength dependent process. Hence for practical applications the Huang plates must be used to perform the SOP transformations by single supermode process.

Dependence of SOP transformation on structural parameters

In this section we shall examine the dependence of the SOP transformation by a Huang plates on its structural parameters. Huang plate is a variably spun birefringent fiber element with spin rate slowly varying from zero to very fast or vice versa. The spin rate at the un-spun end is zero, at the fast spun end is very high quantified by the parameter $Q_{\max}$, and the variation in the spin rate is slow (modeled by Eq. (2.39)). In Eq. (2.39) the term γ was said to control the location of the maximum slope of Q. By the means of simulation we shall investigate the effect of varying $Q_{\max}$, γ and total length (L) of the fiber on the SOP transformation behavior of Huang plates. The analysis is important from a practical point of view as we can determine the tolerance levels for these parameters. Knowing the tolerance levels is essential to identify the stringent requirements while designing the fiber draw process for Huang plates. In the simulation we shall use the un-spun end as the input end, and the initial SOP as **'x'**-aligned linearly polarized light. We shall vary one parameter while keeping the others constant to study the effects on the SOP transformation.

Effect of varying Q_{max}

Keeping γ, L as constants we vary Q_{max} from 10 to 50 in steps of 10 and plot the SOP of the output light at the high-spun end on a Poincairé sphere. Figure 2-53 shows the spin variation along the fiber length for different Q_{max} levels. Figure 2-54 and Figure 2-55 show that as Q_{max} increases the SOP of the output light approaches the north-pole of the Poincairé sphere. We conclude that Q_{max} is an important parameter governing the performance of Huang plates and $Q_{max} > 40$ is required to achieve practically useful SOP transformation.

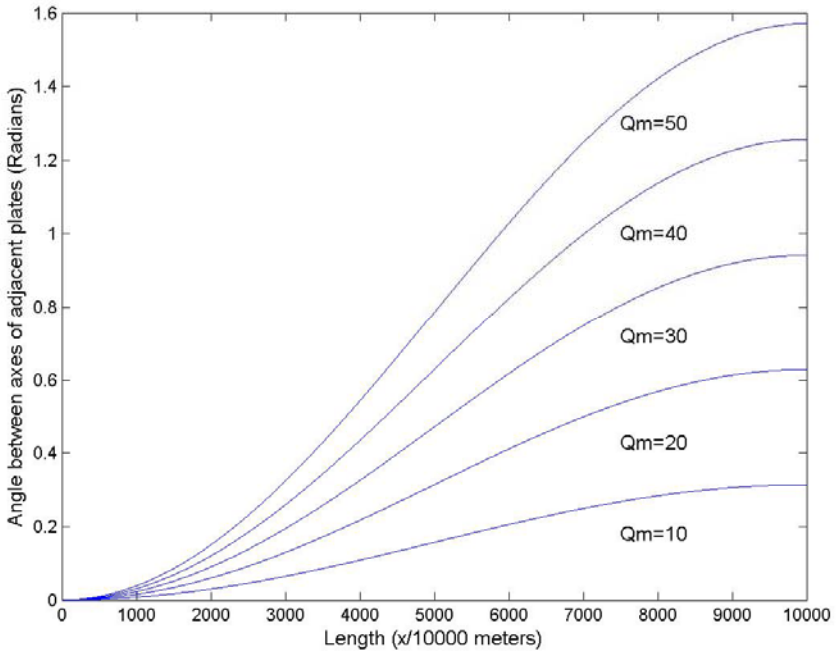

Figure 2-53 Spin variation at different Q_{max} levels

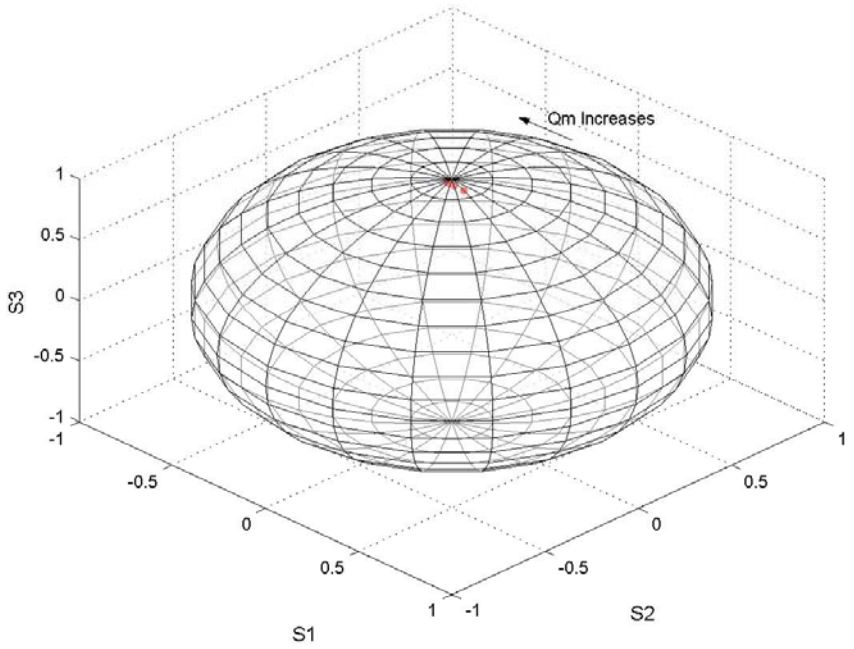

Figure 2-54 Dependence of SOP transformation on $Q_{\max}$

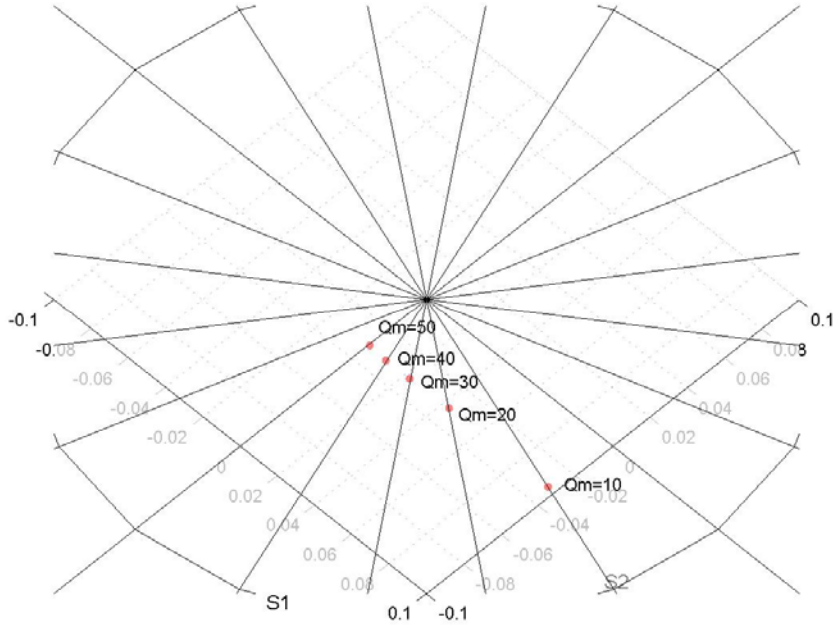

Figure 2-55 Dependence of SOP transformation on $Q_{\max}$ -zoomed

Ideally the spin rate at the high-spun end should be infinite; however there is a limit on how fast the preform can be spun during the linear draw. For example a value of Q_{max} =50 was used in our simulations corresponding to a practically achievable spin rate. Consequently the principal state of polarization at the high-spun end of a practical Huang plate is not quite the circular polarization state. This can also be seen from Figure 2-55 where the point representing the output SOP, for Q_{max} =50 is located very close to the North Pole of the Poincairé sphere but not at the pole. As a result of this, when circularly polarized light is launched in to the high-spun end of a practical Huang plate most of the light is launched in the desired supermode and the remaining light is launched in the other supermode. This causes some beating between the two supermodes along the fiber length as shown by the thickness of curves in Figure 2-56.

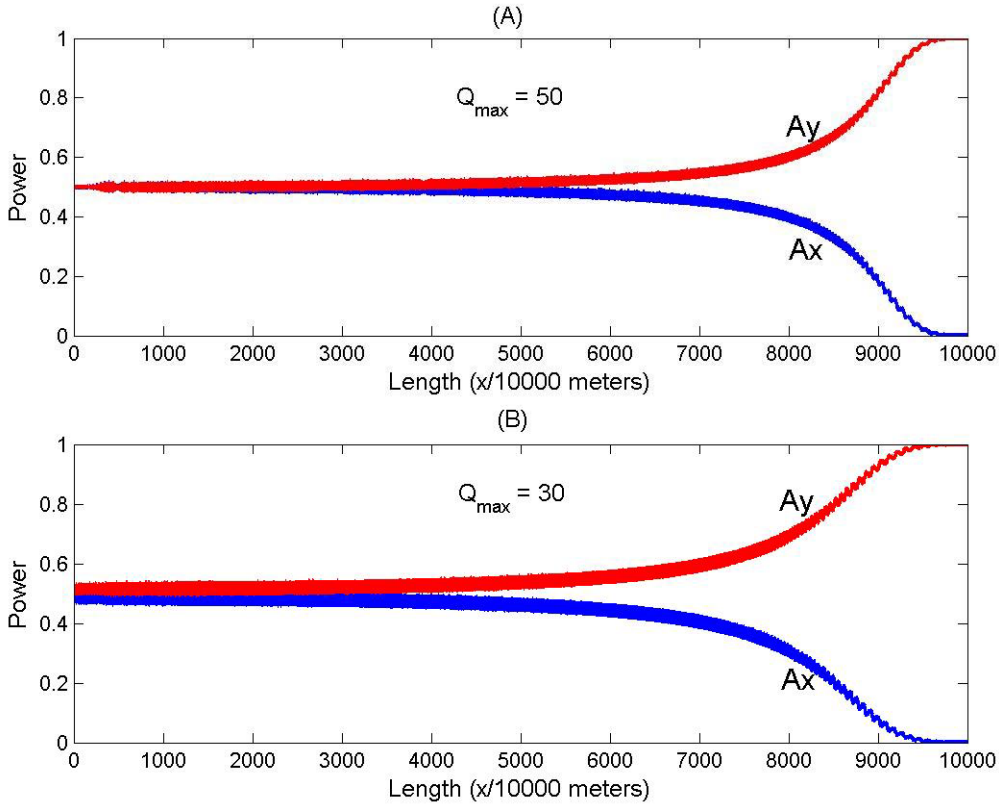

Figure 2-56 Effect of Q_{max}

From the above discussion one would expect that, if the value of Q_{max} is made smaller then for circularly polarized input light at the high-spun end, comparatively more power will be launched in the un-desired super mode and the magnitude of beating between the supermodes will be larger. This is shown in Figure 2-56 where, Q_{max} = 50 for Part (A) and Q_{max} = 30 for Part (B). Clearly, the curves in Part (B) are thicker as compared to the curves in Part (A), indicating greater amount of beating between the two supermodes for Q_{max} = 30.

Effect of varying γ

Keeping Q_{max} , L as constants we vary γ from 0.5 to 2.5 in steps of 0.5 and plot the SOP of the output light at the high-spun end on a Poincairé sphere. Figure 2-57 shows the spin variation along the fiber length for different γ levels. Figure 2-58 and Figure 2-59 show that as γ increases above a value of 0.5 the SOP of the output light does not change much and appears as a same point on the Poincairé sphere. We conclude that if $\gamma > 0.5$ the tolerance level for γ-value is high. In other words the manner in which the spin rate varies from zero-to-very fast is not important as long as it varies slowly.

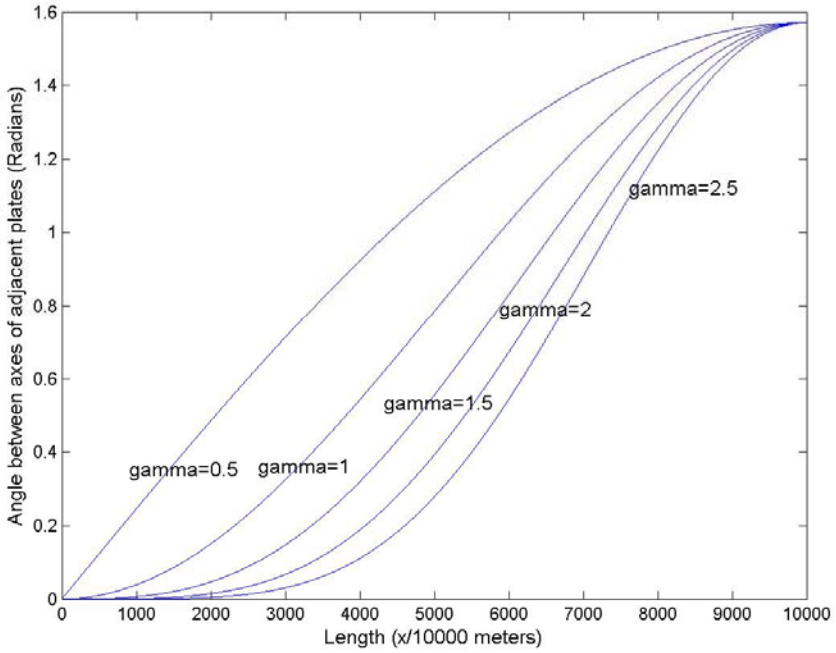

Figure 2-57 Spin rate variation for different γ - levels

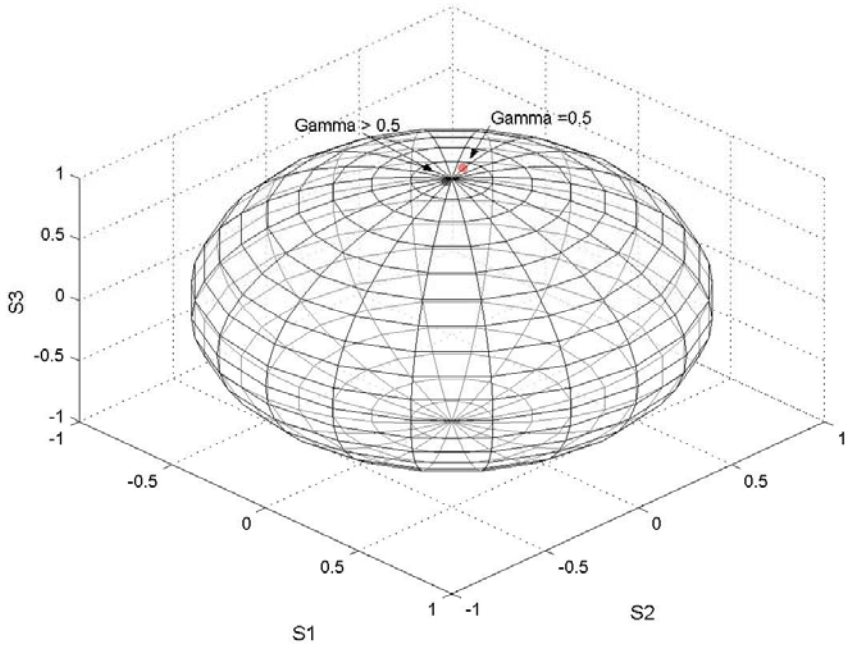

Figure 2-58 Dependence of SOP transformation on γ - value

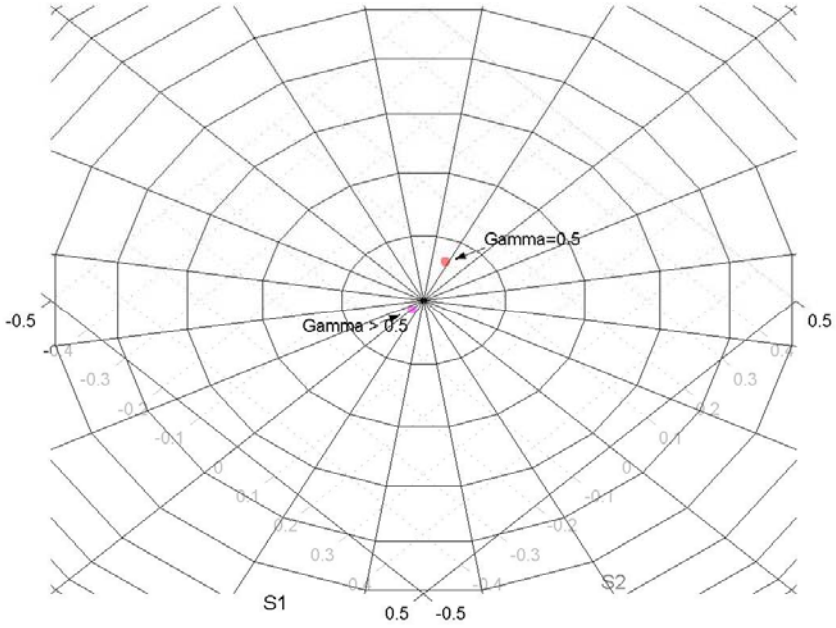

Figure 2-59 Dependence of SOP transformation on γ - level (zoomed)

Effect of varying fiber length L

From Figure 2-6 and Figure 2-7 we can see that for $Q_{\max} = 50$ and $\gamma = 1$, SOP of the output light rapidly approaches the right circular polarization state after 70 *cm* along the fiber. Keeping $Q_{\max}$, γ as constants we vary L from 10 *cm* to 70 *cm* in steps of 10 *cm* and plot the SOP of the output light at the high-spun end on a Poincairé sphere. Figure 2-60 shows that as length (L) approaches 70 *cm* (35 un-spun fiber beatlengths) the SOP of the output light approaches the North Pole on the Poincairé sphere. We conclude that for $Q_{\max} = 50$, fiber length (L) > $35 \times beatlength$ (L_b) is required to achieve a practically useful SOP transformation.

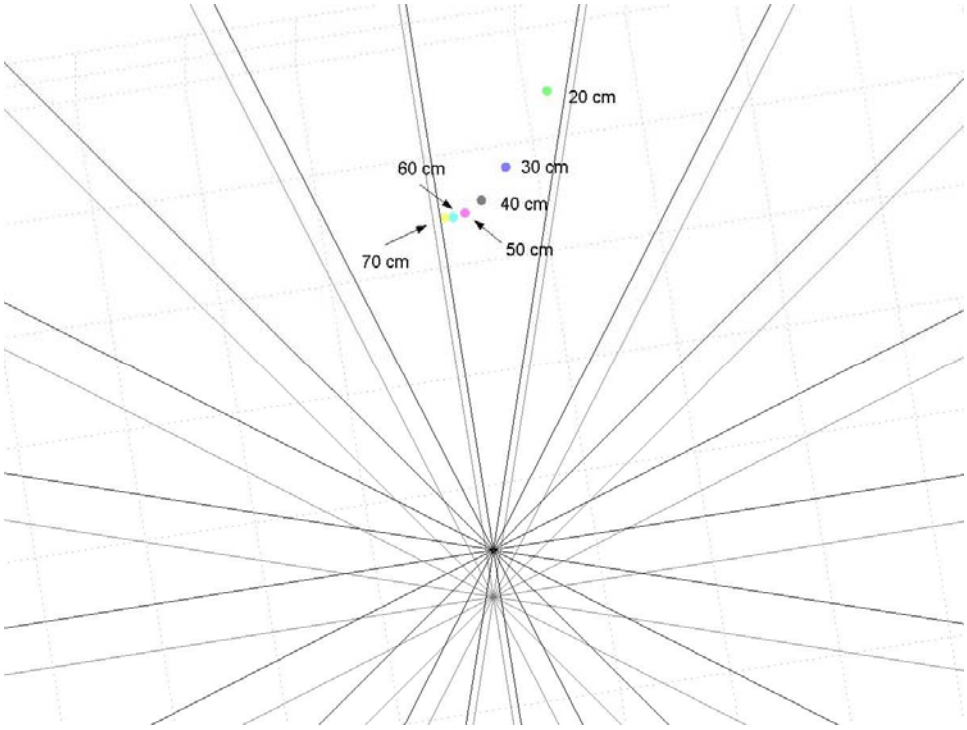

Figure 2-60 Dependence of SOP transformation on length- zoomed

2.6 *Cascaded structures*

In the previous sections we presented a detailed description of the operation of Huang plates and showed that they behave like bulk-optics quarter waveplates with a favorable feature of being inherently wideband. Higher order (half and full wave- like) structures can be constructed by appropriately cascading two Huang plates. The behavior of the cascaded system depends on whether they are cascaded at the un-spun end or the high-spun end and whether the two sections have same spin (clockwise or anti-clockwise) or opposite spin. Naturally the structures of interest should be the ones that can be drawn in one continuous draw without resorting to a tedious procedure of post-draw cascading.

All fiber half waveplate

All-fiber half waveplate- like behavior can be obtained by cascading two Huang plates with opposite spin at the un-spun end. From the point of view of fabrication the preform is spun very fast to start with and the spin rate is gradually reduced to zero and then it is spun in the opposite sense and the spin rate is slowly increased to a large value. It is not required that the maximum spin rate at the beginning and the end of the fiber be the same. The lengths of the two sections can also be different. As in the case of Huang plates the only requirement is that the spin rate in the fast-spun region is large and the variation of the spin rate should be slow. A simulation model consisting of a stack of birefringent waveplates can be constructed similar to that described in section 2.4. Figure 2-61 shows the spin rate variation used in our simulation model.

From analysis point of view it is more convenient to treat the structure as one system however the operation can be readily viewed by treating it as two separate quarter wave sections. Let the first section have clockwise spin and the second section have anti-clockwise spin. If a left circular light is launched in to the section with clockwise spin, the SOP transformation takes place by the single supermode process and the principal axis aligned linearly polarized light is obtained at its un-spun end. This linearly polarized light is also aligned along the principal axis of next section as it is a continuous structure. Since the direction of the spin of the next section is anti-clockwise the principal axis aligned linearly polarized input light exits as a right hand circular light after the SOP transformation by the single supermode process. This behavior is analogous to the bulk-optic half waveplates which are often used to transform handedness of circularly polarized light.

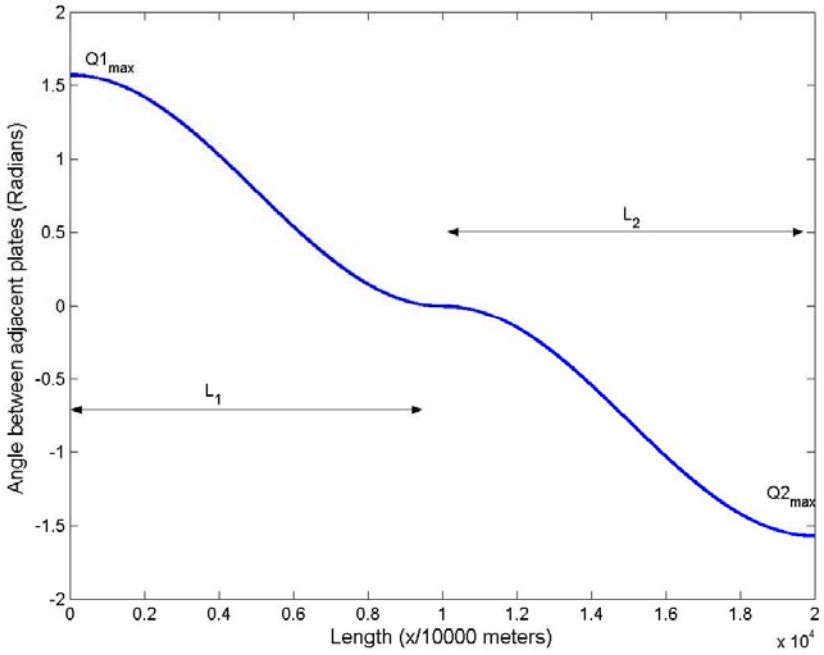

Figure 2-61 Spin rate variation for all-fiber half wave plates

The composite structure can be analyzed by following the same procedure adopted in section 2.3. The section with the opposite spin can be analyzed by putting $-\tau(z)$ for $\tau(z)$ in Eq. (2.25) and following the same steps thereon.

We simulated the behavior of the composite structure. The simulation parameters used were same as those used for simulating the Huang plates. Left circularly polarized light was used as an input to the section with clockwise spin. Figure 2-62 and Figure 2-63 show the evolution of the amplitude and the phase in the local coordinates. Equal power is launched in both the modes at the input end, in the course of the transmission all the power is coupled to the **'y'**-mode after which the power is coupled back to the **'x'**-mode and both the modes carry a same amount of power at the output end. The phase difference evolves from $-\pi/2$ to $\pi/2$ radians. Figure 2-64 and Figure 2-65 show the evolution of the SOP on the Poincairé sphere and the initial and the final SOP in the local coordinates respectively. Figure 2-66-to-Figure 2-69 show the evolution of the SOP in the fixed coordinates.

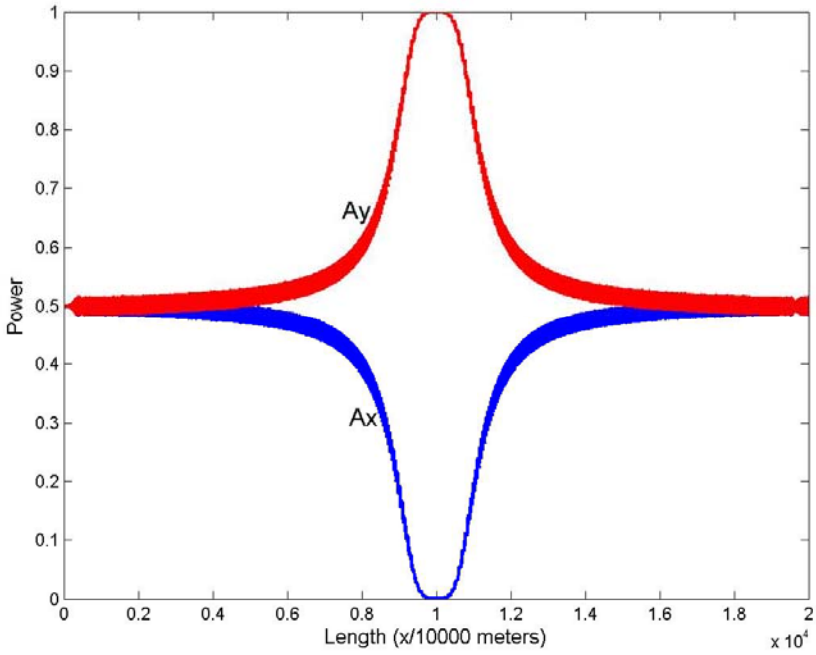

Figure 2-62 Evolution of amplitude in local coordinates

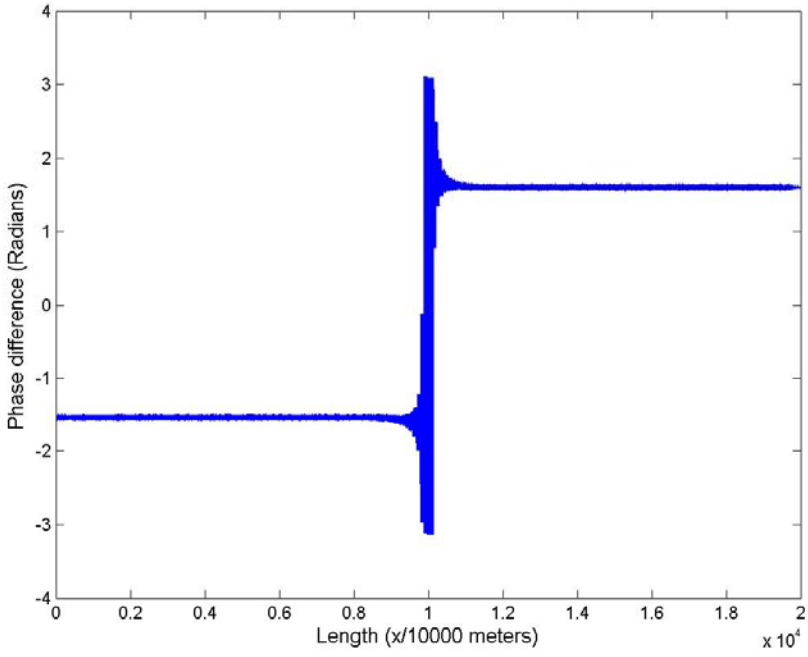

Figure 2-63 Evolution of phase difference in local coordinates

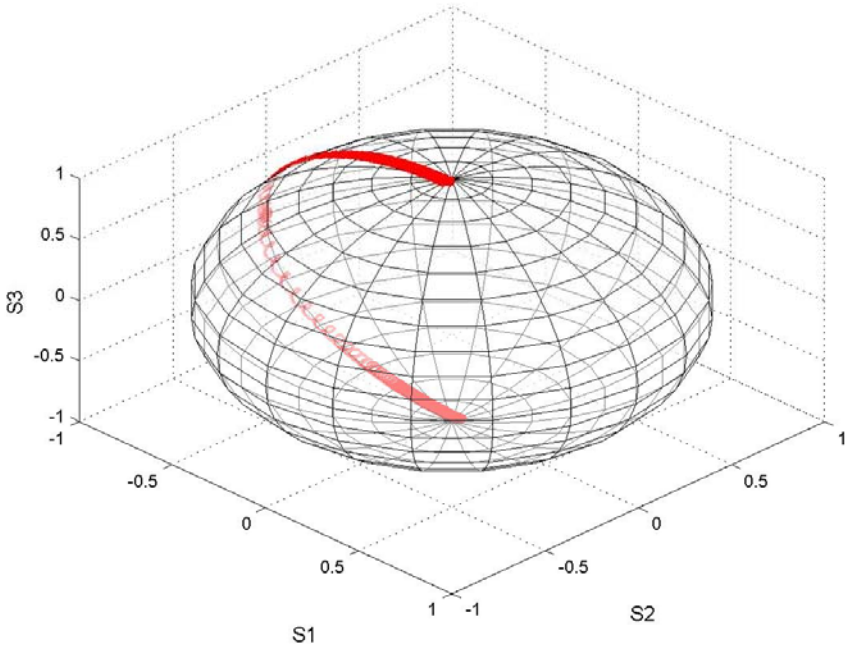

Figure 2-64 Evolution of SOP on Poincairé sphere (local coordinates)

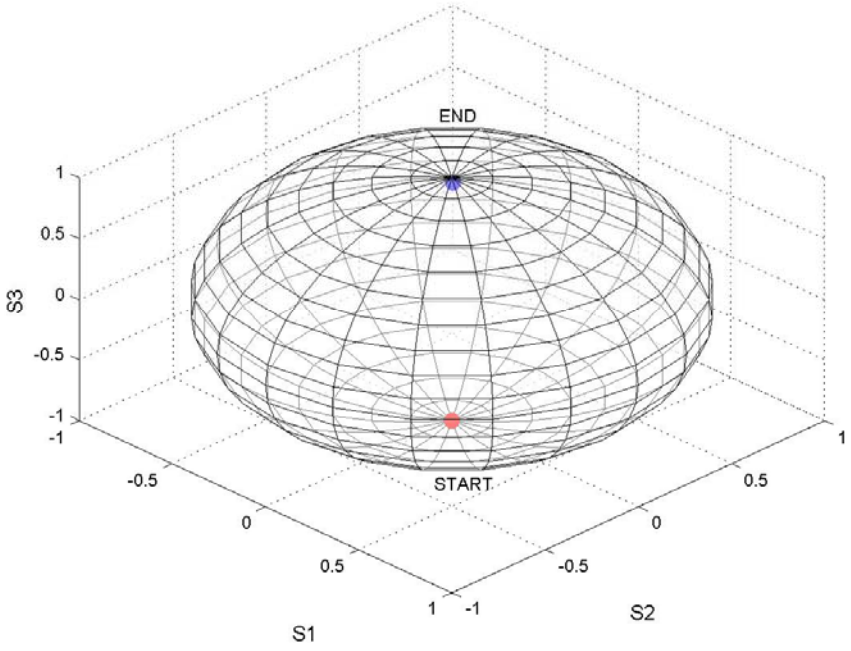

Figure 2-65 Initial and final SOP on Poincairé sphere (local coordinates)

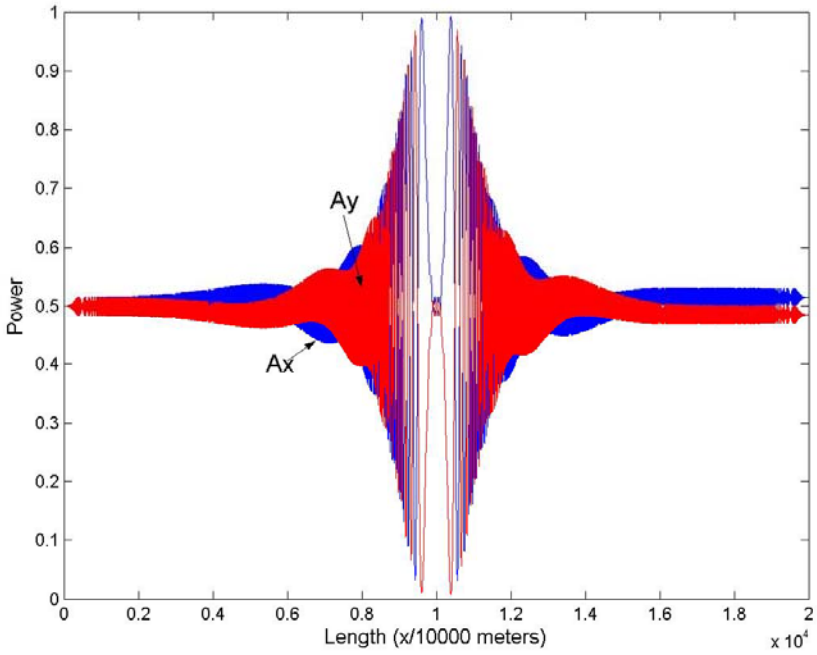

Figure 2-66 Evolution of amplitude in fixed coordinates

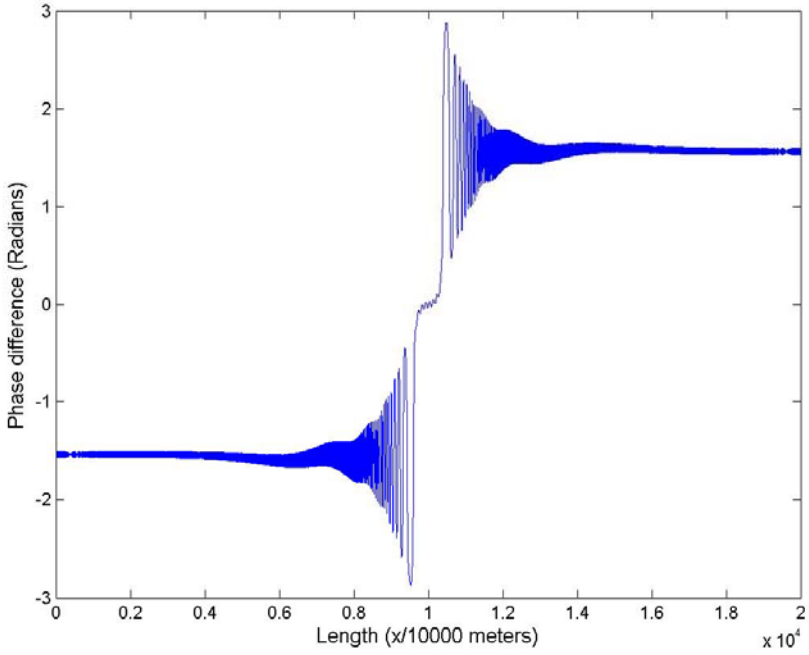

Figure 2-67 Evolution of phase difference in fixed coordinates

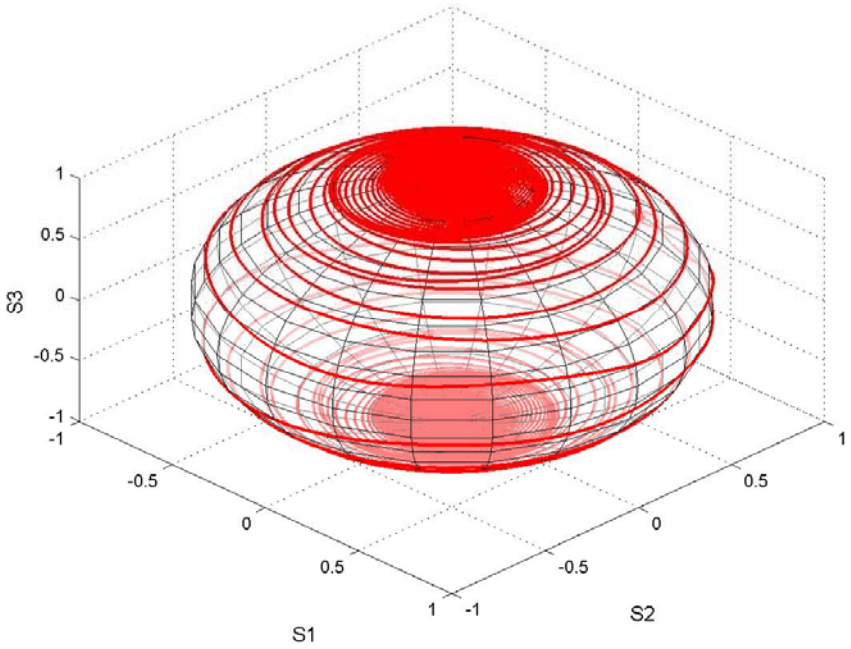

Figure 2-68 Evolution of SOP on Poincairé sphere (fixed coordinates)

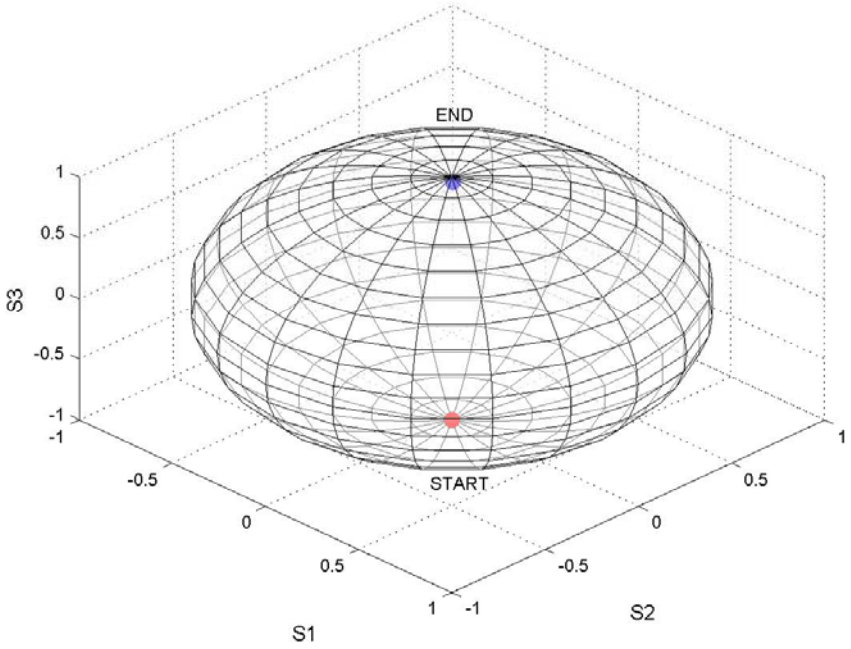

Figure 2-69 Initial and final SOP on Poincairé sphere (fixed coordinates)

For θ-oriented linearly polarized input light the SOP transformation takes place by the dual super mode process. Equal power division property causes the **'x'**-mode and the **'y'**-mode to carry equal power at the un-spun end of the first section. In other words the next section is excited by a SOP that launches equal power in the **'x'**-mode and the **'y'**-mode at its input. Irrespective of the phase difference between the **'x'**-mode and the **'y'**-mode at its input the output at the high-spun end of this section will always be a linearly polarized light. The output linearly polarized light can shown to be oriented at an angle:

$$\alpha = \rho + \frac{\pi}{2} - \theta \qquad 2.68$$

Form Eq. (2.68) if the orientation of the input linear light changes by $\Delta\theta$ the orientation of the output linear light changes by $-\Delta\theta$. This behavior is similar to bulk-optic half waveplates.

All-fiber full waveplate

All-fiber full waveplate- like behavior can be obtained by cascading two Huang plates with the same spin at the un-spun end. From a point of view of fabrication the preform is spun very fast to start with and the spin rate is gradually reduced to zero and then is again gradually increased to very fast. A simulation model consisting of a stack of birefringent waveplates can be constructed similar to that described in section 2.4. Figure 2-70 shows the spin rate variation used in our simulation model.

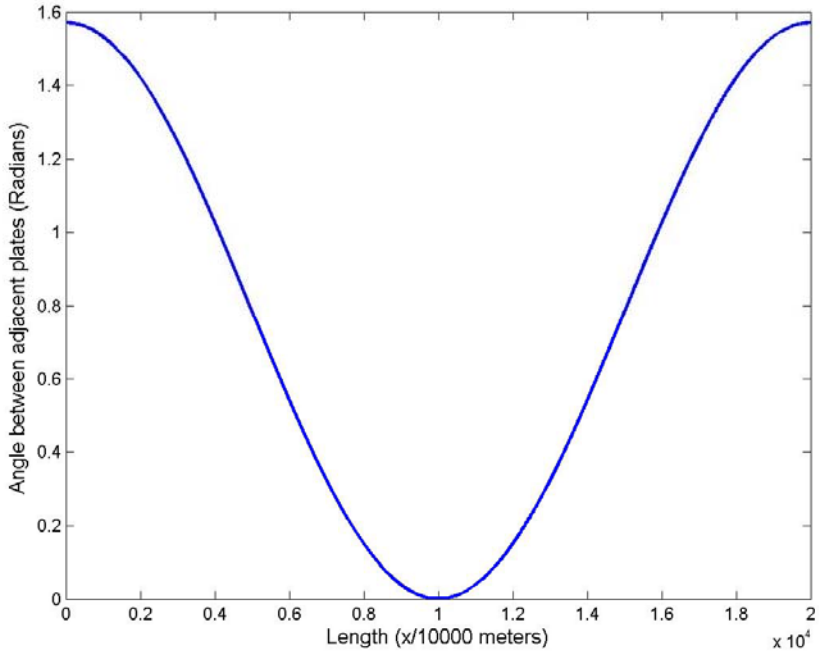

Figure 2-70 Spin rate variation for all-fiber full wave plates

We simulated the behavior of the composite structure. Right circularly polarized light was used as an input. The SOP transformation takes place by the single supermode process. Figure 2-71 and Figure 2-72 show the evolution of the amplitude and the phase in the local coordinates. Equal power is launched in both the modes at the input end, in the course of the transmission all the power is coupled to the **'x'**-mode after which the power is coupled back to the **'y'**-mode and both the modes carry same amount of power at the output end. The phase difference evolves from $\pi/2$ radians to 0 back to $\pi/2$ radians. Figure 2-73 and Figure 2-74 show the evolution of the SOP on the Poincairé sphere and the initial and the final SOP in the local coordinates respectively. The SOP transformation behavior is analogous to bulk-optic full waveplates.

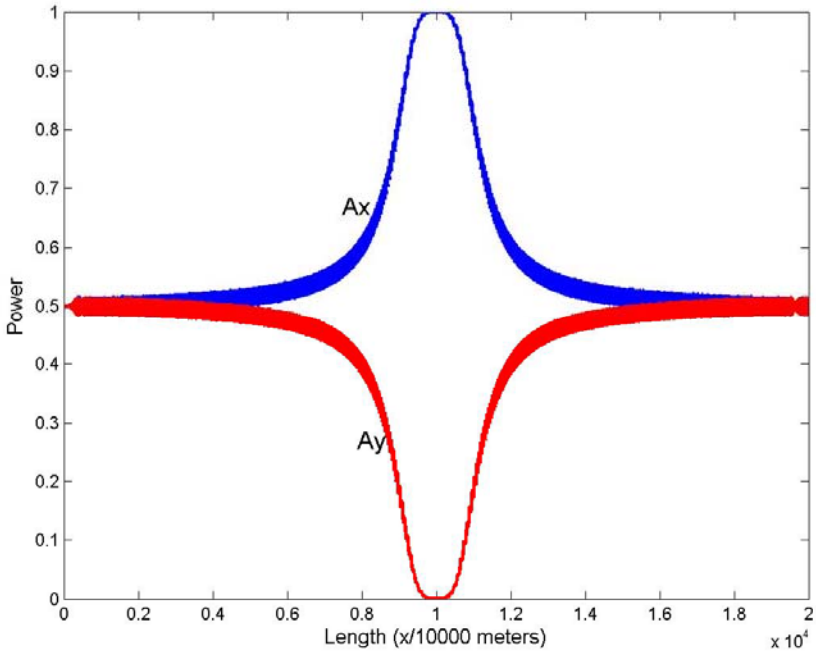

Figure 2-71 Evolution of amplitude in local coordinates

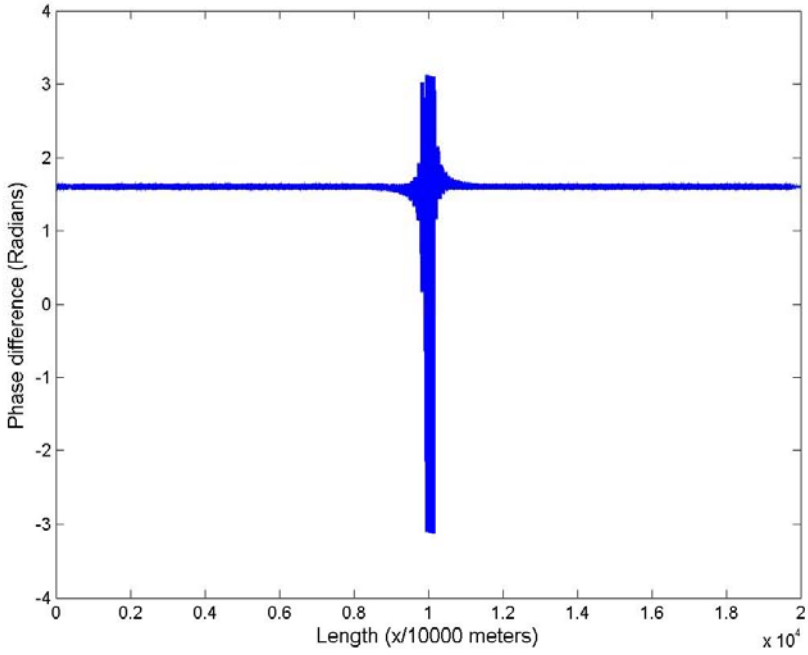

Figure 2-72 Evolution of phase difference in local coordinates

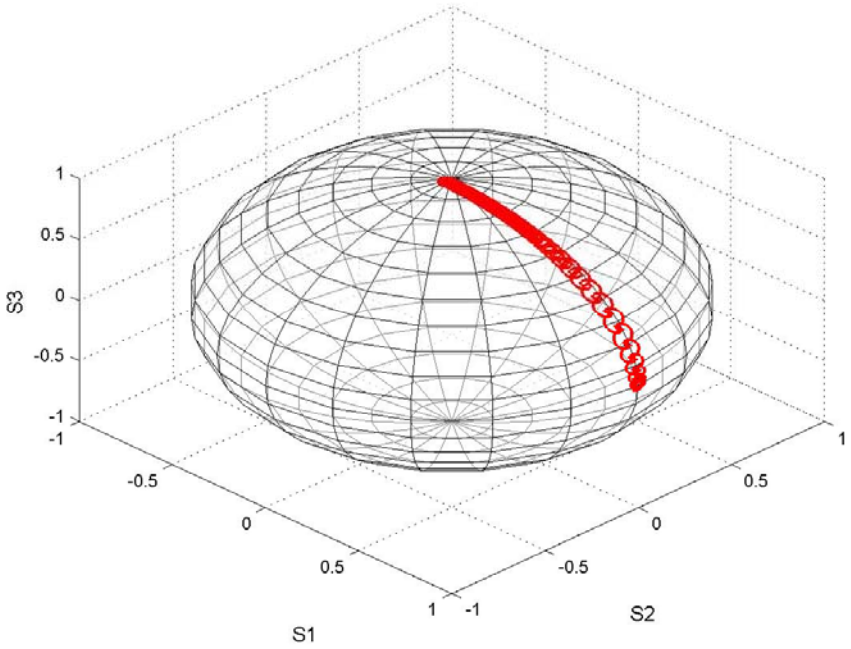

Figure 2-73 Evolution of SOP on Poincairé sphere (local coordinates)

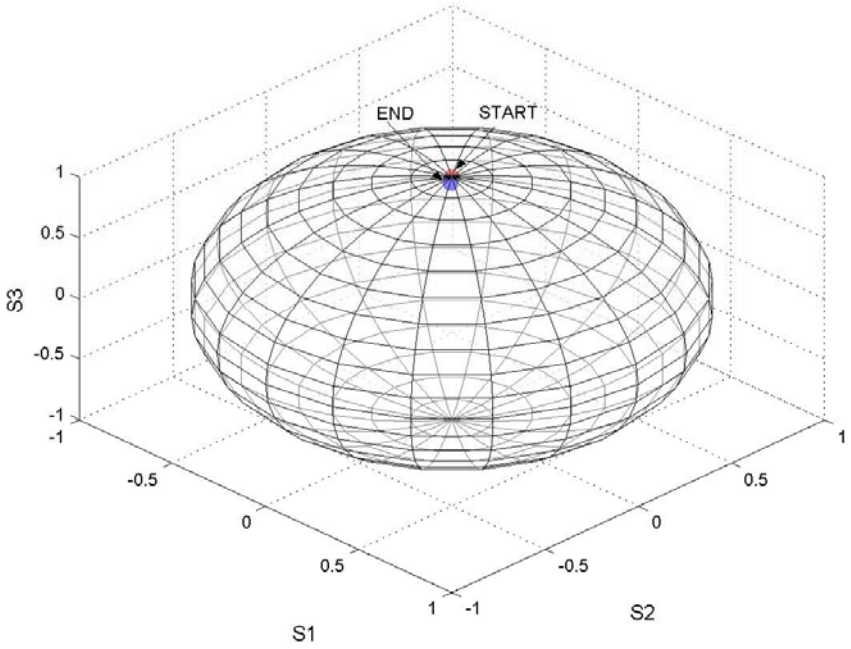

Figure 2-74 Initial and final SOP on Poincairé sphere (local coordinates)

For θ-oriented linearly polarized input light the SOP transformation takes place by the dual super mode process. Following the same argument as that given for the half-waveplates linearly polarized light is obtained at the output end. Output linear light can be shown to be oriented at an angle:

$$\alpha = \theta - \rho$$
$$\rho = \rho_1 + \rho_2 \qquad 2.69$$

Where ρ_1 and ρ_2 are the global structural parameters of the two sections making the composite structure. Form Eq. (2.69) if the orientation of the input linear light changes by $\Delta\theta$ the orientation of the output linear light also changes by $\Delta\theta$ in the same direction. This behavior is similar to bulk-optic full waveplates.

2.7 *PMD Analysis*

PMD characterization of an optical device is important from a systems point of view in order to calculate the PMD penalty that a device will introduce if it is used in the system. One can think of PMD as the maximum deferential group delay (DGD) between the two principal polarization states. In the case of Huang plates if the SOP of the input light matches the principal state of polarization at the input end (principal axes aligned linear at the un-spun end and orthogonal circular at the high-spun end) then only one supermode (section 2.3) is involved during the transmission. In such a case the SOP transformation is wavelength independent and the device will not introduce any PMD penalty in the system.

If the SOP of the input light does not match the principal state of polarization at the input end then SOP transformation takes place by the dual supermode process. In this case both the supermodes are excited and they beat along the fiber length. Two super modes are associated with different group velocities causing the DGD. Thus a Huang plate will introduce some PMD penalty if it is used to transform the SOP by the dual supermode process.

We computed PMD of a Huang plate by simulating a PMD measurement by the polarizer analyzer method [23]. Left circularly polarized light was used as an input from the un-spun end. The wavelength of the input light was varied from 1 μm –to- 2 μm in steps of 0.01 μm. The analyzer at the output high-spun end was simulated by looking at the output power along a fixed direction at the output high-spun end. Figure 2-75 shows the power at the output of the polarizer plotted against the wavelength (microns). It can be seen that there are 7 peaks in the wavelength range 1 μm –to- 2 μm. The value for PMD can be calculated using the equation:

$$\mathbf{PMD}\,(ps/km) = \frac{\mathbf{N}\,\lambda_1\lambda_2}{L(\lambda_2 - \lambda_1)} \cdot \frac{1}{c} \qquad 2.70$$

Putting $\lambda_1 = 1\ \mu m$, $\lambda_2 = 2\ \mu m$, **N**= 7, L= 1m, c = 3 x 10^{-7} *km/ps* in Eq. (2.70), we get:

$$\mathbf{PMD}\ (ps/km) = 46.67 \qquad 2.71$$

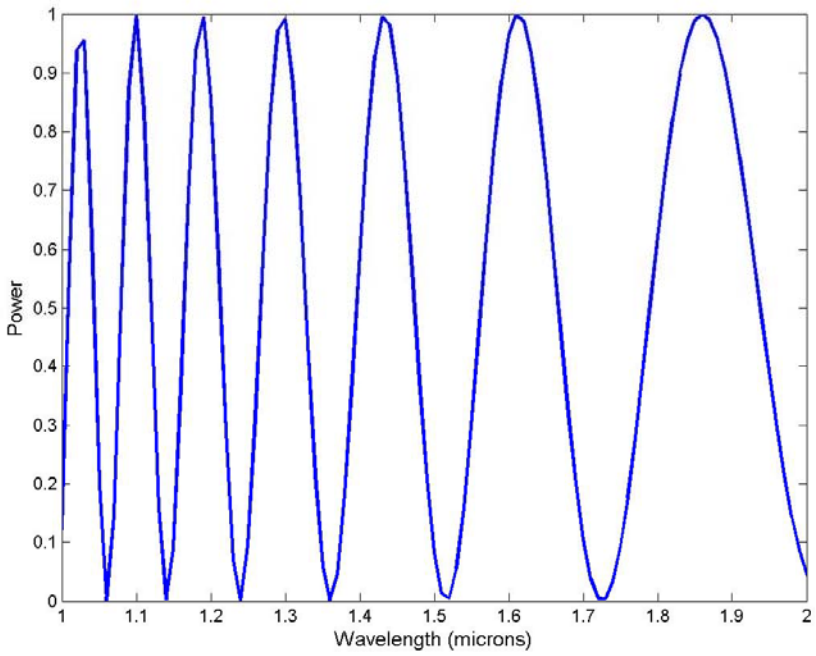

Figure 2-75 Polarizer- analyzer method for PMD calculations

2.8 *Summary*

In this chapter we discussed the SOP transformation characteristics of a variably spun birefringent fiber element in general and Huang plates in particular. We developed a simulation model consisting of a stack of birefringent waveplates and used this model to study the SOP transformation behavior of Huang plates and composite structures. We found that the simulation results confirm well with the theoretical predictions. We also employed the simulation as a tool to understand the tolerances of the different structural parameters on the operation of Huang plates. In the following chapter we will present the experimental results.

Chapter 3. Experimental verification of all-fiber wide band quarter-wave plates

3.1 Introduction

Many commercial and laboratory application of fiber optics require an ability to manipulate, change and control the state of polarization of light. This is usually accomplished with bulk-optic wave plates which are inherently narrowband, bulky, and often require careful manual tuning and adjustments. H.C. Huang has recently demonstrated that a variably spun birefringent fiber with a spin rate slowly varying from zero to very fast (or vice versa) will transform the state of polarization (SOP) from linear to circular (and vice versa). Such a fiber element is similar in many ways to a quarter-wave plate. [1] The most remarkable feature of the Huang fiber is that the transformation of linear to circular polarization is independent of wavelength over the entire single mode range of the fiber.

In this chapter we present the results of experiments at Virginia Tech which show that the Huang fiber indeed functions like a quarter-wave plate over a broad wavelength band.

3.2 Characteristics of Huang plates

In an optical fiber SOP transformations take place either intentionally (PM fibers) or unintentionally (stress induced birefringence). Practical optical fibers always have some intrinsic birefringence as the result of perturbations and imperfections during the fabrication process resulting in the loss of degeneracy between two polarization modes of a single mode fiber. This degeneracy can be characterized by the beat length (L_b) of the fiber. Incident linear light undergoes all the possible SOP changes in half the beat length. However these SOP changes are highly sensitive to input SOP, wavelength, physical surroundings etc and are in general extremely difficult to control with repeatability hence of little practical value.

Bulk optic waveplates work on the principle that an accurate phase difference can be produced due to group delay between rays traveling along the ordinary and extraordinary axes in inherently birefringent crystals like quartz, mica or stack of birefringent polymer films. This phase difference can be adjusted ($\pi/2$ for a $\lambda/4$ plate) to obtain the desired SOP transformation (linear to circular and vice versa for $\lambda/4$ plate) at a particular wavelength. However the phase difference at any other wavelength will be different, hence the narrow band nature of these waveplates.

The principal states [11] of the bulk wave plate are linear polarizations along the two principal axes. The birefringence is the difference in phase velocities for these principal states. If a linear light is incident on a bulk optic quarter waveplate along one of the axes (ordinary or extra-ordinary) no SOP transformation takes place and the output light is linear with same orientation. However if the input linear light is oriented so that it makes an angle of 45^0 with respect to the principal axes then the output light is circularly polarized. If the linear light makes an angle of - 45^0 (i.e. rotated by 90^0) then the output light is circular with opposite handedness. If the input SOP is circular then the output light is linear and is oriented at $\pm 45^0$ with respect of the axes depending on the handedness of the input circular light. This behavior of the bulk optic quarter waveplate is reciprocal in that it behaves the same if the light is input on either face of the wave plate.

In the Huang plates the principal axes of a birefringent fiber rotate along the fiber with slowly increasing rotation rate per unit length. At the un-spun end the axis rotation per unit length is zero while at the high-spun end there are several rotations of the internal axes within one birefringence beat length (Figure 3-1). These quarter-wave fibers can be made by applying a variable spin to a birefringent prefrom during the drawing of the fiber or by heating and twisting a birefringent fiber. The operation of the Huang plate can be best seen by comparing its principal polarization states with those of a bulk wave plate. [7]

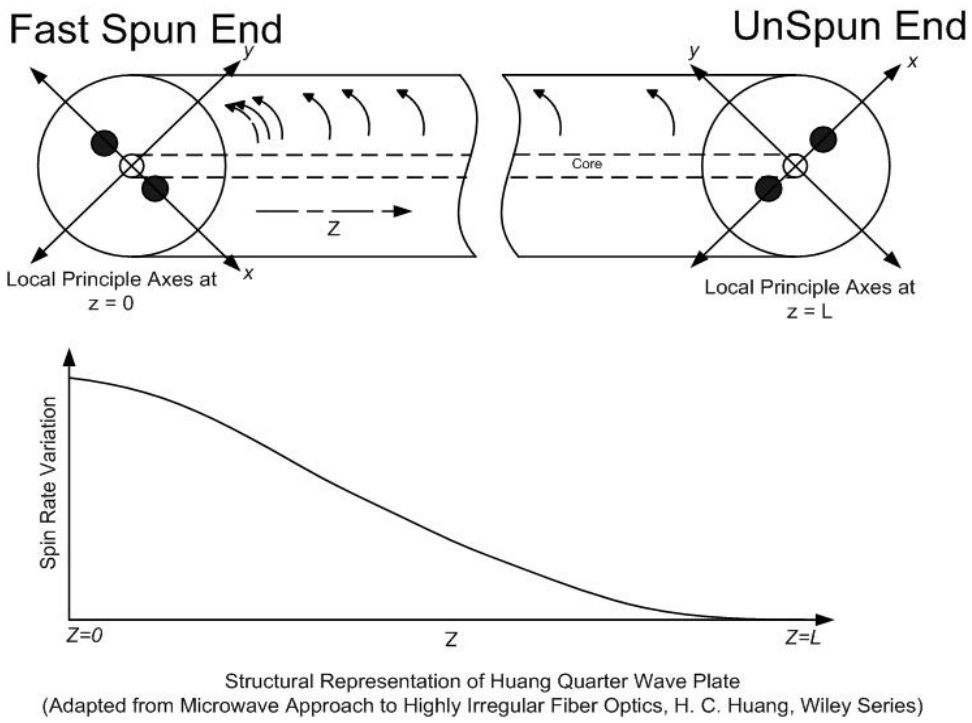

Figure 3-1 Structure of Huang plates

The principal states of the Huang quarter wave fiber show an evolution from linear to circular from un-spun end to high-spun end along the fiber. At the un-spun end the principal polarization states are linear and directed along the internal birefringence axes. At the high-spun end the corresponding principal polarization states are orthogonal circular polarizations. The remarkable feature of the Huang plate is that the transformation from linear to circular polarization from the un-spun end to high-spun end is independent of wavelength.

The polarization properties of both the bulk wave plate and the Huang plate can be obtained from a linear combination of their principal polarization states. For example, linear polarization at 45^0 to the birefringence axes of the un-spun end of the Huang fiber will exit the high-end as a sum of two equal but opposite circular polarizations. The state of output polarization will be linear at some angle with respect to the internal birefringence axes. This angle is determined by the accumulated phase difference between the two principal states at that wavelength.

The Huang fiber functions like a quarter-wave plate but with an interesting asymmetry. The birefringence axes of the un-spun end act like 45 degree excitation of a bulk quarter-wave plate as shown in Figure 3-2. At the high-spun end axes equivalent to the principal states of a quarter-wave plate can also be found. However, the equivalent quarter-wave axes at the high-spun end rotate with wavelength (refer Figure 2-44) while they are fixed with respect to the internal birefringence axes at the un-spun end.

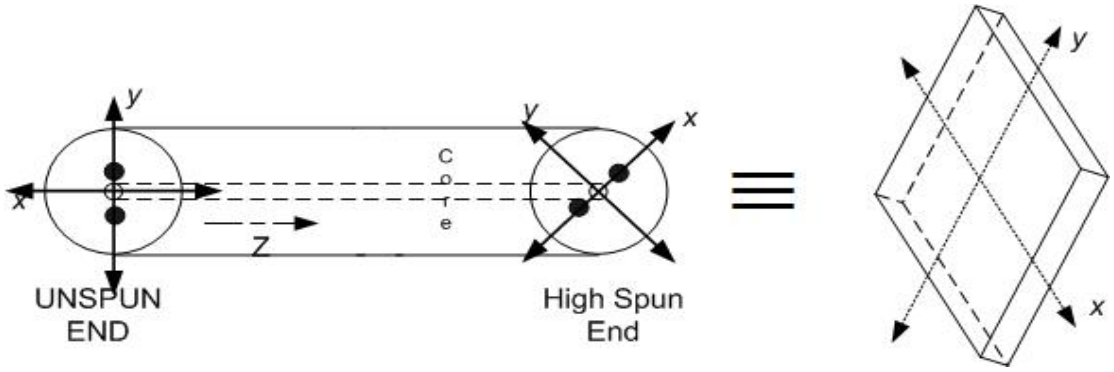

Figure 3-2 Equivalence with bulk-optic quarter-wave plate

3.3 Experiments on Huang plates

In this section we will experimentally explore polarization transformation properties of the Huang quarter-wave fiber. In particular, we see the transformation of linear to circular polarization and from circular to linear polarization starting from either the un-spun or the high-end of the fiber. Measurements are made at both 1310 nm and 1550 nm demonstrating the wavelength independence of the quarter-wave transformation.

Experiment setup

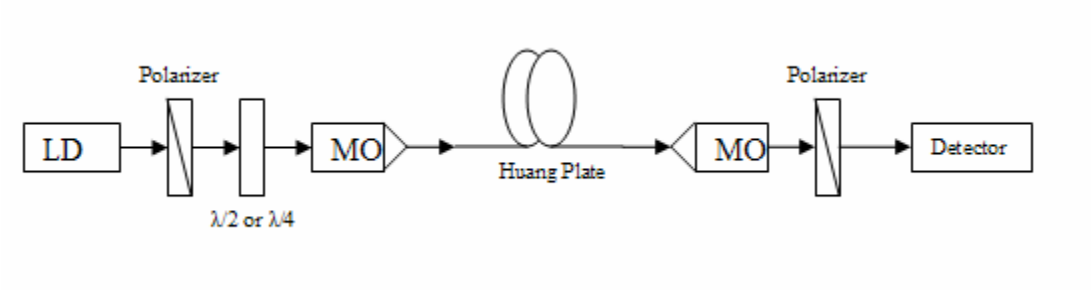

Figure 3-3 Experiment setup

The experimental setup is shown in Figure 3-3. Light from the source diode (**LD**: 1310 nm or 1550 nm) is passed through a microscope objective (**MO**) to obtain a parallel beam. It is then passed through a polarizer. The light at the output of the polarizer has an extinction ratio of 30 dB. This linearly polarized light is passed through a HWP/QWP shown as $\lambda/2$ *or* $\lambda/4$ in the figure. Any orientation of the linear polarization can be obtained by rotating the HWP. Circular state of polarization can be obtained by adjusting the axes of QWP at 45^{o} with respect to the orientation of the linearly polarized light. The best circular light thus obtained has an extinction ratio of 0.4 dB. Thus we can obtain all the states of polarization required for this experiment. The light with the desired SOP is then launched in to the Huang plate (~20 cm long) by focusing it using a MO. At the other end the light coming out of the Huang plate is made parallel and focused on to a detector via a polarizer. The output SOP can be analyzed by rotating the polarizer and recording the power using a power meter.

Huang plate is asymmetric in that it behaves differently when the light is launched from the other end. Hence once all the measurements were completed from one end (say high-spun end) the entire set up was reversed and the experiment was repeated from the other end (un-spun end).

Input at un-spun end (1310 nm)

The results for linearly polarized light launched into the un-spun end at a wavelength of 1310 nm are summarized in Table 3-1. Using the principal states model, we expect that linear light launched along the birefringence axes will be transformed to a circular polarization state at the output. By analogy with the bulk quarter-wave plate we expect a linearly polarized output if light is launched at 45 degrees to the birefringence axes. The results in Table 3-1 confirm these expectations although the best circular light at the high-spun end has an extinction ratio of only 2.7 dB. We attribute this to the short length of the fiber under test causing incomplete SOP transformation.

Change in the orientation of input light (degrees)	Orientation of Pmax in Laboratory coordinates	Extinction (dB)	SOP
0	140	2.71	**Circular**
45	95	16.32	**Linear**
90	50	3.19	**Circular**
135	5	16.91	**Linear**
180	320	3.07	**Circular**
225	275	16.29	**Linear**
270	230	3.55	**Circular**
315	185	16.22	**Linear**

Table 3-1 Table showing SOP of output light when linearly polarized light is input at un-spun end. First column shows the orientation of input light with respect to internal birefringent axes at un-spun end

The output changes from circular to linear for rotations of the input polarization orientation of 45 degrees. The output angles for maximum and minimum extinction are also 45 degrees apart as would be expected from the principal states model. Note that it was not possible to get an accurate measurement of the orientation of the birefringence axes at un-spun end by imaging the end of the fiber. The orientations of the axes were taken as the angles that produced the output SOP with the smallest ellipticity.

When circularly polarized light is input at the un-spun end the two principal states will be equally excited. The output will be linearly polarized since it is a sum of two equal and opposite circular polarizations with some phase difference between them. By analogy with a bulk quarter-wave plate the output will be linearly polarized at an angle 45 degrees from the linearly polarized output using linear input excitation. Indeed, with circularly polarized input light the output is found to be linear (Extinction ratio ~16 dB) and is oriented along 50 degrees in laboratory co-ordinates. When the handedness of the circularly polarized input is reversed by rotating the QWP the output at the high-spun end is again linear but is now oriented at 140 degrees.

Input at high-spun end (1310 nm)

The experiments were repeated with light launched into the high-spun end of the Huang fiber. If circular polarization was launched into the high-spun end, the output at the un-spun end was observed to be linear with an extinction ratio of 15.5 dB. It was oriented at 55 degree in local co-ordinates. When the handedness of the input circular light was reversed the output was again observed to be linear but the orientation was rotated by 90 degrees to 145 degrees in local co-ordinates.

The transformation of a circular to a linear polarization state is expected from the principal states model and the direction of linear polarization at the un-spun end will lie along the internal birefringence axes. Thus the orientation of the principal axes at the un-spun end is determined to be 55 degrees in laboratory co-ordinates.

Linearly polarized light was then launched into the high-spun end and its orientation was rotated using the HWP. The experimental results for the input orientations that produced linear or circular outputs are summarized in Table 3-2.

Input at High Spun End	Output at Un-Spun End		
Change in the orientation of input light (degrees)	Orientation of Pmax in Laboratory coordinates	Extinction (dB)	SOP
0	55	3.28	**Circular**
45	10	18.55	**Linear**
90	325	2.53	**Circular**
135	280	19.57	**Linear**
180	235	2.91	**Circular**
225	190	18.43	**Linear**
270	145	3.47	**Circular**
315	100	18.33	**Linear**

Table 3-2 Table showing the SOP of output light when linearly polarized light is input at high-spun end. First column shows the orientation of input light with respect to principal axes at high-spun end.

The input orientations that produce linear or circular states of polarization are 45 degrees apart as would be expected from the analogy to a bulk quarter-wave plate. The output angles at the un-spun end for linear polarization are 45 degrees from the internal birefringence axes (determined to be located at 55^0 in laboratory coordinates) which also agrees with theoretical expectations.

The best circular light at the un-spun end has an extinction ratio of 2.53 dB and the best linear extinction ratio is 19.57 dB. This is probably due to incomplete SOP transformation due to the short length of the fiber under test. For each orientation of the HWP the power was measured at 55 and 145 degrees, the angles that correspond to the orientation of the principal axes at the un-spun end. Power division factor defined as the ratio of the power along principle axes was plotted and is shown in Figure 3-4. The output power is almost equally divided between the two axes. Equal division of power is expected because linear polarization input at the high-spun end should excite both principal states equally.

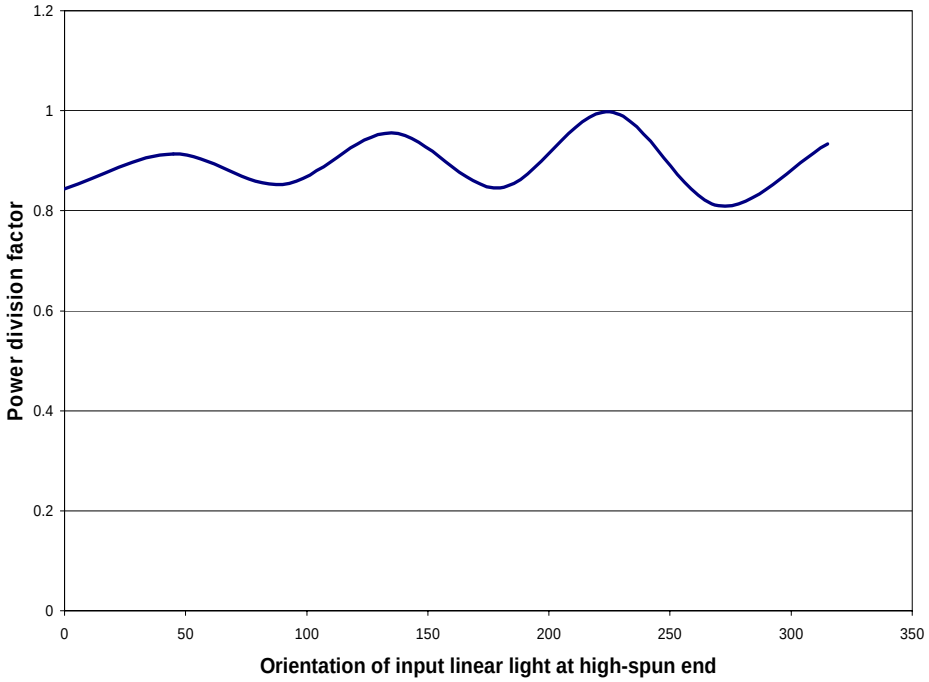

Figure 3-4 Power division factor

Measurements at 1550 nm

The measurements were repeated at 1550 nm with results given in Table 3-3 and Table 3-4. The results are the same as found at 1310 nm which confirms the wavelength independence of the quarter-wave transformation. It is somewhat surprising that no rotation of the effective quarter-wave axes at the high-spun end was found between 1310 nm and 1550 nm. Equivalent axes at high-spun end rotate with wavelength (Figure 2-44). The axes will be oriented at same angle at many wavelengths depending on period of rotation. This could possibly be the reason for not seeing any effective change in the orientation of axes at high-spun end.

Input at Un-Spun End	Output at HighSpun End		
Change in the orientation of input light (degrees)	Orientation of Pmax in Laboratory coordinates	Extinction (dB)	SOP
0	140	2.32	**Circular**
45	95	14.43	**Linear**
90	50	2.06	**Circular**
135	5	15.77	**Linear**
180	320	2.13	**Circular**
225	275	14.09	**Linear**
270	230	2.45	**Circular**
315	185	15.39	**Linear**

Table 3-3 Table showing the SOP of output light when linearly polarized light is input at un-spun end

Input at High Spun End	Output at Un-Spun End		
Change in the orientation of input light (degrees)	Orientation of Pmax in Laboratory coordinates	Extinction (dB)	SOP
0	55	2.57	**Circular**
45	10	15.53	**Linear**
90	325	2.15	**Circular**
135	280	16.14	**Linear**
180	235	2.08	**Circular**
225	190	18.12	**Linear**
270	145	2.33	**Circular**
315	100	18.19	**Linear**

Table 3-4 Table showing the SOP of the output light when linearly polarized light is input at high-spun end

3.4 Summary

The wavelength-independent transformation between linear and circular polarization of a Huang quarter-wave fiber has been demonstrated in our experiments. The experiments also serve to clarify some of the open questions with regard to applications of these quarter-wave fiber devices. The fact that the transformation to circular polarization is not perfect is probably due to loss of some fiber from the high-spun end during setup of the experiments. This, however, raises the question of the ultimate performance of these fibers. This question was investigated by analysis and by numerical simulation in the previous chapter (chapter 2).

Chapter 4. Conclusions and Future work

4.1 *Conclusions*

We studied the polarization transformation behavior of a variably spun birefringent fiber element (Huang plate) in detail by the means of simulations and experiments. The results of simulations and experiments show that a Huang plate indeed functions like a bulk-optic quarter waveplate with a favorable feature of being inherently wideband. We developed an intuitive simulation model based on a stack of birefringent plates and used this model to verify the theoretically predicted polarization transformation behavior. The simulation results were found to be in a good agreement with the theory.

We studied the dependence of polarization transformation behavior of Huang plates on different structural parameters, by the means of simulation. It was found that the structure has loose tolerances with regards to the total length of the fiber and the manner in which the spin rate is varied as long as the variation is slow. These are important from a practical point of view as they translate to an easier fiber draw process. Achieving sufficiently fast spin-rate at the fast-spun end was found to be a serious limitation that would limit the ultimate performance of this device. There will always be a trade-off between the achievements of a large number of rotations per beat length at the high-spun end while still having a high birefringence at the un-spun end. We investigated PMD characteristics of Huang plates and computed a value of PMD for our simulation model.

Polarization transformation behavior of composite structures made by appropriately cascading Huang plates was found to be similar to bulk-optic half waveplates and full waveplates.

4.2 *Future work*

We attempted to draw Huang plates by spinning a birefringent preform while drawing. However the spinning mechanism was not efficient and we had little control over the variation of the spin rate. Efforts must be continued to improvise the spinning mechanism and marking the beginning and the end of the fiber while drawing. Drawing experience would answer open questions regarding the manufacturing limitations. Experiments on Huang plates of different lengths, and different maximum spin rates would help to verify the simulation results on tolerances.

The other issue of importance for most systems applications is the polarization mode dispersion (PMD) of the device since PMD will impose a minimum pulse-length. Preliminary measurements indicate that the PMD of one of the test fibers is small as expected from our simulations. However, detailed measurements with a high resolution instrument are required to get the exact value for PMD.

References

1. H.C. Huang, “Passive Fiber-Optic Polarization Control,” U.S. Patent No. 4,943,132 (1990)
2. H.C. Huang, “Passive Fiber-Optic Polarization Control Element,” U.S. Patent No. 5,096,312 (1992)
3. H.C. Huang, “Fiber-optic analogs of bulk-optic wave plates,” appl. Opt., vol. 36, pp. 4241-4258 (1997)
4. G.G. Stokes, Proc of the Royal Soc. 6, 195, 1852. Reprinted in Mathematical and Physical Papers, vol. 3, pp. 259, Cambridge University press, London, 1901.
5. R. C. Jones “A new calculus for treatment of optical systems,” J. Opt. Soc. America., vol. 31, pp. 488-503 (1941).
6. S. C. Rashleigh, “Origins and control of polarization effects in single mode fibers,” IEEE J. Lightwave Technology., vol LT-1, pp. 312-331 (1983).
7. C.D.Poole, N.S.Bergano, R.E.Wagner, and H.J.Schulte: "Polarization Dispersion and Principal States in a 147-km Undersea Lightwave Cable", Journal of Lightwave Technology, LT-6, pp.1185-1191, 1988
8. R.H. Stolen, V. Ramaswamy, P. Kaiser, and W. Pleibel, “Linear polarization in birefringent single-mode fibers,” Appl. Phys. Lett., vol. 33, pp. 699-701 (1978).
9. H.C. Lefevre, “Single-mode fibre fractional wave devices and polarization controllers,” Electron. Lett., vol. 16, pp. 778-780 (1980).
10. H.C. Huang, “Practical circular polarization maintaining optical fiber,” Appl. Opt., vol. 36, pp. 6968-6975 (1997).
11. C. D. Poole and J. A. Nagel, “Polarization effects in lightwave systems” in Optical Fiber Telecommunications IIIA, I. P. Kaminow and T. L. Koch, eds. (Academic Press, San Diego, 1997).
12. H. C. Huang and Y.C. He, “Polarization behavior of spun fiber versus conventional fiber under strong and slight twisting,” Microwave. Opt. Tech. Lett., vol. 9, pp. 37-41 (1995)
13. H.C. Huang, “Generalized theory of coupled local normal modes in multi-wave guides,” Sci. Sin., vol.9, pp. 142-154 (1960).
14. L. Curz, M.V.Andres, and M.A. Hernandez, “Faraday effect in standard optical fibers: dispersion of effective Verdet constant,” Appl. Opt., vol. 35, pp. 922-927 (1996).
15. P. McIntyre and A. W. Snyder, “Light propagation in twisted anisotropic media: Application to photoreceptors,” J. Opt. Soc. Am., vol. 68, pp. 149-157 (1978).
16. S. Huard., Polarization of Light. 1997, New York: John Wiley and Sons.
17. E. Collett., Polarized Light: Fundamentals and Applications. 1993, Marcel Dekker, Inc
18. S. C. Rashleigh and R. H. Stolen, “Preservation of Polarization in Single-mode fibers,” Opt. Soc. Am., Invited talk.
19. E. Hecht., Optics. 4 ed. 2002, Pearson Education, Inc.
20. A. Ghatak and K. Thyagarajan., Introduction to fiber optics. 1999, Cambridge University Press.
21. W. Shurcliff., Polarized Light. 1962, Harvard University Press.

22. H. C. Huang, “Generalized theory of coupled local modes in multi-wave guides,” Sci. Sin., vol. 9, no. 1, pp. 142-154 (1960)
23. D. Derickson, Editor., Fiber optic test and measurement. 1998, Prentice-Hall, Inc.

Appendix

MATLAB code for input at un-spun end

```
clear all;

Lb=0.02; %in meters
L=1; %in meters
gamma = 1;
iterations=10000;
delta_z = L/iterations;
delta_beta = 2*pi/Lb*delta_z;

z = [0:delta_z:L];
Qm = 50;

%Equation defining the fiber structure. The spin rate varies from zero to
%very fast.
Q = Qm*(0.5 - 0.5.*cos(pi.*z/L)).^gamma;%input un-spun end
%_____________________________________________

tau_z = (2*pi.*Q)./Lb;
delta_tau_z= abs(atan(tan(tau_z * 0.0001)));
plot(delta_tau_z(1:iterations))

%Defining Initial SOP
%_____________________________________________
%LINEAR
% theta= 90;
```

```
% X(1)=cos(theta*pi/180)+0*i;
% Y(1)=sin(theta*pi/180)+0*i;
%_____________________________________________
%CIRCULAR
theta= 45;
X(1)=cos(theta*pi/180)*(1+0*i);
Y(1)=sin(theta*pi/180)*(0-1*i);
%_____________________________________________

Xfixed(1)=X(1);
Yfixed(1)=Y(1);
%_____________________________________________

for j = 1:iterations-1
   out = [exp(i*delta_beta) 0;0 exp(-i*delta_beta)]*[X(j);Y(j)];

   %Rotating back to fixed coordinates_____________________________
   total_theta = sum(delta_tau_z(1:j));
   temp1=[cos(total_theta) -sin(total_theta); sin(total_theta) cos(total_theta)]*out;
   Xfixed(j+1)=temp1(1);
   Yfixed(j+1)=temp1(2);

%_____________________________________________________________________
   temp = [cos(delta_tau_z(j+1)) sin(delta_tau_z(j+1));-sin(delta_tau_z(j+1))
cos(delta_tau_z(j+1))]*out;

   X(j+1)=temp(1);
   Y(j+1)=temp(2);
   j
end
```

```
%plotting amplitude and phase variation in local coordinates
figure(2)
plot(abs(X).^2,'linewidth',2)
hold on
plot(abs(Y).^2,'r','linewidth',2)
xlabel('Length (x/10000 meters)','fontsize',12)
ylabel('Power','fontsize',12)
text(2000,0.7,'Ax','fontsize',15)
text(2000,0.3,'Ay','fontsize',15)


rho = atan(abs(Y(length(Y))./abs(X(length(Y))))*180/pi



figure(3)
plot(angle(Y./X),'linewidth',2)
xlabel('Length (x/10000 meters)','fontsize',12)
ylabel('Phase difference (Radians)','fontsize',12)


P0=(abs(X)).^2 + (abs(Y)).^2;
P1=(abs(X)).^2 - (abs(Y)).^2;
P2=2.*(abs(X)).*(abs(Y)).*cos(angle(Y./X));
P3=2.*(abs(X)).*(abs(Y)).*sin(angle(Y./X));

S0=P0./P0;
S1=P1./P0;
S2=P2./P0;
S3=P3./P0;
```

```
%plotting SOP evolution in local coordinates on Poincaire sphere
figure(4)
colormap([1 1 1;1 1 1])
sphere(20)
alpha(0.5)
VIEW(45,45)
hold on
plot3(S1,S2,S3,'r','linewidth',2)
xlabel('S1','fontsize',12)
ylabel('S2','fontsize',12)
zlabel('S3','fontsize',12)
axis([-1 1 -1 1 -1 1])


figure(5)
v=length(S1);
S1n=[S1(1),S1(v)];
S2n=[S2(1),S2(v)];
S3n=[S3(1),S3(v)];
colormap([1 1 1;1 1 1])
sphere(20)
alpha(0.5)
VIEW(45,45)
hold on
plot3(S1n(1),S2n(1),S3n(1),'r.','markersize',30)
hold on
plot3(S1n(2),S2n(2),S3n(2),'b.','markersize',30)
xlabel('S1','fontsize',12)
ylabel('S2','fontsize',12)
zlabel('S3','fontsize',12)
```

```
axis([-1 1 -1 1 -1 1])
hold off


%Plotting amplitude and phase variation in fixed coordinates
figure(6)
plot(abs(Xfixed).^2)
hold on
plot(abs(Yfixed).^2,'r')
xlabel('Length (x/10000 meters)','fontsize',12)
ylabel('Power','fontsize',12)
text(2000,0.7,'Ax','fontsize',15)
text(2000,0.3,'Ay','fontsize',15)

figure(7)
plot(angle(Yfixed./Xfixed))
xlabel('Length (x/10000 meters)','fontsize',12)
ylabel('Phase difference (Radians)','fontsize',12)

P0=(abs(Xfixed)).^2 + (abs(Yfixed)).^2;
P1=(abs(Xfixed)).^2 - (abs(Yfixed)).^2;
P2=2.*(abs(Xfixed)).*(abs(Yfixed)).*cos(angle(Yfixed./Xfixed));
P3=2.*(abs(Xfixed)).*(abs(Yfixed)).*sin(angle(Yfixed./Xfixed));

S0=P0./P0;
S1=P1./P0;
S2=P2./P0;
S3=P3./P0;
```

```
%plotting SOP evolution in fixed coordinates on Poincaire sphere
figure(8)
colormap([1 1 1;1 1 1])
sphere(20)
alpha(0.5)
VIEW(45,45)
hold on
plot3(S1,S2,S3,'r','linewidth',2)
xlabel('S1','fontsize',12)
ylabel('S2','fontsize',12)
zlabel('S3','fontsize',12)
axis([-1 1 -1 1 -1 1])
hold off


figure(9)
v=length(S1);
S1n=[S1(1),S1(v)];
S2n=[S2(1),S2(v)];
S3n=[S3(1),S3(v)];
colormap([1 1 1;1 1 1])
sphere(20)
alpha(0.5)
VIEW(45,45)
hold on
plot3(S1n(1),S2n(1),S3n(1),'r.','markersize',30)
hold on
plot3(S1n(2),S2n(2),S3n(2),'b.','markersize',30)
xlabel('S1','fontsize',12)
ylabel('S2','fontsize',12)
zlabel('S3','fontsize',12)
```

```
axis([-1 1 -1 1 -1 1])
hold off
```

MATLAB code for input at high-spun end

```
clear all;

Lb=0.02; %in meters
L=1; %in meters
gamma = 1;
iterations=10000;
delta_z = L/iterations;
delta_beta = 2*pi/Lb*delta_z;

z = [0:delta_z:L];
Qm = 50;

%Equation defining the fiber structure. The spin rate varies from very fast to
%zero.
Q = Qm*(0.5 + 0.5.*cos(pi.*z/L)).^gamma;%input un-spun end
%_____________________________________________

tau_z = (2*pi.*Q)./Lb;
delta_tau_z= abs(atan(tan(tau_z * 0.0001)));
plot(delta_tau_z(1:iterations))

%Defining Initial SOP
%_____________________________________________
%LINEAR
theta= 69.51+90;
```

```
X(1)=cos(theta*pi/180)+0*i;
Y(1)=sin(theta*pi/180)+0*i;
%_____________________________________________
%CIRCULAR
% theta= 45;
% X(1)=cos(theta*pi/180)*(1+0*i);
% Y(1)=sin(theta*pi/180)*(0-1*i);
%_____________________________________________

Xfixed(1)=X(1);
Yfixed(1)=Y(1);
%_____________________________________________

for j = 1:iterations-1
   out = [exp(i*delta_beta) 0;0 exp(-i*delta_beta)]*[X(j);Y(j)];

   %Rotating back to fixed coordinates_____________________________
   total_theta = sum(delta_tau_z(1:(length(delta_tau_z)-j)));
   temp1=[cos(total_theta) -sin(total_theta); sin(total_theta) cos(total_theta)]*out;
   Xfixed(j+1)=temp1(1);
   Yfixed(j+1)=temp1(2);

%_____________________________________________________________________
   temp = [cos(delta_tau_z(j+1)) sin(delta_tau_z(j+1));-sin(delta_tau_z(j+1))
cos(delta_tau_z(j+1))]*out;

   X(j+1)=temp(1);
   Y(j+1)=temp(2);
   j
end
```

```
%plotting amplitude and phase in local coordinates
figure(2)
plot(abs(X).^2,'linewidth',2)
hold on
plot(abs(Y).^2,'r','linewidth',2)
xlabel('Length (x/10000 meters)','fontsize',12)
ylabel('Power','fontsize',12)
text(8000,0.7,'Ay','fontsize',15)
text(8000,0.3,'Ax','fontsize',15)

figure(3)
plot(angle(Y./X),'linewidth',2)
xlabel('Length (x/10000 meters)','fontsize',12)
ylabel('Phase difference (Radians)','fontsize',12)

P0=(abs(X)).^2 + (abs(Y)).^2;
P1=(abs(X)).^2 - (abs(Y)).^2;
P2=2.*(abs(X)).*(abs(Y)).*cos(angle(Y./X));
P3=2.*(abs(X)).*(abs(Y)).*sin(angle(Y./X));

S0=P0./P0;
S1=P1./P0;
S2=P2./P0;
S3=P3./P0;


%plotting SOP evolution in local coordinates on poincaire sphere
figure(4)
colormap([1 1 1;1 1 1])
sphere(20)
alpha(0.5)
```

```
VIEW(45,45)
hold on
plot3(S1,S2,S3,'r','linewidth',2)
xlabel('S1','fontsize',12)
ylabel('S2','fontsize',12)
zlabel('S3','fontsize',12)
axis([-1 1 -1 1 -1 1])

figure(5)
v=length(S1);
S1n=[S1(1),S1(v)];
S2n=[S2(1),S2(v)];
S3n=[S3(1),S3(v)];
colormap([1 1 1;1 1 1])
sphere(20)
alpha(0.5)
VIEW(45,45)
hold on
plot3(S1n(1),S2n(1),S3n(1),'r.','markersize',30)
hold on
plot3(S1n(2),S2n(2),S3n(2),'b.','markersize',30)
xlabel('S1','fontsize',12)
ylabel('S2','fontsize',12)
zlabel('S3','fontsize',12)
axis([-1 1 -1 1 -1 1])
hold off


%plotting amplitude and phase in fixed coordinates
figure(6)
plot(abs(Xfixed).^2)
```

```
hold on
plot(abs(Yfixed).^2,'r')
xlabel('Length (x/10000 meters)','fontsize',12)
ylabel('Power','fontsize',12)
text(8000,0.7,'Ay','fontsize',15)
text(8000,0.3,'Ax','fontsize',15)


figure(7)
plot(angle(Yfixed./Xfixed))
xlabel('Length (x/10000 meters)','fontsize',12)
ylabel('Phase difference (Radians)','fontsize',12)

P0=(abs(Xfixed)).^2 + (abs(Yfixed)).^2;
P1=(abs(Xfixed)).^2 - (abs(Yfixed)).^2;
P2=2.*(abs(Xfixed)).*(abs(Yfixed)).*cos(angle(Yfixed./Xfixed));
P3=2.*(abs(Xfixed)).*(abs(Yfixed)).*sin(angle(Yfixed./Xfixed));

S0=P0./P0;
S1=P1./P0;
S2=P2./P0;
S3=P3./P0;

%plotting SOP evolution in fixed coordinates on poincaire sphere
figure(8)
colormap([1 1 1;1 1 1])
sphere(20)
alpha(0.5)
VIEW(45,45)
hold on
plot3(S1,S2,S3,'r','linewidth',2)
```

```
xlabel('S1','fontsize',12)
ylabel('S2','fontsize',12)
zlabel('S3','fontsize',12)
axis([-1 1 -1 1 -1 1])
hold off


figure(9)
v=length(S1);
S1n=[S1(1),S1(v)];
S2n=[S2(1),S2(v)];
S3n=[S3(1),S3(v)];
colormap([1 1 1;1 1 1])
sphere(20)
alpha(0.5)
VIEW(45,45)
hold on
plot3(S1n(1),S2n(1),S3n(1),'r.','markersize',30)
hold on
plot3(S1n(2),S2n(2),S3n(2),'b.','markersize',30)
xlabel('S1','fontsize',12)
ylabel('S2','fontsize',12)
zlabel('S3','fontsize',12)
axis([-1 1 -1 1 -1 1])
hold off
```

Vita

Harsh Sanghvi was born in Mumbai, India. In 2001 he obtained a bachelors degree in electronics and telecommunications engineering from Mumbai University, India. In 2004 he completed his M.S. degree in electrical engineering from Virginia Polytechnic Institute and State University. Harsh is an avid reader and likes to play with hi-tech electronics gadgets.